THE TWO-DIMENSIONAL TURBULENT MIXING OF DENSITY STRATIFIED FLOWS IN A MOVING AIRSTREAM

J. HARRIS-BASS

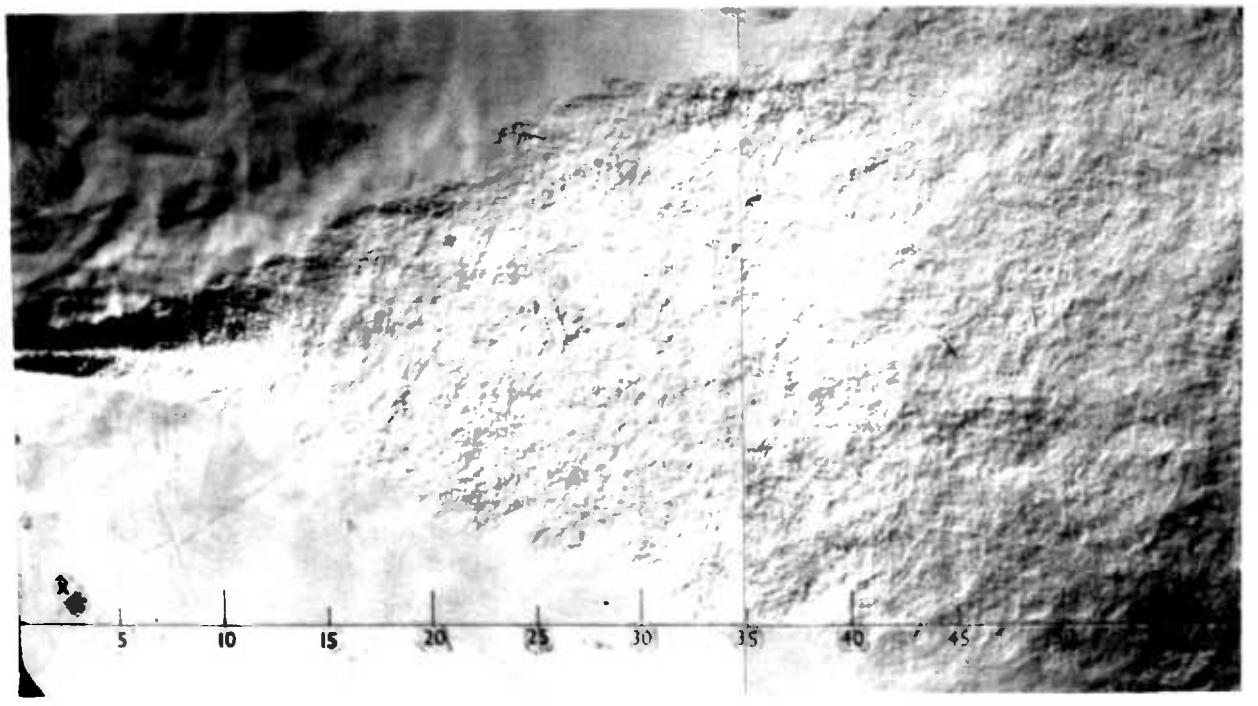
Thesis submitted for the degree of
Doctor of Philosophy
in the Faculty of Engineering of the
University of London

DEPARTMENT OF AERONAUTICS

IMPERIAL COLLEGE OF SCIENCE AND TECHNOLOGY

UNIVERSITY OF LONDON

NOVEMBER 1972



Turbulent jet mixing

$u_m = 0$

CONTENTS

	Page
Summary	i
Acknowledgements	ii
Nomenclature	iii
1. Introduction and Survey of Literature	
1.1 Introduction	1
1.2 Survey of Literature	2
2. Apparatus and Test Facilities	
2.1 Facilities	9
2.1.1 Primary Streams	9
2.1.2 Secondary Streams	11
2.2 Instrumentation and Traverse Gear	12
2.2.1 Velocity measurements	14
2.2.1.1 Measurement of Jet Velocity	15
2.2.2 Concentration measurements	16
2.2.2.1 Katharometer calibration	17
2.2.3 Temperature measurements	19
3. Experiments, Data Reduction and Results	
3.1 Experiments	20
3.2 Data Reduction	22
3.3 Results of Profile measurements	24
3.3.1 Velocity Profiles	24
3.3.2 Concentration Profiles	25
3.3.3 Temperature Profiles	27
3.4 Conservation of Momentum, Mass and Heat	28
3.4.1 Momentum Balances	29
3.4.2 Mass Balances	29
3.4.3 Heat Balances	30

Page

4. Theoretical Considerations

4.1 The turbulent plane jet in a moving airstream 32

4.2 Turbulent jet mixing for incompressible flow at constant pressure with density stratification 36

4.3 Excess Momentum Flux parameter approach 43

4.4 Jet Entrainment 46

4.5 Extraction of turbulent Schmidt and Prandtl numbers from experimental results 48

5. Correlations

5.1 Centre-line decays of velocity, concentration and temperature 55

5.1.1 Velocity decay 55
5.1.2 Concentration decay 57
5.1.3 Temperature decay 58

5.2 The spread of velocity, concentration and temperature 58

5.3 Centre-line measurements of turbulent Schmidt and Prandtl numbers 60

5.4 Jet entrainment 62

6. Conclusions and Suggestions for future work

6.1 Conclusions 63

6.2 Suggestions for future work 63

Appendix I 65

Appendix II 67

References 73

List of figures

SUMMARY

Experimental results are presented for the turbulent mixing of plane jets of air, cold carbon dioxide and hot carbon dioxide issuing into a cold moving airstream, and for the turbulent mixing of plane jets of cold air issuing into a heated moving airstream. The diffusion of momentum, mass and heat have been considered. Transverse and centre-line distributions of velocity, concentration and temperature have been obtained and compared for velocity ratios in the range $5.38 \geqslant {}^{u_j}/_{u_m} \geqslant 0.16$, for the near-downstream region $0 \leqslant {}^{x}/_{s} \leqslant 50$. The Reynolds Analogy has been found not to apply to flows of this nature. Measurements have been made of the turbulent Schmidt and Prandtl numbers for these flows.

ACKNOWLEDGEMENTS

I wish to place on record my thanks to Mr. John Stollery, under whose supervision this work has been conducted, for his many helpful suggestions, continued interest, encouragement and guidance during its duration.

My thanks are also due to Mr. "Mac" McAra and Mr. John Coles of the Departmental workshop for their time and many useful practical hints during the experimental work.

Finally, my thanks are due to Vivien, my wife, for her encouragement throughout my research and her patience with my spelling in the typing of this manuscript.

NOMENCLATURE

Symbols

A, B, E, F	constants in equations 4.2.8 and 4.2.9.
A_1, A_2	constants in § 4.4.
A', B'	constants in § 4.4.
C	Mass fraction; concentration by mass.
C_{D_s}	drag coefficient based on slot height.
Cp	specific heat at constant pressure.
D	drag.
D_{12}	laminar coefficient of diffusion of one gas to another.
D_t	turbulent diffusion coefficient in § 4.5.
H	$\frac{\theta_j}{s} - C_{D_s}$; excess momentum flux parameter.
h_o	enthalpy.
J	$\int_{-\infty}^{+\infty} \rho u(u-u_m)dy$; excess momentum flux.
K	mole fraction; concentration by volume.
K_1, K_2, K_3	dimensional constants in § 4.5.
Le	Lewis Number.
M	molecular weight.
$\dot{m}$	mass flow rate.
$\dot{m}_e$	$\dot{m}/\rho_m u_m$; mass flow rate parameter in § 4.4.
N	$= (N_j + N_m)$; number of molecules in gas.
Pr	Prandtl Number.
s	slot height

Sc	Schmidt Number.
T	temperature.
u	x-component velocity.
u_o	$= (u_{max} - u_m)$; velocity difference on jet or wake axis.
v	y-component velocity.
x,y	Cartesian coordinates.

Greek symbols

β	$= (M_j/M_m - 1)$; molecular weight parameter.
γ	C_p/C_v ; ratio of specific heats.
δ	characteristic width of jet or wake.
ϵ	eddy kinematic viscosity or eddy diffusivity.
τ	$\rho\epsilon\,(du/dy)$; shear stress.
η	y/δ ; similarity variable.
μ	laminar coefficient of viscosity.
ν	μ/ρ ; kinematic viscosity.
ρ	density.
θ_j	$\left(\frac{\rho_j u_j}{\rho_m u_m}\left[\frac{u_j}{u_m} - 1\right] s\right)$; initial momentum thickness at the slot.
κ	thermal conductivity.
σ	gradient used in §4.5.
ψ	stream function.

Subscripts

j	jet.
m	mainstream.
$\mathfrak{c}$	centre-line.
max	maximum

u	velocity
c	concentration
T	temperature
t	turbulent

1. INTRODUCTION AND SURVEY OF LITERATURE

1.1 INTRODUCTION

The problem of turbulent mixing of two plane gas streams has received considerable attention during recent years as the survey of the literature shows.

A most important problem arises when one gas is injected into an entirely different one moving in the same direction. The practical motivation for an investigation of such a flow is in the film cooling of combustion chambers.

The phenomena of turbulent mixing between two moving streams of gases of differing density is difficult to resolve and the analytical treatments of this problem are greatly impeded by the present knowledge of the fundamentals of turbulent transport of momentum, mass and temperature.

One of the simplifying factors often applied to flows of this nature is the analogy between heat and mass transfer, sometimes loosely termed the Reynolds Analogy. To test this analogy in the initial region of a two-dimensional jet, $(0 \leqslant {}^{x}/_{s} \leqslant 50)$ an initial density ratio of $\rho_j / \rho_m = 1.52$ has been generated by two separate means, a) by injecting carbon dioxide into cold air, and b) by heating the outside airstream and injecting cold air into it. Transverse and centre-line profiles of velocity, concentration and temperature have

been measured and compared using an excess momentum flux parameter approach.

To complete the cycle, the carbon dioxide was then heated, until an initial density ratio of $\rho_j / \rho_m = 1.0$ was reached, and an investigation of simultaneous mass and heat transfer conducted.

Turbulent Schmidt and Prandtl numbers are extracted from the experimental data, according to four methods of prediction, and compared.

1.2 SURVEY OF LITERATURE

This survey indicates that two principal types of analytical and experimental approaches have been adopted in turbulent mixing studies. The first approach deals with mean properties only, the fluctuations being expressed in terms of the mean. The second approach treats the mean and fluctuation properties separately. Recent developments in experimental techniques have made possible the measurement of turbulent fluctuations and consequently enhanced the importance of the second approach.

Kuethe[1] made the first extensive investigation of the mixing region between two moving streams with different velocities. He extended Tollmien's[2] exact solution (employing Prandtl's mixing length hypothesis) for the mixing of a plane jet issuing into air at rest and obtained an approximate method for computing the

velocity profile. This semi-empirical theory has subsequently been found to disagree with experimental data. Abramovich[3] obtained velocity, concentration and temperature profiles of a free jet using Prandtl's mixing length hypothesis and Taylor's vorticity theorem. He found that the concentration and temperature profiles as predicted by Taylor's theorem were in better agreement with experiments carried out by himself and others than those predicted by Prandtl's hypothesis. Szablewski[4] investigated theoretically the diffusion of heat with a hot air jet for large differences in the density of the two streams but small velocity difference. He used Prandtl's mixing length hypothesis to predict the velocity and temperature along the jet axis in addition to describing the rate of spread of the jet in terms of the width of the mixing region. In the book by Schlichting[5] it is shown how Goertler used Prandtl's new hypothesis and obtained a simpler exact solution to the problem of the free jet than the solution given previously by Tollmien. Ragsdale et al[6] measured the isothermal mixing between a heavy slow moving jet of Bromine and air. They suggested a formula for the dimensionless eddy viscosity and tested it experimentally for a range of Reynolds numbers. Alpinieri[7] measured the subsonic mixing of two co-axial streams of different density. His main conclusion was that unity ratios of none of the velocity, mass flux or momentum

flux ratios of the two streams produces a satisfactory criterion for the minimum mixing rate. He also concluded that the transport coefficients in a turbulent flow cannot be considered to be principally dependent upon the difference of two flow quantities when this difference approaches zero. Schetz[8] placed particular emphasis on the form of the model for the eddy viscosity. Good agreement was found between theory and experiment using a unified model based on that of Clauser[9]. Zakkay et al[10] experimentally determined momentum and mass eddy diffusivities and turbulent Schmidt and Prandtl numbers. Ghia et al[11] used a semi-empirical, analytical solution together with an eddy viscosity formulation based on Prandtl's new (1945) hypothesis. Experimental data was used to correlate appropriate values for some of the parameters. For low speed flow across a flat plate, Morkovin[12] found excessive scatter when attempting to determine the eddy diffusivities of momentum, mass and heat by differentiating experimental results. His suggestion was to produce eddy coefficients by taking the total momentum, mass or temperature flux and divide it by the respective mean velocity, mean concentration or mean temperature gradient. Use of dimensionality constants led to turbulent Schmidt and Prandtl numbers. Forde[13] studied the mixing of supersonic coaxial compressible streams of Carbon Dioxide and air.

He concluded that subsonic turbulent mixing theories were applicable for his supersonic conditions when a mixing similarity parameter was determined empirically.

Among those who used an integral method, assuming a velocity distribution function, Squire and Trouncer[14] obtained a solution for the case of two moving axisymmetric streams. Forstall and Shapiro[15] compared Squire and Trouncers results with their experimental results and found that 1) mass transport is more rapid than momentum transport and 2) that the turbulent Schmidt and Prandtl numbers were both approximately 0.70 and independent of velocity ratio. It should be pointed out that Forstall and Shapiro only made measurements with foreign gases and that their values for turbulent Prandtl number are based on the results of other workers. Hinze[16] has however stated that the cosine distribution used by Forstall and Shapiro for their velocity profile does not apply to the mixing process when the mainstream and jet velocities are of the same magnitude, (i.e. when $u_j/u_m \simeq 1.0$). Landis and Shapiro[17] extended the work of Forstall and Shapiro to include the thermal transport case. They found that the temperature spreads faster than the momentum but found that the normalized temperature profile was not the same as for velocity and concentration, a result also established by Corrsin and Uberoi[18]. Keagy and Weller[19], who studied the injection of gases from a sharp-edged orifice into still air found that the density difference

between the two gases is a very important factor in the mixing process. They agreed that the concentration profiles were wider than the corresponding velocity profiles, thus confirming that mass diffuses more rapidly than momentum. El-Ehwany[20] found, from plane jet mixing of various gases in a moving airstream, that the velocity, concentration, momentum flux and mass flux profiles could be represented by one distribution. However, both he and Keagy and Weller found difficulty in correlating data for a light gas (Helium). El-Ehwany also used the excess momentum parameter to correlate his data for decays and spreads. In their investigation of a plane jet in a parallel airstream, Bradbury and Riley[21] showed that as long as an effective shift in the origin of the flow is allowed for, the flow some distance downstream of the nozzle is dependent only on the overall excess momentum flux and independent of the precise nozzle conditions. The structure of the jet was noticed to change as it spread downstream, from that of a pure jet type flow towards a self-preserving jet type of structure, but this change seemed much slower than that suggested by a straightforward application of Townsend's[22] large-eddy hypothesis. This finding is in accordance with work by Maczynski[23] who studied a round jet immersed in an airstream having the same velocity.

Turbulent flows are characterised by a random fluctuating motion superimposed on a time-smoothed mean flow. The instantaneous values of the flow properties

can therefore be expressed as the sum of the mean flow and a fluctuating flow. In the preceding survey, the work considered has been concerned mainly with determining, both experimentally and theoretically, the local mean flow distribution for momentum, mass and temperature. Subsequent determination of turbulent shear stress has been performed using various transport theories. This mean property approach is sufficient for many practical applications, but only through the actual measurement of the fluctuating components is it possible to understand the mechanism of the turbulent mixing process. Early work on fluctuation measurements was done by Corrsin[24] both by himself and with Uberoi[18]; this latter work measuring velocity fluctuations in hot jets. Liepmann and Laufer[25] pioneered the cross-wire technique for measuring velocity fluctuations in a half-jet.

However, very little work seems to have been done on the turbulence in the mixing region between two moving streams with density stratification. D'Souza et al[26] and Montealegre et al[27] measured the velocity fluctuations and the axial turbulence intensities in the mixing region of a Freon-12 jet issuing into a moving airstream at low subsonic speeds. Attempts by both sets of workers to obtain values for the density fluctuations however, proved unfruitful. This was put down to the type of probe used which was of the aspirator type and was found to be measuring fluctuations in the probe rather than in the flow field. Recently, Sebacher[28] has tried

an electron-beam technique without very much success, but it has led to the laser anemometer of which great results are expected. More recently a pulsed hot-wire probe has been developed by Bradbury and Castro[29], which is based on simple time-of-flight measurements and will thus not be affected by variations in density. It is hoped that this probe will be able to measure fluctuations in a mixing region and it is being further developed by MacQuaid and Wright[30] to measure density fluctuations.

2. APPARATUS AND TEST FACILITIES

2.1 FACILITIES

All the tests were conducted in a converted working section of the 18x18 inch closed working-section, open return windtunnel of the Aeronautics Department of Imperial College, London. The effect of this conversion, as shown in Fig. 2.1, was to reduce the horizontal plane of the tunnel from 18 inches to 9 inches. This also reduced the span of the jet exit and thus reduced the amount of gas emitted.

2.1.1 PRIMARY STREAMS (AIR AND HOT AIR)

The tunnel has a 6 foot long working section and had, with its new section, a maximum test section velocity of $\sim$180 ft./sec. speed control of the tunnel was achieved by throttling the air at the inlet to the tunnel fan. The turbulent intensity in the working section was found to be higher at lower tunnel speeds but to economize on gas most tests were carried out in the 25-70 ft./sec. range. For the series III tests, in which cold air was ejected into a hot mainstream, heating was provided by four industrial heat guns* blowing into what was known as the heat chamber of the tunnel and also by a grid containing six 1Kw. electric fire bars. The heat chamber

---

*Hellerman Electric Ltd., Crawley, Sussex.

was clad with aluminium plate and it was also found necessary to clad 6-8 feet of the tunnel upstream of the chamber with aluminium foil to reduce the fire risk caused by radiation of the heat up the tunnel. The effect of these heaters was to produce a stream of hot air of between 200-250^{o}C in the centre of the tunnel as shown in Fig. 2.2. Although the depth of this stream was less than the 18 inches of the tunnel, it was sufficient to give a constant mainstream temperature of $\sim$ 180^{o}C from the jet exit to approximately 100 slot widths downstream over the centre of the tunnel and spanning to within $^{1}/_{2}$ inch of the walls. Heat losses were inevitable along the walls, but down the centre of the working section, the temperature was essentially constant. Control of the heaters was by a variable rheostat. This was necessary as the temperature of the mainstream at the jet exit had to be adjusted according to the temperature of the cold air used in the secondary stream which was stored in tanks situated externally and exposed to the elements. Adjustment was made to give a density ratio at the exit of $\varrho_j / \varrho_m = 1.52$.

The grid of heaters were at first omitted from the tunnel and tests for series $\underline{\mathrm{I}}$ and $\underline{\mathrm{II}}$ were conducted. The heater grid was then placed in the tunnel for the series $\underline{\mathrm{III}}$ tests and some marked contradictions were noticed when comparing the results for these three series. The contradictions were due to the very marked increase in

turbulence in the tunnel with the grid in place. All the series were then run with the heater grid in the tunnel.

2.1.2 SECONDARY STREAMS (AIR, CO_2 AND HOT CO_2)

The secondary stream was supplied to the tunnel through a two-dimensional slot similar to that shown in Fig. 2.3(a). The slot width was $^1/8$ inch and the slot spanned the new 9 inch wide section of the tunnel. Its width had originally been 18 inches and some small modifications to its interior were made, as shown in Fig. 2.3(b).

The jet contained a plenum chamber 18 inches long and $^3/8$x3 inches in section. The exit side of this chamber could be altered by using throats of various sizes. The throat used for all these experiments was of $^1/16$ inch diameter holes spaced $^1/8$ inch apart in two rows as shown in Fig. 2.3(b). Upstream of these holes was a very fine gauze screen followed by a short diffuser and 1 inch of parallel sided duct to the jet exit. Pressures in the plenum chamber were such that the throat was always choked and it was found that for this particular design the velocity distribution at the slot exit was two-dimensional to $\pm 2\%$ except within $^1/2$ inch of the tunnel walls. (re: $\int$ 3.1).

Air supply for the secondary stream was contained in two large external tanks at pressures of $\sim$ 500 psi and was controlled by throttle valves, through a common

header tank which was in turn controlled by a pressure regulator valve. A pressure gauge fitted to the low pressure circuit checked the pressure regulator gauge reading.

Carbon dioxide was supplied from high pressure bottles available commercially. The bottles contained a gas equivalent of 1500 cu.ft. at N.T.P. at a maximum pressure of 800 psig. An arrangement was made to utilize more than one bottle at a time by introducing a common manifold connecting four cylinders through high pressure hosing to the header tank mentioned above. Again the pressure was controlled by a pressure regulator valve monitored by a pressure gauge.

To obtain the hot carbon dioxide for the series IV tests, a 4 Kw. heat exchanger was placed just downstream of the header tank. All pipework upstream of the heat exchanger was heavily lagged with glass-fibre wadding for this series of tests.

The maximum Reynolds numbers based on the slot width were, a) 20,000 for air and b) 16,000 for carbon dioxide.

2.2 INSTRUMENTATION AND TRAVERSE GEAR

Measurements consisted of total head, static pressure, concentration by volume and total temperature. In order to obtain simultaneous readings of velocity and concentration or temperature, the probe head was constructed to hold the probes equispaced in a lateral position.

Spacing was $^{3}/_{4}$ inch, enough to ensure that the disturbances to the flow by each probe did not affect the others. This was checked by taking measurements of velocity, concentration and temperature with single probes and then repeating these measurements with the probes mounted in the probe head. The probe head was moved vertically by means of a "slide-rule" traverse driven by a reversible 12v. dc. motor†. Position of the traverse was obtained by a small transducer* of positional accuracy of ±0.001 inch or less. Output voltages from this transducer were connected via a control panel to a Mosely‡ X-Y recorder. A general view of the traverse gear is shown in Fig. 2.4. Longitudinal positioning of the traverse gear downstream of the jet exit was obtained by using removable shutters of known width which were located in the tunnel roof. The shutters were constructed of various sizes to facilitate location of the traverse gear in any position throughout the working section. Mainstream velocity was measured from the reference pressure tappings in the tunnel using a Betz manometer.

---

† Manufactured by Vactric Control Equipment, Morden, Surrey.

* Manufactured by Ether Engineering, Hemel Hempstead, Herts.

‡ Hewlett Packard, Mosely Division, California.

2.2.1 VELOCITY MEASUREMENT

Dynamic head profiles were obtained using an I.R.D. micromanometer* with, for these tests, a transducer whose sensitivity was 250 mv/in. water gauge with a linearity within 2% of full scale output. This was calibrated before and after each set of runs against the Betz manometer. The transducer was connected to the probes by about 12 inches of tubing and this was found to yield a tolerable response time.

The total head probe was of 0.027 inch internal diameter and the static probe was 0.080 inch external diameter and was of standard NPL design.

Output voltages from the transducer (proportional to $^1/2\ \rho u^2$) were fed via a control panel to the Mosely X-Y recorder similarly to the positional transducer output. The sensitivity and linearity of the recorder were sufficiently good to render any errors at this stage of signal processing negligible relative to those at the transducing stage.

During the course of the series $\bar{I}$ tests further measurements were taken using both a hot wire probe of standard DISA† design and a pulsed hot wire probe. The philosophy behind this latter probe is fully explained in the paper by Bradbury and Castro[29]. It was hoped that the pulsed hot-wire probe could be used in this study

---

* Hilger-IRD Ltd., Camden Road, London, NW1.

† DISA, Denmark

to measure turbulent properties in density stratified flows but the time available necessitated only a mean flow investigation. Figs. 2.5 and 2.6 show the results of the measurements made with these two probes in the series $\underline{I}$ tests compared with some results by Bradbury[37] for a plane air jet.

2.2.1.1 MEASUREMENT OF JET VELOCITY

Pressures inside the jet plenum chamber were kept such that the throat of the jet was always choked. This resulted in a turbulent jet being produced at the slot exit as can be seen from Figs. 2.7(a) and (b), which show the profiles inside and outside the exit compared with the theoretical flat-plate boundary-layer results for the same conditions. These figures demonstrate that the flows were turbulent.

The jet velocities were calculated using the standard one-dimensional gas dynamic equations (as used previously by El-Ehwany[20]). Thus the jet velocity may be expressed as,

$$u_j = \left[\frac{\gamma}{R_j T_o}\right]^{1/2}\left[\frac{2}{\gamma+1}\right]^{\frac{\gamma+1}{2(\gamma-1)}}\left[\frac{p_o}{\rho_j}\right]\left[\frac{A^*}{A_j}\right]$$

Since $\left[A^*/A_j\right]$ is fixed by the slot design, the jet velocity may be calculated for any given plenum chamber pressure and temperature.

Measurements made across the span of the jet of velocity profiles showed that the experimentally measured maximum velocities were within ± 3% of those given by the above equation.

2.2.2 CONCENTRATION MEASUREMENT

Analysis of gas-mixture constituents on a continuous basis was achieved by using a microkatharometer‡ of the through-flow type with the heated wires directly in the sample stream. This together with a total passage volume of only $2.6\mu/1$, enables a short response time to be obtained which is not possible with the more conventional diffusion type of katharometer where the heated wires are in a side passage and depend upon the relatively slow molecular diffusion from the sample stream. Unfortunately, however, the through-flow katharometer is very sensitive to flow rate and it is therefore important to ensure that the pressure drop across the cell is constant during sampling. The design philosophy of this type of katharometer is outlined by Préau and Guiochon[31].

A schematic of the pipework and electrical circuitry for the katharometer is shown in Fig. 2.8. The probe used was of the total head type with an internal diameter of 0.070 inches. The sampling conditions used yielded a response time of 0.5 sec. for a sampling velocity

---

‡ Developed by the Distiller's Company Ltd., and marketed by Servomex Controls of Crowborough, Sussex.

at the probe tip of about 42 ft./sec. (48 ml./sec.). The traversing speed was kept at speeds sufficiently low to eliminate the risk of concentration profile distortion due to the 0.5 sec. time response of the cell. To determine the traversing speed, several runs were made, in both directions across the slot, at gradually slower speeds until the velocity and concentration axes coincided. At this point observation showed that the profiles were symmetrical.

As with the velocity profiles, the concentration profiles were plotted by the X-Y recorder.

2.2.2.1 KATHAROMETER CALIBRATION

The cell was calibrated for mixtures of carbon dioxide in air by injecting mixtures of known composition into the cell, using a known, constant, cell pressure drop and pressure within the cell. The calibration mixtures were made up in a 100 ml syringe. The calibrations obtained were valid for the cell during subsequent operation provided that the cell pressure drop and cell pressure were maintained the same as for the calibration.

The total probable uncertainty in mole fraction measurements amounted to not more than 2.5% of full scale readings and arose from the cumulative effects of drift in the bridge supply voltage, drift in cell pressure drop and uncertainty in calibration.

The calibration and analysis were carried out with a cell pressure drop of 8 inches of alcohol and a vacuum of 19.5 inches of alcohol upstream of the cell. These figures were arrived at because of the need for a short time response which was governed by the travelling time of a slug of sampled gas from the probe to the cell.

For the series IV tests, where hot carbon dioxide was used, a further calibration was required. For the cold carbon dioxide, the calibrations obtained had agreed tolerably well with the manufacturers calibrations as shown in Fig. 2.9. However, on heating the gas the thermal conductivity is altered. As outlined by Préau and Guiochon, the thermal conductivity is the quantity which is measured by the katharometer, thus a variation in calibration is expected. For 100% carbon dioxide the calibration was a straightforward measurement at elevated temperatures. However, for other percentages of the gas in the mixture, the following procedure was adopted. The carbon dioxide was blown into the tunnel upstream of the heat chamber and mixed with the air before reaching the heaters. Several samples were taken with 100 ml syringes on the downstream side of the heaters along with voltage measurements and temperature readings. When the contents of the syringes had cooled to room temperature, they were fed through the katharometer in the usual way to obtain their concentration. These points are shown in the elevated temperature calibrations in Fig. 2.9.

2.2.3 TEMPERATURE MEASUREMENT

Measurements of total temperature were made with a Chromel/Alumel (Cr/Al) thermocouple connected to a temperature sensing transducer*. The response of this system was 0.3 sec. per 100^{o}C for increasing temperatures. However, an odd characteristic of the probe was that it could sense a cool temperature quicker than a hot one, this time response being about 40% quicker than the increasing temperature response. This resulted in an asymmetric profile and necessitated the taking of traverses in both directions across the flow in order to achieve a true profile. A check was made on the profiles by taking a point-by-point temperature profile across the jet at various times during the tests. These tests showed the two-part profiles to be accurate to about ± 5%.

A calibration check on the transducer showed it to be accurate to within ± 2% of full scale deflection and after the initial calibration no further attention was required.

As with the velocity and concentration profiles, the temperature profiles were plotted directly by the X-Y recorder.

---

* Manufactured by COMARK Ltd., Littlehampton, Sussex.

3. EXPERIMENTS, DATA REDUCTION AND RESULTS

3.1 EXPERIMENTS

As a preliminary to the main experimental programme, a two-dimensionality check was made of velocity across the jet exit. This showed that to within $^1/2$ inch of the tunnel walls the jet was two-dimensional to within $\pm 2\%$. This is demonstrated in Fig. 3.1.

The experiments themselves were split into four series of tests depending on the constituents of the primary jet. These are detailed below.

SERIES	PRIMARY STREAM	SECONDARY STREAM
I	Air at 15°C	Air at 15°C
II	Air at 15°C	CO_2 at 15°C
III	Air at 160°C	Air at 15°C
IV	Air at 15°C	CO_2 at 165°C

These tests made it possible to study heat and mass transfer independently under the same initial geometric and density conditions. The series IV tests made it possible to examine simultaneous heat and mass

transfer under the same initial conditions as the series I tests. The initial conditions for all the tests are summarized in the following table.

		MASS
	Series I AIR → AIR $\rho_j/\rho_m = 1.00$ $T_j/T_m = 1.00$ $C_j/C_m = 1.00$	Series II CO_2 → AIR $\rho_j/\rho_m = 1.52$ $T_j/T_m = 1.00$ $C_j/C_m \neq 1.00$
HEAT	Series III COLD AIR → HOT AIR $\rho_j/\rho_m = 1.52$ $T_j/T_m \neq 1.00$ $C_j/C_m = 1.00$	Series IV HOT CO_2 → COLD AIR $\rho_j/\rho_m = 1.00$ $T_j/T_m \neq 1.00$ $C_j/C_m \neq 1.00$

Although many velocity ratios were used throughout the tests, comparisons for all the series were based upon six velocity ratios. These ranged from almost pure wake flows to strong jet flows and are listed below.

u_j/u_m	0.16	0.50	1.00	1.53	2.83	5.38

where u_j/u_m is the ratio of jet velocity to mainstream velocity on the centre-line of the jet at the jet exit.

For each run, profiles of $^1/2\ \rho u^2$ and either concentration or temperature (in the case of the series IV tests both concentration and temperature profiles were taken) were recorded for seven streamwise stations within the range $0 \leqslant x/s \leqslant 50$. This range was chosen so that the study could be of the initial mixing region of the jet and could be related to the mixing problems involved in aero-engine combustion chambers. Flows far downstream of the exit have been widely examined, but little attention has been devoted to the initial mixing region. The recorded profiles were produced by an X-Y plotter and subsequently reduced.

3.2 DATA REDUCTION

From the work of Jeans[32], local measurement of volumetric concentration of the injected gas in a mixture will give a local value of the number density according to the following equations:-

$$K = N_j/N \qquad 3.2.1$$

$$1-K = N_m/N \qquad 3.2.2$$

where N is the total number of molecules of the mixture of the gas jet and air per unit volume under a constant pressure and temperature, i.e.:

$$N = N_j + N_m \qquad 3.2.3$$

considering a mixture of two gases in a steady state, the mass density ρ of the mixture under constant pressure and temperature is,

$$\rho = M_j N_j + M_m N_m \qquad 3.2.4$$

and this may be written, from 3.2.1, 3.2.2 and 3.2.4 as,

$$\rho = \rho_m(\beta K + 1) \qquad 3.2.5$$

where ρ_m is the mainstream density and $\beta \left(= \left[M_j/M_m - 1\right]\right)$ is known as the molecular weight parameter.

Pitot-static recordings give ρu^2 and hence the values of local velocity are obtained.

With the heat measurements use was made of the equation of state to obtain the density and this led to the local velocity measurement from the pitot-static recordings.

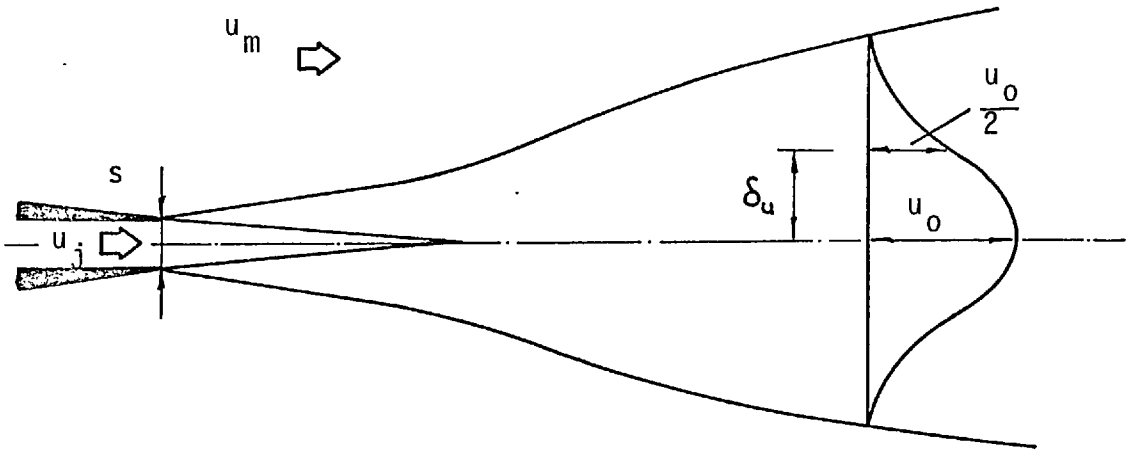
3.3 RESULTS OF PROFILE MEASUREMENTS

3.3.1 VELOCITY PROFILES

The experimentally measured velocity profiles were normalized by plotting

$$\left| \frac{u - u_m}{u_{max} - u_m} \right| \quad \text{against} \quad \left| \frac{y}{\delta_u} \right|$$

where δ_u is the individual half-width at the half-velocity difference point measured from the jet centre line, as shown in the figure below. Though various length scales are defined in the literature δ_u has the great advantage in that it can be measured easily and accurately. Results are shown in Figs. 3.2(a), (b), (c) and (d).



$$u_o = u_{max} - u_m$$

The profiles outside the potential core region ($0 \leqslant {}^{x}/s \leqslant 10$) for the whole range of velocity ratio for all the combinations tested are similar and can be reasonably well expressed by the well known "Gaussian Distribution". This is:-

$$\left| \frac{u - u_m}{u_{max} - u_m} \right| = \exp. \left(-0.6932 \left(\frac{y}{\delta_u}\right)^2\right) \qquad 3.3.1.1$$

This function has been used successfully by many other workers, for example Weinstein et al[33], Eskinazy[34], El-Ehwany[20] and Keagy and Weller[19]. Other profiles have been used, notably the "Cosine Distribution", but as shown in Figs. 3.2 it is not a successful profile for the latter part, or tail, of the function (i.e.: when ${}^{y}/_{\delta_u} > 1.0$).

3.3.2 CONCENTRATION PROFILES

Experimentally measured profiles of concentration were of K, the volumetric concentration. Before normalizing these profiles they were converted to mole-fraction or concentration by mass, C, by the following:-

From 3.2.1, 3.2.2, 3.2.3 and 3.2.4,

$$K = {}^{N_j}/_{N}$$

$$1-K = {}^{N_m}/_{N}$$

$$N = N_j + N_m$$

$$\rho = M_j N_j + M_m N_m$$

now, concentration by mass, C,

$$= M_j N_j / M_j N_j + M_m N_m$$

$$= 1 \Big/ 1 + \frac{M_m}{M_n} \cdot \frac{N_m}{N_j}$$

$$C = 1 \Big/ 1 + \frac{M_m}{M_j} \left(\frac{1-K}{K}\right) \qquad 3.2.2.1$$

The concentration profiles were then normalized by plotting

$$\left|\frac{C}{C_{max}}\right| \quad \text{against} \quad \left|\frac{y}{\delta_c}\right|$$

where δ_c is the individual half-width at the half-concentration point measured from the jet centre-line. Again although other length scales have been defined in the literature, δ_c , like δ_u , has the advantage in that it can be measured easily and accurately. Results are shown in Figs. 3.3(a) and (b).

Again, outside the potential core region $(0 \leqslant x/s \leqslant 10)$ the data shows that the Gaussian distribution is a fair description of the concentration profiles, i.e.

$$\left|\frac{C}{C_{max}}\right| = \exp.\ (-0.6932(\frac{y}{\delta_c})^2) \qquad 3.2.2.2$$

This function has also been used by other workers, particularly Forstall and Shapiro[15], El-Ehwany[20] and Keagy and Weller[19]. Forstall and Shapiro also considered the cosine distribution for concentration and found that both functions represented their data with reasonable accuracy. However, as shown in Figs. 3.3, the results obtained here demonstrate that the cosine function is not as successful for representing the data when $y/\delta_c > 1.0$.

3.3.3 TEMPERATURE PROFILES

The experimentally measured temperature profiles were normalized by plotting,

$$\left|\frac{T-T_m}{T_{max}-T_m}\right| \quad \text{against} \quad \left|\frac{y}{\delta_T}\right|$$

where δ_T is the individual half-width at the half-temperature point measured from the jet centre-line. Results are shown in Figs. 3.4(a) and (b).

Outside the potential core region $(0 \leqslant x/s \leqslant 10)$ the data showed that a fair description for the temperature profiles would be,

$$\left|\frac{T-T_m}{T_{max}-T_m}\right| = \frac{1}{2}\left[1 + \cos\frac{\pi}{2}\left(\frac{y}{\delta_T}\right)\right] \qquad 3.3.3.1$$

This function although slightly different to that found

for the velocity and concentration fits the data better and was used by Landis and Shapiro[17] in a similar form for their work on heated axisymmetric jet mixing. Also shown in Figs. 3.4 is the Gaussian distribution function.

3.4 CONSERVATION OF MOMENTUM, MASS AND TEMPERATURE

A check on the integrated flux of momentum, mass and heat across the jet is a sensitive test of repeatability of initial conditions. Such a check was made at each streamwise station for the two extreme velocity ratio cases tested, (i.e.: $u_j/u_m = 0.16$ and 5.38). The conserved quantities were,

Momentum $$\int_{-\infty}^{+\infty} \rho u (u-u_m)\, d(\tfrac{y}{s}) \qquad 3.4.1$$

Mass $$\int_{-\infty}^{+\infty} \rho u C\, d(\tfrac{y}{s}) \qquad 3.4.2$$

Heat $$\int_{-\infty}^{+\infty} \rho u Cp\, (T-T_m)\, d(\tfrac{y}{s}) \qquad 3.4.3$$

The conserved quantity in equation 3.4.3 is enthalpy. For the series III tests the temperatures used ($<200^{o}C$) were not enough to cause the specific heat at constant pressure to alter and it was considered constant at 0.239 Btu/lb.^{o}C. For the series IV tests, however, Cp was not constant. However, considering a total enthalpy

balance for the flow, it can be shown that there is a linear relationship between Cp and the concentration measurement C. Thus a value for Cp was used at a particular position, based on the concentration at that point.

3.4.1 MOMENTUM BALANCES

The check on the integrated momentum flux down the jet yielded a scatter of about ± 5%. This error is due to the superposition of individual errors in the components that make up the product $\rho u(u-u_m)$ in the integral.

Measurements of $^1/2\ \rho u^2$ are, however, accurate to within about 3% and at $^x/s = 50$ the scatter on velocity measurements was ± 2% of the free-stream velocity. This does increase slightly to about ± 5% further downstream, as a check at $^x/s = 200$ showed, but in all cases the scatter was random and not systematic showing that it was due to measurement errors.

The momentum balances according to equation 3.4.1 are shown in Figs. 3.5(a), (b), (c) and (d).

3.4.2 MASS BALANCES

A check downstream on the mass flux from the jet for the series II and IV tests showed an observed scatter in integrated species flux of typically about 7% for the strong jet case of $u_j/u_m = 5.38$ and up to about 14% for the wake case of $u_j/u_m = 0.16$. The discrepancy between these two results demonstrates the difficulty in making

mean flow measurements in strong wake flows. This may be explained by the wake flow consisting basically of a core of fully developed continuous turbulence in which bulges are formed by the moving outwards of large-eddy motions. These large-eddies are of comparable size to the width of the wake but contain small scale eddies of a magnitude about one order less. These small scale eddies, which originate mostly in the core region are entrained into the large scale motions of the bulges. This mechanism is to some extent demonstrated in the Schlieren photographs for $u_j/u_m = 0.2$ shown in APPENDIX I.

Measurements of mass-fraction, however, are accurate to within about 3% of unity and yield effective measurements to within about 6% when a two component gas such as Carbon Dioxide is used.

Mass balances according to equation 3.4.2 are shown in Figs. 3.6(a) and (b).

3.4.3 HEAT BALANCES

A downstream check on the heat flux from the jet for the series III and IV tests revealed a scatter in integrated heat flux of typically about 15% for both the jet and wake cases. In common with the individual profiles for each velocity ratio all the tests with heat showed a greater scatter of results. These errors were due primarily to the measuring technique employed which

was only accurate to approximately 7% and had quite different time constants depending on whether the probe was being heated or cooled. Thus at the edges of the jet where the turbulence is highest, the probe was subjected to very varied conditions, resulting in subsequent errors. The integrated heat flux results reflect these errors but are still good compared with other results in heated jet mixing, (e.g. Landis and Shapiro[17], Corrsin and Uberoi[18]).

The heat balances according to equation 3.4.3 are shown in Figs. 3.7(a) and (b).

4. THEORETICAL CONSIDERATIONS

4.1 THE TURBULENT PLANE JET IN A MOVING AIRSTREAM

Since this flow is of interest in the present work it is appropriate to afford some time in defining the terms used. The figure shown in § 3.3.1 shows the flow of a plane jet emerging from a slot of width s into a moving airstream of constant velocity u_m. The jet velocity, u_j, is assumed to be constant and uniform at the slot exit. In the immediate vicinity of the slot a region develops in which the centre-line velocity remains constant and equal to u_j, and in this region plane mixing-layers develop. These shear layers are similar to those studied by Kuethe[1]. Eventually these layers join and the jet becomes fully turbulent. Particular cases of this flow have been fairly rigorously dealt with in the literature and further duplication here is unnecessary. One of these cases, that of the pure plane jet, has been shown (Tollmein[2], etc.) for $u_m = 0$ to develop from a fully turbulent region into a strictly self-preserving one where u_{max} is proportional to $x^{-1/2}$ and δ is proportional to x. For $u_m \neq 0$ however, Spalding[35], following Abramovich[3], has suggested that for downstream of the slot, the fully turbulent flow will develop into a self-preserving flow in which $(u_{max}-u_m)$ will be proportional to $x^{-1/2}$ and δ will be

proportional to $x^{+\frac{1}{2}}$. This would imply that the flow in a jet would behave similarly to that in a wake far downstream from the slot.

If we now consider the gross development of jets and wakes in a constant pressure, with steady mean flow, the equations of momentum and continuity are,

$$u \frac{\partial u}{\partial x} + v \frac{\partial u}{\partial y} = \frac{1}{\rho} \left(\frac{\partial \tau}{\partial y} \right) \qquad 4.1.1$$

$$\frac{\partial u}{\partial x} + \frac{\partial v}{\partial y} = 0 \qquad 4.1.2$$

Assuming, as with Prandtl's new hypothesis, that the shear stress relationship is,

$$\tau = \rho \epsilon \left(\frac{\partial u}{\partial y} \right)$$

with $\epsilon = K \delta (u_{max} - u_{min})$, and that, as according to Duncan et al[36], the v component of the turbulence may be related as,

$$u_{max} \cdot \frac{\partial \delta}{\partial x} \sim \sqrt{\overline{v}^2}$$

where $\sqrt{\overline{v}^2}$ is the root mean square of the v component of the turbulence, then

$$\frac{\partial \delta}{\partial x} = \frac{\text{constant} \cdot \delta \left(\frac{\partial u}{\partial y} \right)}{u_{max}}$$

but, $\epsilon = \text{constant} \cdot \delta \cdot (u_{max} - u_{min}) = \delta^2 \left(\frac{\partial u}{\partial y} \right)$

thus,

$$\delta\left(\frac{\partial u}{\partial y}\right) = \text{constant} \cdot (u_{max} - u_{min})$$

or, $$\frac{\partial \delta}{\partial x} = \text{constant} \cdot \left(1 - \frac{u_{min}}{u_{max}}\right) \qquad 4.1.3$$

Thus the case when $u_m \ll u_{max}$,

$$\frac{\partial \delta}{\partial x} = \text{constant} \qquad \text{or} \qquad \delta \sim x$$

Correspondingly, using the momentum conservation equation together with a similarity solution in the form,

$$\frac{u}{u_{max}} = \text{fn}\left(\frac{y}{\delta}\right)$$

we obtain, $u_{max} \sim x^{-1/2}$.

In the case of the wake where u_{min} will represent the velocity at the centre-line, $u_{\mathfrak{C}}$ and u_{max} the freestream velocity, u_m, from 4.1.3,

$$\frac{\partial \delta}{\partial x} = \text{constant} \cdot \left(1 - \frac{u_{\mathfrak{C}}}{u_m}\right)$$

Then, for $(u_{\mathfrak{C}} - u_m) \ll u_m$,

$$\delta \frac{\partial \delta}{\partial x} = \text{constant} \cdot C_D$$

where C_D is the drag coefficient across the wake.
This leads to,

$$(u_{\mathfrak{C}} - u_m) \sim x^{-1/2} \qquad \text{and} \qquad \delta \sim x^{+1/2}$$

Results of Weinstein et al[33] which Spalding[35] tried to correlate are in agreement with the above result

for a near jet. The fact that the measurements were confined to close to the slot ($^{x}/_{s} \leqslant 60$) accounts for the apparent errors in Spalding's predictions.

Bradbury[37] has since suggested that the self-preservation in a flow of this nature will be developed from an apparent origin which is different from the actual origin of the flow at the slot exit, and that the nozzle itself is a source of excess momentum flux. This work follows Townsend[22] and by dimensional analysis suggests that,

$$\frac{u_{max} - u_m}{u_m} = C \left(\frac{x - x_o}{\theta} \right)^{-1/2}$$

and

$$\frac{\delta}{\theta} = G \left(\frac{x \quad x_o}{\theta} \right)$$

where x_0 is the apparent shift in the origin of the flow and θ is the momentum thickness of the jet, defined as,

$$\theta = \frac{1}{\rho_m u_m^2} \int_{-\infty}^{+\infty} \rho u (u - u_m) \, dy$$

This suggests that equation 4.1.4 will be similar to that obtained for a jet issuing into still air. These arguments, in fact, seem to indicate that self-preservation in a jet issuing into a moving stream is not possible throughout the entire flow field as has indeed been suggested by Townsend[22], but two types of self-preservation would appear to be able to exist in limited regions of the

flow. Near to the slot exit where $u_{max} \gg u_m$, a self-preserving flow in which $u_{max} \sim x^{-1/2}$ and $\delta \sim x$ as explained by Bradbury[37] and far downstream where $(u_{max} - u_m) \ll u_m$ when $(u_{max} - u_m) \sim x^{-1/2}$ and $\delta \sim x^{+1/2}$ as suggested by Spalding[35]. The laws for the centre-line velocity decay and for the spread of jets and wakes may be summarized as,

TYPE OF FLOW	CONDITION	CENTRE-LINE DECAY	SPREAD
PLANE JET	$u_m = 0$ or $u_{max} \gg u_m$	$x^{-1/2}$	x
PLANE WAKE	$(u_{max}-u_m) \ll u_m$	$x^{-1/2}$	$x^{+1/2}$

4.2 TURBULENT JET MIXING FOR INCOMPRESSIBLE FLOW AT CONSTANT PRESSURE WITH DENSITY STRATIFICATION

The governing equations for steady two-dimensional flow are,

Momentum:
$$\rho u \frac{\partial u}{\partial x} + \rho v \frac{\partial u}{\partial y} = \frac{\partial}{\partial y}\left[\rho \epsilon \frac{\partial u}{\partial y}\right] \qquad 4.2.1$$

Mass:
$$\frac{\partial}{\partial x}(\rho u) + \frac{\partial}{\partial y}(\rho v) = 0 \qquad 4.2.2$$

Energy:
$$\rho u \frac{\partial h_o}{\partial x} + \rho v \frac{\partial h_o}{\partial y} = \frac{\partial}{\partial y}\left[\frac{\rho \epsilon}{Pr_t} \frac{\partial h_o}{\partial y}\right] + \dot{z}_i \qquad 4.2.3$$

Species Diffusion:
$$\rho u \frac{\partial c}{\partial x} + \rho v \frac{\partial c}{\partial y} = \frac{\partial}{\partial y}\left[\frac{\rho \epsilon}{Sc_t} \frac{\partial c}{\partial y}\right] + \dot{w}_i \qquad 4.2.4$$

where $i = 1,2,\ldots N$

Since, in the present analysis, only flows without chemical reaction are considered, the rate of formation of species i is equal to zero, as is the energy that would be required to be used in those formations, i.e., $\dot{w}_i$ and $\dot{z}_i = 0$.

The analytical solution of these equations is greatly impeded by the present limited knowledge of the fundamentals of turbulent transport (momentum, mass, energy and species diffusion) and theoretical results are always empirical in the sense that the variation of the transport properties along and across the flow must be obtained from experiment. The usual technique in solving these equations is, therefore, by introducing some sort of transformation (in which the transport coefficients $\left(\rho\epsilon\right)$, $\left(\rho\epsilon/Pr_t\right)$ and $\left(\rho\epsilon/Sc_t\right)$ are normally included) to render them into a set of linear differential equations of known form. The scaling of the flow properties (i.e. the total enthalpy h_o, or the concentration, C) from the transform plane to the real plane will be entirely dependent upon the variation of these transport coefficients. Most of the analytical treatments of this problem have assumed that the turbulent Schmidt and Prandtl numbers are constant along and across the layer, and hence they have consentrated on the variation of the kinematic eddy viscosity, .

The most common assumption is to consider that Pr_t and $Sc_t = 1.0$. The governing equations, 4.2.1, 4.2.2, 4.2.3 and 4.2.4 can then be written according to the Von Mises transformation as,

Momentum:
$$\frac{\partial u}{\partial x} = \frac{\partial}{\partial \psi}\left[\rho^2 \epsilon u \frac{\partial u}{\partial \psi}\right] \qquad 4.2.5$$

Energy:
$$\frac{\partial h_o}{\partial x} = \frac{\partial}{\partial \psi}\left[\rho^2 \epsilon u \frac{\partial h_o}{\partial \psi}\right] \qquad 4.2.6$$

Diffusion:
$$\frac{\partial c}{\partial x} = \frac{\partial}{\partial \psi}\left[\rho^2 \epsilon u \frac{\partial c}{\partial \psi}\right] \qquad 4.2.7$$

From 4.2.5 and 4.2.6 a possible solution is

$$h_o = Au + B \qquad 4.2.8$$

and from 4.2.5 and 4.2.7 a possible solution is

$$C = Eu + F \qquad 4.2.9$$

where A,B,E and F are constants.
The assumption usually made at this point is that Cp is constant which leads to 4.2.8 being written in terms of temperature, T, as

$$T = A_1 u + B_1 \qquad 4.2.8(a)$$

where A_1 and B_1 are further constants.

Hence from 4.2.9 we obtain,

$$\left[\frac{C - C_m}{C_j - C_m}\right] = \left[\frac{u - u_m}{u_j - u_m}\right] \qquad 4.2.10$$

and from 4.2.8(a) we obtain,

$$\left[\frac{T - T_m}{T_j - T_m}\right] = \left[\frac{u - u_m}{u_j - u_m}\right] \qquad 4.2.11$$

and thus from 4.2.10 and 4.2.11,

$$\left[\frac{u - u_m}{u_j - u_m}\right] = \left[\frac{C - C_m}{C_j - C_m}\right] = \left[\frac{T - T_m}{T_j - T_m}\right] \qquad 4.2.12$$

This expression is known as the Reynolds Analogy for unit Lewis number, applied by many with little caution to engineering problems connected with heat and mass transfer. Its greatest fault is to assume Cp constant in the mass transfer case of foreign gas injection.

Several authors have attempted analytical treatments to the problem in which the Schmidt and Prandtl numbers are not unity. There follows a short account of some of them.

An approximate technique by Libby[38] has yielded solutions for the jet mixing problem with non-constant density and with arbitrary initial conditions. Essentially the method consists of the transformation

and linearization of the equations of motion, mass, energy and species diffusion, so that they resemble the form of the parabolic heat conduction equation. In order to obtain this form, the product $(\rho\epsilon)$ must be assumed to be a function of the axial coordinate only. The solution of the problem in transformed coordinates is then straightforward. However, the transformation back to the physical plane requires the specification of the coefficients of transport of momentum, mass and energy.

The greatest amount of attention has been focused on the formulation of the coefficient of momentum transport or eddy viscosity. A knowledge of the eddy viscosity together with an empirical knowledge of the turbulent Schmidt and Prandtl numbers can then be used to determine the coefficients of mass and energy transport.

In order to correlate the extensive experimental data due to Reichardt on the decay of an incompressible jet, Prandtl postulated the constant exchange hypothesis. This hypothesis was adapted by Crane and Pack[39] in an attempt to obtain an analytical solution for an isothermal plane gas jet exhausting into still air. They used the momentum and species diffusion equations 4.2.1 and 4.2.4, and assumed incompressible flow of the gas and constant eddy viscosity across the jet. The following transformation was used,

$$z = \int_0^y \left(\frac{\rho}{\rho_m}\right) dy \qquad ; \qquad \xi = \int_0^x \left(\frac{\epsilon(x)}{\epsilon_o}\right) dx$$

where ϵ_o is Prandtl's constant exchange coefficient. The usual stream functions were used,

$$\rho u = \frac{\partial \psi}{\partial y} \qquad ; \qquad \rho v = -\frac{\partial \psi}{\partial x}$$

For a first approximation ($\rho_j/\rho_m = 1.0$) the momentum equation was reduced to that obtained by Bickley[40] for a laminar jet. Crane and Pack considered Bickley's stream function as a starting point for the solution. The second approximation was obtained by expanding Bickley's stream function in a Rayleigh-Janzen series in powers of a parameter related to the concentration. Their results for velocity have indicated that if the injected gas is heavier than the surrounding atmosphere, the velocity on the axis, u_{max}, will be less than it would be if both fluids had the same density. This result is in disagreement with the physics of the problem and also with the experimental results shown here and by El-Ehwany[20] and Keagy and Weller[19], all of whom found that the increased density causes the velocity to fall less rapidly than for the constant density case.

Crane's approximate expression for the momentum flux was found to be insensitive to changes of density far

downstream from the slot as would be expected from small density ratio experiments such as those of Corrsin and Uberoi[18].

An attempt has been made by Schetz[8] to solve the two-dimensional problem following the method of Libby. The method produced a solution similar to that of Pai[41] for the velocity results, but in order to obtain stagnation enthalpy and concentration results he had to resort to the Reynolds Analogy. To transform back to the physical plane, Shetz reduces the usual complex relations to simple power laws of the form,

$$(y/s) = m^{0.75} F(\tilde{\varphi})$$

$$(x/s) = \text{constant}.m^{1.44} G(\tilde{\varphi})$$

although no experimental measurements are given to substantiate these formulae.

In general, the kinematic eddy viscosity, ϵ, is a function of x and y, but the above analyses have used or suggested at least three formulae for ϵ which may be summarized by

$$\epsilon = \left[\frac{\rho_{max}}{\rho}\right]^n \bar{\epsilon}$$

where $\bar{\epsilon}$, a function of x and y, is the kinematic eddy viscosity for incompressible flow, and $n = 0$, 1 or 2. $n = 0$ means that ϵ is constant across the mixing layer as used by Crane and Pack. $n = 1$ corresponds to

a constant dynamic viscosity coefficient ($\rho\epsilon$) and was suggested by Libby. $n = 2$ permits the transformation from the compressible boundary-layer to an incompressible form and was suggested by Libby and Ting[42], and used by Shetz.

Hill and Nicholson[43] have shown, by comparing measured profiles in a supersonic mixing-layer with the theoretical profiles calculated with $n = 0$, 1 and 2, that $n = 2$ was not in agreement with the experimental results although $n = 0$ and 1 seem to agree fairly well.

Zakkay et al[10] have shown from an experimental investigation of the turbulent mixing of two dissimilar gases in a coaxial configuration that a similarity approach may be used to determine values of the eddy viscosity, turbulent diffusion coefficient and Lewis Number. However, this work although worth mentioning is based on a Reynolds Analogy assumption.

4.3 EXCESS MOMENTUM PARAMETER APPROACH

It has been suggested by Bradbury[37], El-Ehwany[20] and Maczynski[23], by analogy with Schlichting's[5] solution on the downstream behaviour of a free wake behind a circular cylinder and directly from dimensional analysis, that the far downstream development of a jet will depend on the momentum increment or decrement in the wake and not on the body details. However, in any

experiment the slot geometry and model will affect the flow in the region close to the slot because of the initial boundary-layer thickness at the slot. Both the present experimental results and others show that one can assume, providing that the jet velocity is above 2.5 times the free stream velocity and that the density ratio, ρ_j / ρ_m , is greater than 1.0, that the effects of the model will have become negligibly small downstream of the potential core region. It has been shown, however, by El-Ehwany[20] and Keagy and Weller[19] that when the density ratio, ρ_j/ρ_m , is less than 1.0, (in both cases Helium gas issuing into air) it is the momentum deficit between the momentum in the boundary layer on the model and the momentum in the jet that is the important parameter. This is also the important parameter when $\rho_j/\rho_m > 1.0$ and $u_j/u_m < 2.5$. It is therefore important to calculate the local excess momentum flux, $\int_{-\infty}^{+\infty} \rho u(u-u_m)dy$ rather than assuming this to be equal to $\rho_j u_j(u_j-u_m)s$. It is the connection between these two quantites and the compensation for the drag of the model which must be considered. Thus,

$$\int_{-\infty}^{+\infty} \rho u(u-u_m)\,dy = \text{constant} = \rho_j u_j(u_j-u_m)s - D$$

$$\frac{1}{\rho_m u_m^2}\int_{-\infty}^{+\infty} \rho u(u-u_m)\,d\left(\frac{y}{s}\right) = \frac{\rho_j u_j}{\rho_m u_m}\left(\frac{u_j}{u_m}-1\right) - \frac{D}{\rho_m u_m^2 s}$$

now, let H, the excess momentum parameter be this constant. Then,

$$\frac{H}{s} = \frac{\rho_j u_j}{\rho_m u_m}\left(\frac{u_j}{u_m} - 1\right) - \frac{D}{\rho_m u_m^2 s}$$

and thus $$\frac{H}{s} = \frac{\rho_j u_j}{\rho_m u_m}\left(\frac{u_j}{u_m} - 1\right) - C_{D_s} \qquad 4.3.1$$

where C_{D_s} is the drag coefficient of the model based on slot width and $\frac{\rho_j u_j}{\rho_m u_m}\left(\frac{u_j}{u_m} - 1\right)$ is the initial momentum thickness at the slot usually denoted by $\theta_{j/s}$.
Then by analogy with Schlichting[5] and as shown by Stollery et al[44], one would expect the suggestions of §4.1 to become, for wake flows,

$$\left|\frac{u_{max} - u_m}{u_m}\right| \sim \left(\left|\frac{x}{H}\right|\right)^{-1/2} \qquad 4.3.2$$

$$\left|\frac{\delta_u}{H}\right| \sim \left(\left|\frac{x}{H}\right|\right)^{+1/2} \qquad 4.3.3$$

and for jet flows,

$$\left|\frac{u_{max}}{u_m}\right| \sim \left(\left|\frac{x}{H}\right|\right)^{-1/2} \qquad 4.3.4$$

$$\left|\frac{\delta_u}{H}\right| \sim \left|\frac{x}{H}\right| \qquad 4.3.5$$

By assuming the Reynolds Analogy to be correct (i.e., for a Schmidt and Prandtl number of unity) the concentration and temperature decays and spreads may be

shown to be,

$$\left| C_{max}\left(1 - \frac{u_j}{u_m}\right) \right| \sim \left(\left| \frac{x}{H} \right| \right)^{-1/2} \qquad 4.3.6$$

$$\left| \frac{\delta_C}{H} \right| \sim \left| \frac{x}{H} \right| \qquad 4.3.7$$

and,

$$\left| T_{max}\left(1 - \frac{u_j}{u_m}\right) \right| \sim \left(\left| \frac{x}{H} \right| \right)^{-1/2} \qquad 4.3.8$$

$$\left| \frac{\delta_T}{H} \right| \sim \left| \frac{x}{H} \right| \qquad 4.3.9$$

These results, however, are not expected from all experimental investigation as this would imply either that both the turbulent Schmidt and Prandtl numbers were unity or that the constants of proportionality were equal.

4.4 JET ENTRAINMENT

If one characterises the flow in a jet by two stations in the downstream direction, where velocities u_1 and u_2 affect areas of the flow A_1 and A_2, then by the conservation of momentum,

$$\rho_1 A_1 u_1 = \rho_2 A_2 u_2$$

or

$$\frac{\rho_2 A_2 u_2}{\rho_1 A_1 u_1} = \frac{u_1}{u_2}$$

if station 1 is nearer to the jet source than station 2 then due to velocity decay, $u_1 > u_2$, or $u_1/u_2 > 1$ which means that,

$$\rho_2 A_2 u_2 > \rho_1 A_1 u_1$$

but, if mass were conserved then these would be equal. Thus quantities of air must be entrained into the plume of the jet.

From the analysis of the previous section (§4.3), a result may be deduced for the jet entrainment rate. For a jet issuing into still air, the total mass flow rate, $\dot{m}$, represented by the integral $\int_{-\infty}^{+\infty} \rho u \, dy$ has a finite value. Hence the rate of mass entrained by the jet is,

$$\frac{1}{\rho u_{max}} \cdot \frac{d}{dx}\left(\int_{-\infty}^{+\infty} \rho u \, dy\right) = \left(\frac{1}{\rho u_{max}}\right) \cdot \frac{d\dot{m}}{dx} = \text{constant}$$

when the surrounding air is moving, i.e.: u_m is finite, the integral $\int_{-\infty}^{+\infty} \rho u dy$ is infinite and thus cannot serve as a measure for the amount of fluid which has been significantly influenced by the jet. It would be possible to define the entrainment rate as,

$$\left[\rho u_{max}\right] \cdot \frac{d\dot{m}_e}{dx} = \frac{d}{dx} \int_{-\infty}^{+\infty} \rho (u - u_m) \, dy$$

where $\dot{m}_e$ is a dimensionless mass flow rate given by $\dot{m}/\rho_m u_m$; but this definition would be inappropriate

because for very small relative velocities, the expression tends to zero. However, the zone of influence of the jet increases by turbulent diffusion at a rate which is not equal to zero. Thus, as a first approximation, the general equation which governs the entrainment has been shown by El-Ehwany[20] to be,

$$\left[\frac{1}{\int_{-\infty}^{+\infty} f(\eta)\,d\eta}\right] \frac{d}{dx}\left(\frac{\dot{m}_e}{H}\right) = \left(\frac{u_{max} - u_m}{u_m}\right)\frac{d}{dx}\left(\frac{\delta_u}{H}\right) + \left(\frac{\delta_u}{H}\right)\frac{d}{dx}\left(\frac{u_{max} - u_m}{u_m}\right)$$

where $f(\eta) = \exp.(0.6932(\frac{y}{\delta_u})^2)$ as shown before. Now, when $u_j >> u_m$, in the strong jet case, this equation shows, in conjunction with equations 4.3.4 and 4.3.5, that the entrainment rate will be, to a first approximation, and assuming ρ to be constant,

$$\frac{d\dot{m}_e}{dx} = A'\left(\left|\frac{x}{H}\right|\right)^{-1/2}$$

where A' is a constant. For the wake case, when $u_j < u_m$, using equations 4.3.2 and 4.3.3, it yields,

$$\frac{d\dot{m}_e}{dx} = B'\Big/\left(\left|\frac{x}{H}\right|\right)$$

where B' is a constant.

4.5 EXTRACTION OF TURBULENT SCHMIDT AND PRANDTL NUMBERS FROM EXPERIMENTAL RESULTS

The problem of turbulent mixing of two dissimilar gases has received a considerable amount of attention

during recent years but in nearly all analyses some form of application of the Reynolds Analogy has been used. Despite several warnings (Stollery et al[44], El-Ehwany[20], etc.) this analogy has been applied to several practical problems with little regard to whether or not it is entirely relevant. Indeed, in only a few cases have workers attempted to extract values for turbulent Schmidt and Prandtl numbers from their results to check on its relevance.

In his new (1945) hypothesis, Prandtl proposed that the turbulent exchange coefficients ϵ_u, ϵ_c and ϵ_T, could be defined as,

$$\left.\begin{aligned} \epsilon_u &= k_u\, \delta_u \left[u_{max} - u_{min} \right] \\ \epsilon_c &= k_c\, \delta_c \left[u_{max} - u_{min} \right] \\ \epsilon_T &= k_T\, \delta_T \left[u_{max} - u_{min} \right] \end{aligned}\right\} \qquad 4.5.1$$

where k_u, k_c, k_T are dimensionless proportionality factors; δ_u, δ_c, δ_T are the characteristic widths of the mixing zones for velocity, concentration and temperature; and u_{max} and u_{min} are the maximum and minimum velocities at a given section.

Based on the laminar flow case, the exchanges of momentum, mass and temperature may be compared by evaluating the ratios of the respective exchange coefficients.

The ratio of the momentum exchange coefficient to the mass exchange coefficient is the Schmidt number.

In laminar flow this is written as,

$$Sc = \frac{\nu}{D_{12}} = \frac{\mu}{\rho D_{12}}$$

The corresponding ratio in turbulent is the turbulent Schmidt number, which may be written as,

$$Sc_t = \epsilon_u / \epsilon_c = \frac{k_u \delta_u [u_{max} - u_{min}]}{k_c \delta_c [u_{max} - u_{min}]}$$

If one now considers the constants of proportionality to be equal, (not strictly true but valid for a first approximation) then for a given section,

$$Sc_t \sim \delta_u / \delta_c \qquad 4.5.2$$

Similarly, in the laminar case, the ratio of the momentum exchange coefficient to the temperature exchange coefficient is the Prandtl number, which is,

$$Pr = \frac{\mu C_p}{K}$$

The corresponding ratio in turbulent flow is the turbulent Prandtl number which is written as,

$$Pr_t = \epsilon_u / \epsilon_T = \frac{k_u \delta_u [u_{max} - u_{min}]}{k_T \delta_T [u_{max} - u_{min}]}$$

again, considering the constants of proportionality to be equal, for a given section,

$$Pr_t \sim \delta_u / \delta_T \qquad 4.5.3$$

This analysis results in a very simple relationship for both the turbulent Schmidt and Prandtl numbers which is also simple to implement in practice since the characteristic half-widths of velocity, concentration and temperature are easily measured accurately.

Unlike laminar Schmidt and Prandtl numbers, which are properties of the fluid and independent of the flow pattern so long as the flow is laminar, the turbulent Schmidt and Prandtl numbers must be determined in part by the nature of the turbulent process and hence depend on the dynamics of the flow.

It was this fact which led Forstall and Shapiro[15], following the integral technique of Squire and Trouncer[14], to make their analysis. Both these groups of workers concluded that since slope was a more delicate test of shape, a slope coefficient based on the profile shape at the half-width position might be a more accurate measurement of turbulent Schmidt and Prandtl number. Although Forstall and Shapiro only extended Squire and Trouncer's work to measure turbulent Schmidt number, a similar extension may be made to measure turbulent Prandtl number.

The analysis is based then on a slope coefficient defined at the half-width position as,

$$\sigma = f'\left(\tfrac{1}{2}\right)$$

The values for the turbulent Schmidt numbers are then evaluated by taking the ratio of the slope coefficient for

momentum and mass, i.e.

$$Sc_t = \sigma_u / \sigma_c = \left[\left(\frac{\partial u}{\partial y}\right) \Big/ \left(\frac{\partial C}{\partial y}\right) \right] \quad 4.5.4$$

This may be extended for the turbulent Prandtl number, as a similar slope coefficient may be found for the temperature profiles. Then,

$$Pr_t = \sigma_u / \sigma_T = \left[\left(\frac{\partial u}{\partial y}\right) \Big/ \left(\frac{\partial T}{\partial y}\right) \right] \quad 4.5.5$$

As stated above, although the measurement of slope is a more delicate test, measuring slopes from plotted data is not an easy procedure nor is it as accurate as measuring a length as in the half-widths above. Forstall and Shapiro did, however, find that the slope coefficients for velocity and concentration had no systematic differences and that they appeared to be independent of velocity ratio.

Zakkay et al[10] did not, however, find that across the whole mixing region the turbulent Schmidt and Prandtl numbers remained constant. On the contrary their results showed remarkable variation.

Their technique was based on the conservation equations, solutions to which were obtained by making assumptions concerning the transport coefficients. In their analysis, a reverse approach was made in that the conservation equations were used as defining equations

for the transport properties. The flow quantities and their derivatives were obtained by experiment. After some algebra, the following, somewhat complicated, expressions were derived.

$$Sc_{t_{\ell}} = \lim_{y \to 0} \left[\frac{\left(\frac{\partial u}{\partial x}\right) \cdot \left(\frac{\partial^2 C}{\partial y^2}\right)}{\left(\frac{\partial C}{\partial x}\right) \cdot \left(\frac{\partial^2 u}{\partial y^2}\right)} \right] \qquad 4.5.6$$

and

$$Le_{t_{\ell}} = \lim_{y \to 0} \left[\frac{D_t \left(\frac{\partial^2 T}{\partial y^2} - T \frac{\partial^2 C}{\partial y^2} \right)}{\left(\frac{1}{2} u \frac{\partial T}{\partial x} - D_t T \frac{\partial^2 C}{\partial y^2} \right)} \right] \qquad 4.5.7$$

where D_t is the turbulent diffusion coefficient and is defined by,

$$(\rho D_t)_{\ell} = \lim_{y \to 0} \left[\frac{\rho u \left(\frac{\partial C}{\partial x}\right)}{2 \left(\frac{\partial^2 C}{\partial y^2}\right)} \right] \qquad 4.5.8$$

The turbulent Prandtl number is evaluated from,

$$Pr_{t_{\ell}} = Le_{t_{\ell}} \cdot Sc_{t_{\ell}} \qquad 4.5.9$$

Further analysis in this work makes use, inconsistently, of the Reynolds Analogy and is therefore of little practical use.

Morkorin[12] starts on a different theme and only mentions the possibility of extracting the turbulent Schmidt and Prandtl numbers in passing. His suggestion is that the momentum, mass and temperature eddy coefficients

may be expressed equal to the total momentum, mass or temperature flux divided by the respective mean velocity, mean concentration or mean temperature gradient. Although this is not dimensionally consistent with the eddy viscosity a dimensional constant may be inserted to give,

$$\epsilon_u = \frac{K_1 \int_{-\infty}^{+\infty} \rho u (u - u_m)\, dy}{\left[\partial u / \partial x\right]_{\mathfrak{L}}}$$

$$\epsilon_c = \frac{K_2 \int_{-\infty}^{+\infty} \rho u C\, dy}{\left[\partial C / \partial x\right]_{\mathfrak{L}}}$$

$$\epsilon_T = \frac{K_3 \int_{-\infty}^{+\infty} \rho u (T - T_m)\, dy}{\left[\partial T / \partial x\right]_{\mathfrak{L}}}$$

where K_1, K_2 and K_3 are constants. In the usual way, taking these constants to be equal, the turbulent Schmidt and Prandtl numbers may be found by writing,

$$Sc_t = \epsilon_u / \epsilon_c \qquad 4.5.11$$

$$Pr_t = \epsilon_u / \epsilon_T \qquad 4.5.12$$

The results of all the above expressions applied to the tests described earlier in this text ($\S$ 3) are presented and discussed in the following chapter.

5. CORRELATIONS

5.1 CENTRE-LINE DECAY OF VELOCITY, CONCENTRATION AND TEMPERATURE

5.1.1 VELOCITY DECAY

The data obtained for the decay of centre-line velocity are shown in Figs. 5.1(a), (b), (c) and (d) for all the series of tests. They are plotted using the excess momentum parameter, H/S, as suggested by equations 4.3.2 and 4.3.4. The figures show that despite the density differences, the data fall on two lines depending on whether u_j/u_m is greater or less than unity, with those data which are around $u_j/u_m = 1.0$ tending to lie between the two, which is to be expected since these flows are not strictly self-preserving. (Bradbury[37], Townsend[22], Wyganski[45], etc.) As a comparison, the predictions for a plane jet due to Förthmann and a plane wake due to Schlichting are shown in these figures. The data, although correlating fairly satisfactorily, do not correspond to the lines predicted by the free jet or free wake models of the previous chapter, but indicate that,

1) In a constant density flow the asymptotic theory for the plane wake is relevant for the wake and weak jet flows. For the strong jet flows, the data approaches the asymptotic theory for the plane jet.

2) With an initial density ratio of $\rho_j/\rho_m = 1.52$, obtained either by means of gas injection or by heat, the strong jet flow data again approaches the asymptotic theory for plane jets. For the wake flow, however, the data tends more to a rate of decay of $(u_{max}) \sim (|x/H|)^{-0.40}$.

This is contrary to El-Ehwany[20], who, using his own and Foley's[46] data, found good agreement between the experimental results and the two asymptotic theories. Nevertheless, it is a result which has also been observed in some unpublished results of Burns, which are shown in Fig. 5.2.

A summary of the centre-line velocity decays for the jet and wake flows are shown in Fig. 5.9(a).

It is worth noting at this point, following El-Ehwany, that the values of the excess momentum flux parameter, H/S, are the average values of the dimensionless local excess momentum flux at the downstream stations for each run. Tables 1-6 in Appendix II show examples of these calculations. From these tables the constancy of the momentum flux is again (re: § 3.4.1) shown to be fairly satisfactory (within experimental and numerical integration accuracy) throughout the flow field. It is also interesting to note the effect of the initial boundary-layer thickness at the slot, that is, the effect of the slot drag coefficient, C_{D_s}, as given by equation 4.3.1. For $u_j/u_m \gg 1.0$, C_{D_s} can be seen to have negligible effect and the excess

momentum flux parameter, H/S, becomes equal to the initial momentum thickness, $\theta_{j/s}$. As $u_j/u_m \longrightarrow 1.0$, so the influence of C_{D_s} becomes more pronounced, until for $u_j / u_m < 1.0$, it becomes very significant, i.e.: for u_j/u_m just > 1.0 (weak jet case),

$$\frac{H}{s} = \frac{\rho_j u_j}{\rho_m u_m}\left(\frac{u_j}{u_m} - 1\right) - C_{D_s} < \frac{\rho_j u_j}{\rho_m u_m}\left(\frac{u_j}{u_m} - 1\right)$$

and for $u_j/u_m < 1.0$ (wake case),

$$\left|\frac{H}{s}\right| = -\left(\frac{\rho_j u_j}{\rho_m u_m}\left(\frac{u_j}{u_m} - 1\right) - C_{D_s}\right) > \left|\frac{\rho_j u_j}{\rho_m u_m}\left(\frac{u_j}{u_m} - 1\right)\right|$$

Here the momentum deficit due to the boundary-layer thickness is very significant $\left(C_{D_s} \simeq 40\% \text{ of } \left[\frac{\rho_j u_j}{\rho_m u_m}\left(\frac{u_j}{u_m} - 1\right)\right] \right)$ and cannot be ignored, thus demonstrating the importance of using the excess momentum parameter rather than just the excess momentum flux.

5.1.2 CONCENTRATION DECAY

The centre-line concentration data are plotted using the parameters of equation 4.3.6 in Figs. 5.3(a) and (b). The data show that the experimental result for both jet and wake flow is $(C_{max}) \sim (\left|\frac{x}{H}\right|)^{-0.55}$; indicating a slightly faster rate of decay of mass or concentration than momentum. This is especially so in the wake case. However, comparing with El-Ehwany's and Burns' results, (the latter shown in Fig. 5.4) which are

for other gases, shows another variation dependent upon the gas used and thus on initial density ratio.

5.1.3 TEMPERATURE DECAY

The centre-line temperature data are plotted using the parameters of equation 4.3.8 in Figs. 5.5(a) and (b). The data demonstrates for the experimental results a rate of decay of temperature of

$(T_{max}) \sim (\left|\frac{x}{H}\right|)^{-0.60}$ for strong jet flows and

$(T_{max}) \sim (\left|\frac{x}{H}\right|)^{-0.25}$ for wake flows.

A comparison of the centre-line concentration and temperature decays for the jet and wake flows are shown in Fig. 5.9(b).

5.2 THE SPREAD OF VELOCITY, CONCENTRATION AND TEMPERATURE

From the analysis in §4, the general form of the jet (or wake) spread parameter can be written as,

$$\left|\frac{\delta}{H}\right| = K(\left|\frac{x}{H}\right|)^{n}$$

Spreads of velocity, concentration and temperature are shown in Figs. 5.6(a), (b), (c) and (d), 5.7(a) and (b) and 5.8(a) and (b) respectively. The asymptotic forms of the spreads of velocity for the plane jet and plane wake according to Förthmann and Schlichting are shown for comparison in Figs. 5.6(a), (b), (c) and (d). A comparison of the spreads of velocity, concentration

and temperature are shown in Fig. 5.9(c).

The results of the centre-line decays and half-width spreads are perhaps best summarized by the following table,

		JETS ($u_j \gg u_m$)	WAKES ($u_j < u_m$)
DECAYS	$\rho_j/\rho_m = 1.00$ VELOCITY	$5.12(\lvert\frac{x}{H}\rvert)^{-0.50}$	$5.87(\lvert\frac{x}{H}\rvert)^{-0.50}$
	$\rho_j/\rho_m = 1.52$ VELOCITY	$4.76(\lvert\frac{x}{H}\rvert)^{-0.50}$	$3.78(\lvert\frac{x}{H}\rvert)^{-0.40}$
	CONCENTRATION	$3.86(\lvert\frac{x}{H}\rvert)^{-0.55}$	$3.86(\lvert\frac{x}{H}\rvert)^{-0.55}$
	TEMPERATURE	$4.10(\lvert\frac{x}{H}\rvert)^{-0.60}$	$1.56(\lvert\frac{x}{H}\rvert)^{-0.25}$
SPREADS	$\rho_j/\rho_m = 1.00$ VELOCITY	$1.11(\lvert\frac{x}{H}\rvert)^{1.00}$	$1.46(\lvert\frac{x}{H}\rvert)^{0.50}$
	$\rho_j/\rho_m = 1.52$ VELOCITY	$1.11(\lvert\frac{x}{H}\rvert)^{1.00}$	$1.46(\lvert\frac{x}{H}\rvert)^{0.50}$
	CONCENTRATION	$1.09(\lvert\frac{x}{H}\rvert)^{1.10}$	$1.09(\lvert\frac{x}{H}\rvert)^{1.10}$
	TEMPERATURE	$1.17(\lvert\frac{x}{H}\rvert)^{1.10}$	$1.44(\lvert\frac{x}{H}\rvert)^{0.85}$

In summary it can be seen that for jet flows in particular, temperature spreads and decays faster than concentration which in turn spreads and decays faster

than velocity. Thus in jets, heat will diffuse faster than mass, which will diffuse faster than momentum. In wakes, however, this has not been found to be the case. In this flow, mass appears to diffuse faster than heat, which diffuses faster than momentum. Hence it can be seen that the turbulent Schmidt and Prandtl numbers for similar experiments in the same facility will not be unity and the analogy between heat and mass transfer does not strictly apply.

5.3 CENTRE-LINE MEASUREMENTS OF TURBULENT SCHMIDT AND PRANDTL NUMBERS

From the final remarks of the previous two sections, it would seem that the Reynolds Analogy for a particular experimental facility is not wholly justified. It has been shown by Eckert[47] that if the turbulent Schmidt number is constant throughout the flow but less than one, the mass will spread more and decay less than the momentum. Similarly, it has been shown by Spalding[35], that if the turbulent Prandtl number is less than one and constant, the temperature will spread quicker and decay quicker than the momentum.

Although it has been recognized for some time that the Reynolds Analogy inadequately describes the connection between the transport of momentum and mass or thermal energy in a turbulent flow, very few workers have ventured to consider it and even fewer to measure the turbulent Schmidt and Prandtl numbers from their results.

In Figs. 5.10(a), (b), (c) and (d) the results of the various predictions for turbulent Schmidt number from ∫4 are shown applied to the results of the experiments from ∫3; and in Figs. 5.11(a), (b), (c) and (d) the results for turbulent Prandtl number are shown.

The first observation from these figures is that the more complicated the theory, the more erratic the results seem to become. This is undoubtedly because for the Zakkay and Morkovin theories gradients in both the streamwise and transverse directions have to be measured and these are significantly more difficult to make accurately from experimental profiles than straightforward measurements. In the Zakkay theory in particular, second order gradients are required which accentuate any small error made in measuring the initial gradient.

From these figures it can be seen that after the initial region of the potential core, where the external boundary-layer at the slot influences the flow, both numbers appear to settle down to a reasonably constant value which seems to depend on velocity ratio. However, as shown in Figs. 5.12 and 5.13, where both numbers are shown plotted against velocity ratio, u_j/u_m, this effect is not as pronounced as may at first seem the case. The predictions of Zakkay et al and Morkovin are removed from these latter figures to give a clearer view of the trends.

From Figs. 5.12 and 5.13 the evaluation of the turbulent Schmidt and Prandtl numbers for strong jets ($u_j/u_m \geqslant 2.5$) appear to be fairly constant as the

flow moves downstream. It is the wake and weak jet cases which tend to vary, more for the Schmidt number than the Prandtl number. On the whole though, both numbers seem to be slightly less for the wake case than for the jet case.

Results of turbulent Schmidt and Prandtl numbers obtained for the experiments of [3] were,

Jet flows:

$Sc_t = 1.25$ $\qquad$ $Pr_t = 0.80$

Wake flows:

$Sc_t = 1.10$ $\qquad$ $Pr_t = 0.65$

5.4 JET ENTRAINMENT

Calculations of mass flow across sections of the jet have been found to increase more rapidly than the increase provided by the natural inflow into the growing jet from the external stream. Hence, as shown in [4] 4.4 the jet must induce an entrainment towards itself. To calculate mass flows for this entrainment it has been found necessary, as with some boundary layer calculations, to integrate only to the 90% profile point owing to the difficulty with experimental results of determining the tail of the profile. Entrainment mass flows are expressed as percentages of the initial mass flow of the jet at the slot. The amount of mass entrained downstream of the slot is shown in Fig. 5.14, for a velocity ratio of $u_j/u_m = 2.83$. The variation of the mass flow entrained with velocity ratio is shown in Fig. 5.15.

6. CONCLUSIONS AND SUGGESTIONS FOR FUTURE WORK

6.1 CONCLUSIONS

1) This investigation has shown that for similar two-dimensional tests in the same experimental facility, the analogy between heat and mass transfer, sometimes loosely termed the Reynolds Analogy, does not strictly apply.

2)a) The Gaussian distribution function represents the profiles of velocity and concentration downstream of the potential core region ($^{x}/s \geqslant 10$).

b) The Cosine distribution function represents the profile of temperature downstream of the potential core region ($^{x}/s \geqslant 10$).

3) The excess momentum flux parameter, $^{H}/S$, satisfactorily correlates the data of centre-line decay and half-width spread for velocity, concentration and temperature.

4) Predictions of the values of turbulent Schmidt and Prandtl number may be made using the simple theory or the method of Forstall and Shapiro.

5) Turbulent Schmidt and Prandtl numbers are, as found in this investigation slightly less in wake flows than in jet flows.

6.2 SUGGESTIONS FOR FUTURE WORK

1) Extensive measurements of the turbulent structure and the density fluctuations in the mixing region

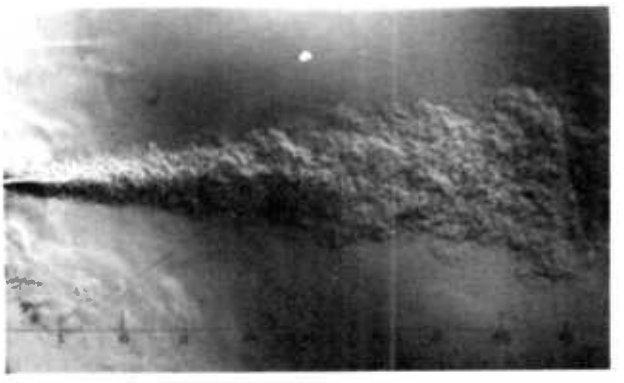
of plane jets and wakes, issuing into a moving stream of a different density are essential to obtain information concerning the eddy diffusivity and mixing mechanisms between two turbulent gas streams.

2) A more accurate theory involving the consideration of the movement of transport across the flow field by the replacement of the molecular properties by combinations of molecular and small scale entity properties.

Appendix I



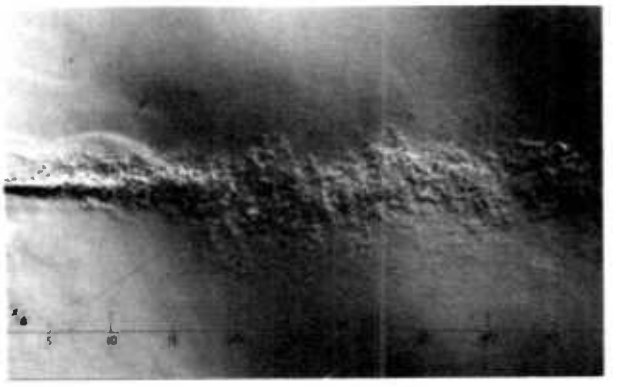
$\frac{u_j}{u_\infty} = 2.50$



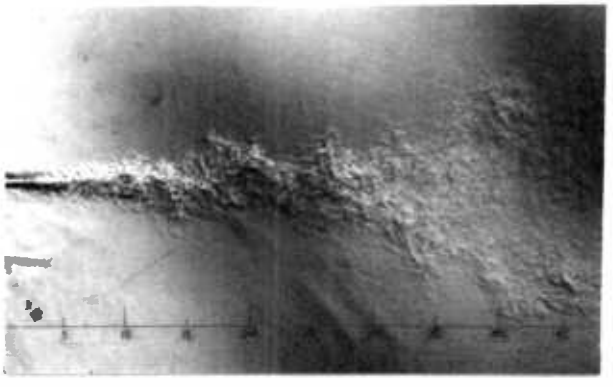
$\frac{u_j}{u_\infty} = 1.50$



$\frac{u_j}{u_\infty} = 1.00$



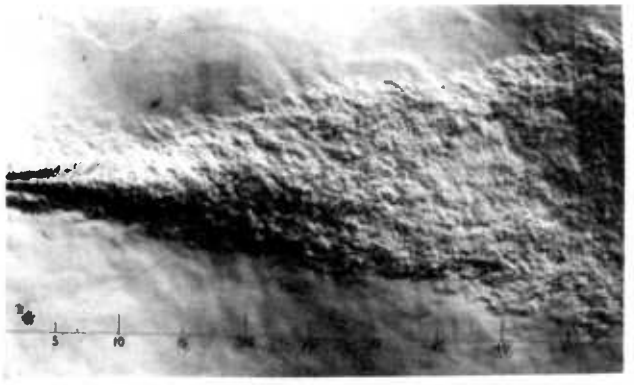
$\frac{u_j}{u_\infty} = 0.50$



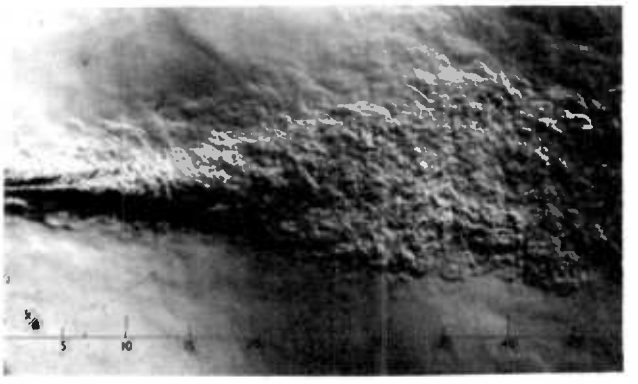
$\frac{u_j}{u_\infty} = 0.20$

Two-dimensional mixing of a Carbon Dioxide jet and a moving airstream

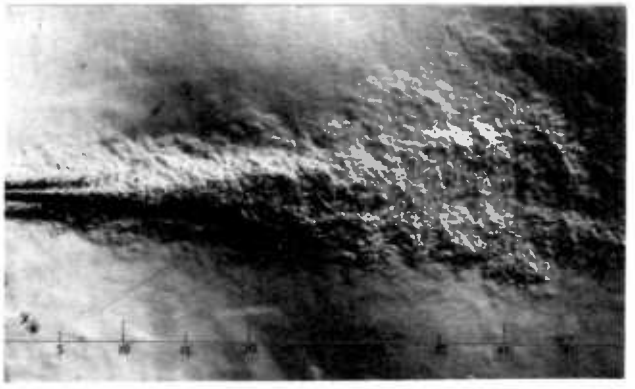
Appendix I



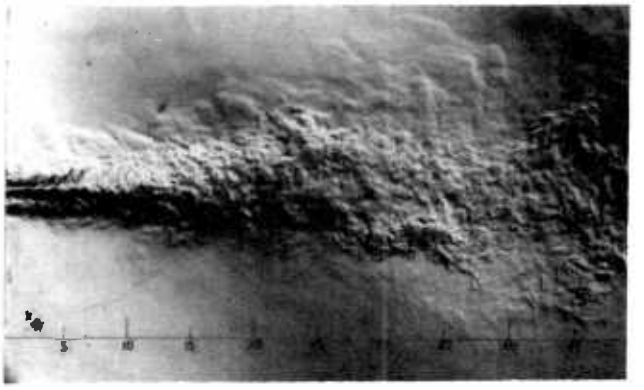
$\frac{u_j}{u_m} = 2.50$



$\frac{u_j}{u_m} = 1.50$



$\frac{u_j}{u_m} = 1.00$



$\frac{u_j}{u_m} = 0.50$



$\frac{u_j}{u_m} = 0.20$

Two-dimensional mixing of a cold air jet (15°c) and a hot moving airstream (165°c)

APPENDIX II

TABLE 1

$u_j/u_m = 5.38$	$\frac{x}{s}$	$\frac{\delta_u}{s}$	$\frac{u_{max}-u_m}{u_j-u_m}$	$\left\|\frac{H}{S}\right\|$
Series I				
$\theta_{j/s} = 24.60$	5	0.53	0.931	24.73
	10	0.81	0.682	24.44
	15	1.08	0.507	24.15
	20	1.51	0.419	23.98
	30	2.03	0.321	24.78
	50	3.00	0.240	24.82
	Average $\left\|H/S\right\|$			24.48
Series II				
$\theta_{j/s} = 37.40$	5	0.54	0.971	36.91
	10	1.04	0.775	37.42
	15	1.57	0.592	37.03
	20	2.10	0.493	37.12
	30	3.03	0.370	36.85
	50	4.65	0.250	37.57
	Average $\left\|H/S\right\|$			37.15
Series III				
$\theta_{j/s} = 37.40$	5	0.56	0.845	37.49
	10	0.98	0.670	36.98
	15	1.63	0.520	37.62
	20	2.43	0.441	37.15
	30	3.72	0.350	37.10
	50	4.63	0.238	36.82
	Average $\left\|H/S\right\|$			37.19
Series IV				
$\theta_{j/s} = 24.60$	5	0.56	0.901	23.97
	10	1.04	0.680	24.83
	15	1.51	0.485	24.70
	20	1.95	0.383	24.13
	30	2.71	0.280	24.62
	50	3.98	0.200	24.50
	Average $\left\|H/S\right\|$			24.45

TABLE 2

$u_j/u_m = 2.83$	$\frac{x}{s}$	$\frac{\delta_u}{s}$	$\frac{u_{max}-u_m}{u_j-u_m}$	$\left\|\frac{H}{S}\right\|$
Series I				
$\theta_{j/s} = 5.17$	5	0.57	0.980	5.02
	10	0.62	0.929	5.32
	15	0.82	0.759	4.98
	20	1.06	0.654	5.14
	30	1.44	0.518	5.19
	50	2.20	0.387	5.27
	Average $\left\|H/S\right\|$			5.15
Series II				
$\theta_{j/s} = 7.85$	5	0.56	0.940	7.70
	10	1.02	0.751	7.73
	15	1.52	0.649	7.90
	20	1.96	0.560	7.52
	30	3.06	0.461	7.97
	50	4.37	0.358	7.42
	Average $\left\|H/S\right\|$			7.71
Series III				
$\theta_{j/s} = 7.85$	5	0.56	0.840	7.81
	10	1.01	0.648	7.81
	15	1.61	0.518	7.93
	20	2.10	0.440	7.78
	30	3.01	0.349	7.65
	50	4.72	0.231	7.87
	Average $\left\|H/S\right\|$			7.80
Series IV				
$\theta_{j/s} = 5.17$	5	0.57	0.990	5.21
	10	0.97	0.929	5.18
	15	1.36	0.808	5.14
	20	1.71	0.690	5.23
	30	2.28	0.560	5.04
	50	3.23	0.440	5.17
	Average $\left\|H/S\right\|$			5.16

TABLE 3

$u_j/u_m = 1.53$	$\frac{x}{s}$	$\frac{\delta_u}{s}$	$\frac{u_{max}-u_m}{u_j-u_m}$	$\left\lvert\frac{H}{S}\right\rvert$
Series I				
	5	0.54	0.986	0.57
	10	0.59	0.937	0.48
	15	0.75	0.850	0.51
$\theta_{j/s} = 0.81$	20	0.92	0.767	0.58
	30	1.22	0.645	0.49
	50	1.68	0.540	0.50
			Average $\lvert H/S \rvert$	0.52
Series II				
	5	0.56	0.937	0.90
	10	1.02	0.809	0.93
	15	1.96	0.720	1.01
$\theta_{j/s} = 1.23$	20	2.32	0.666	0.89
	30	2.41	0.612	0.92
	50	3.26	0.527	0.97
			Average $\lvert H/S \rvert$	0.93
Series III				
	5	0.55	0.921	0.93
	10	0.90	0.800	0.92
	15	1.44	0.686	0.87
$\theta_{j/s} = 1.23$	20	1.82	0.642	1.04
	30	2.42	0.540	1.10
	50	3.26	0.451	0.98
			Average $\lvert H/S \rvert$	0.97
Series IV				
	5	0.51	0.968	0.60
	10	0.88	0.882	0.57
	15	1.12	0.800	0.52
$\theta_{j/s} = 0.81$	20	1.32	0.733	0.51
	30	1.66	0.643	0.59
	50	2.16	0.530	0.57
			Average $\lvert H/S \rvert$	0.56

TABLE 4

$u_j/u_m = 1.00$	$\frac{x}{s}$	$\frac{\delta_u}{s}$	$\frac{u_{max}-u_m}{u_j-u_m}$	$\left\|\frac{H}{S}\right\|$
Series I				
$\theta_{j/s} = 0$	5	0.52	0.992	0.32
	10	0.57	0.984	0.34
	15	0.67	0.970	0.37
	20	0.81	0.950	0.30
	30	1.00	0.908	0.34
	50	1.23	0.861	0.37
			Average $\left\|H/S\right\|$	0.34
Series II				
$\theta_{j/s} = 0$	5	0.54	0.950	0.41
	10	0.86	0.850	0.38
	15	1.21	0.822	0.43
	20	1.50	0.809	0.44
	30	1.86	0.789	0.41
	50	2.01	0.760	0.42
			Average $\left\|H/S\right\|$	0.41
Series III				
$\theta_{j/s} = 0$	5	0.54	0.931	0.40
	10	0.92	0.821	0.45
	15	1.14	0.795	0.46
	20	1.40	0.775	0.39
	30	1.75	0.745	0.38
	50	2.03	0.700	0.47
			Average $\left\|H/S\right\|$	0.42
Series IV				
$\theta_{j/s} = 0$	5	0.53	0.989	0.31
	10	0.78	0.935	0.30
	15	0.95	0.861	0.36
	20	1.08	0.822	0.30
	30	1.28	0.789	0.32
	50	1.56	0.766	0.31
			Average $\left\|H/S\right\|$	0.31

TABLE 5

$u_j/u_m = 0.50$	$\frac{x}{s}$	$\frac{\delta_u}{s}$	$\frac{u_{max}-u_m}{u_j-u_m}$	$\left\|\frac{H}{S}\right\|$
Series I				
$\theta_{j/s} = -0.25$	5	0.54	0.982	0.68
	10	0.61	0.927	0.66
	15	0.79	0.820	0.69
	20	1.01	0.738	0.62
	30	1.23	0.608	0.67
	50	1.54	0.450	0.67
			Average $\left\|H/S\right\|$	0.66
Series II				
$\theta_{j/s} = -0.38$	5	0.58	0.980	0.83
	10	0.96	0.929	0.82
	15	1.25	0.861	0.79
	20	1.60	0.804	0.85
	30	1.99	0.720	0.83
	50	2.51	0.589	0.82
			Average $\left\|H/S\right\|$	0.82
Series III				
$\theta_{j/s} = -0.38$	5	0.55	0.964	0.81
	10	0.91	0.899	0.86
	15	1.26	0.826	0.82
	20	1.55	0.760	0.85
	30	1.98	0.660	0.82
	50	2.39	0.530	0.84
			Average $\left\|H/S\right\|$	0.83
Series IV				
$\theta_{j/s} = -0.25$	5	0.54	0.997	0.65
	10	0.83	0.956	0.64
	15	1.09	0.849	0.67
	20	1.26	0.758	0.69
	30	1.50	0.635	0.63
	50	1.78	0.480	0.62
			Average $\left\|H/S\right\|$	0.65

TABLE 6

$u_j/u_m = 0.16$	$\frac{x}{s}$	$\frac{\delta_u}{s}$	$\frac{u_{max}-u_m}{u_j-u_m}$	$\left\lvert\frac{H}{S}\right\rvert$
Series I				
$\theta_{j/s} = -0.134$	5	0.54	0.927	0.550
	10	0.70	0.762	0.562
	15	0.91	0.600	0.549
	20	1.10	0.491	0.513
	30	1.42	0.362	0.502
	50	1.86	0.267	0.577
			Average $\lvert H/S \rvert$	0.542
Series II				
$\theta_{j/s} = -0.204$	5	0.55	0.975	0.598
	10	0.97	0.860	0.634
	15	1.30	0.814	0.637
	20	1.73	0.762	0.645
	30	2.21	0.650	0.642
	50	2.71	0.504	0.627
			Average $\lvert H/S \rvert$	0.633
Series III				
$\theta_{j/s} = -0.204$	5	0.55	0.938	0.632
	10	0.94	0.850	0.641
	15	1.29	0.759	0.657
	20	1.63	0.669	0.628
	30	2.12	0.542	0.597
	50	2.69	0.410	0.662
			Average $\lvert H/S \rvert$	0.636
Series IV				
$\theta_{j/s} = -0.134$	5	0.56	0.957	0.548
	10	0.92	0.812	0.563
	15	1.28	0.669	0.552
	20	1.53	0.558	0.526
	30	1.85	0.435	0.561
	50	2.29	0.309	0.504
			Average $\lvert H/S \rvert$	0.542

REFERENCES

1. KUETHE — Investigations of the turbulent mixing regions formed by jets. J. App. Mech. 1935

2. TOLLMIEN — Calculation of the turbulent expansion process. NACA TM 1085(5). 1926

3. ABRAMOVICH — The theory of turbulent jets. MIT Press. 1963

4. SZABLEWSKI — Diffusion of a hot-air jet in air in motion. NACA TM 1288(1). 1950

5. SCHLICHTING — Boundary Layer theory. McGraw Hill N.Y. 1962

6. RAGSDALE, WEINSTEIN, LANZO — Correlation of a turbulent Air-Bromine coaxial-flow experiment. NACA TN D-2121. 1964

7. ALPINIERI — Turbulent mixing of coaxial jets. AIAA Jnl. Vol. 2. 1964

8. SCHETZ — Unified analysis of turbulent jet mixing. NASA CR-1382. 1969

9. CLAUSER — The turbulent boundary layer. Advances in App. Mech. IV. 1956

10. ZAKKAY, KRAUSE, WOO — Turbulent transport properties for axisymmetric heterogeneous mixing. AIAA Jnl. Vol. 2 (1939-). 1964

11. GHIA, TORDA, LAVAN — Turbulent mixing in the initial region of a heterogeneous axisymmetric coaxial jet. NASA CR-1615. 1970

12. MORKOVIN — On eddy diffusivity, Quasi-similarity and diffusion in turbulent boundary layers. AIAA Paper No. 64-432. 1964

13. FORDE — An experimental investigation of the mixing of supersonic turbulent streams of non-similar fluids. McGill University Report 63-3. 1963

14. SQUIRE TROUNCER — Round jets in a general stream. R&M 1974. 1944

15. FORSTALL SHAPIRO — Momentum and mass transfer in coaxial gas jets. J. App. Mech. 17. 1950

16. HINZE — Turbulence. McGraw Hill. N.Y. 1959

17. LANDIS SHAPIRO — The turbulent mixing of coaxial gas jets. Heat Transfer and Fluid Mech. Inst. 1951

18. CORRSIN UBEROI — Further experiments on the flow and heat transfer in a heated turbulent air jet. NACA TN 1865 1949

19. KEAGY WELLER — A study of freely expanding inhomogeneous jets. Proc. Heat Transfer and Fluid Mech. Inst. 1949

20. EL-EHWANY — The turbulent mixing of a two-dimensional jet of foreign gas with a moving airstream. Ph.D. Thesis. London University. 1965

21. BRADBURY RILEY — Spread of a turbulent plane jet issuing into a parallel moving airstream. J. Fluid Mech. 27 II 1966

22. TOWNSEND — The structure of turbulent shear flow. Cambridge University Press 1956

23. MACZYNSKI — A round jet in an ambient co-axial stream. J. Fluid Mech. 13. 1962

24. CORRSIN — Investigations of flow in an axially symmetrical heated jet of air. NACA (wartime report) TIB/ 607(2). 1943

25. LIEPMANN LAUFER — Investigations of free turbulent mixing. NACA TN 1257. 1947

26. D'SOUZA, MONTEALEGRE, WEINSTEIN — Measurements of turbulent correlations in a coaxial flow of dissimilar fluids. NASA CR-960. 1968

27. MONTEALEGRE, D'SOUZA, WEINSTEIN — Evaluation of turbulent correlations in a coaxial flow of dissimilar fluids. NASA CR-961. 1968

28. SEBACHER — Diffusive separation in shock-waves and free jets of Nitrogen-Helium mixtures. AIAA Jnl. Vol. 6 No. 1. 1968

29. BRADBURY, CASTRO — A pulsed-wire technique for velocity measurements in highly turbulent flows. J. Fluid Mech. 49, IV (657-691). 1971

30. McQUAID, WRIGHT — Measurement of turbulent fluctuating velocities in gas mixtures using a pulsed-wire. To be published. 1972

31. PRÉAU, GUIOCHON — Rapid Analysis by Gas Chromatography V: A catharometer with rapid response. J. Gas Chromatog. IV (343-346). 1966

32. JEANS — An introduction to the kinematics of Gases. Cambridge University Press 1948

33. WEINSTEIN, OSTERLE, FORSTALL, PITTSBURGH — Momentum diffusion from a slot jet into a moving secondary airstream. ASME (55-A-60). 1960

34. ESKINAZY — Mixing of wakes in a turbulent shear flow. NASA D-83. 1959

35. SPALDING — Convective Mass Transfer Arnold. London. 1963

36. DUNCAN, THOM, YOUNG — A treatise on the mechanics of fluids. Arnold. London. 1960

37. BRADBURY — An investigation into the structure of a turbulent plane jet. Ph.D. Thesis. London University. 1963

38. LIBBY — Theoretical analysis of turbulent mixing of reactive gases with application to supersonic combustion of Hydrogen. ARS. Jnl. 32. 1962

39. CRANE PACK — The mixing of a jet of gas with an atmosphere of a different gas at a large distance from the orifice. Quart. Jnl. of Mech. and App. Maths. 14. 1961

40. BICKLEY — Phil. Mag. (7) 23/727. 1937

41. PAI — Fluid Dynamics of Jets. D van Nostrand Co. Inc.. (London). 1956

42. LIBBY TING — Remarks on eddy viscosity in compressible mixing flows. J.A.S. Vol. 27 (10). 1960

43. HILL NICHOLSON — Compressibility effects on fluid entrainment by turbulent mixing layers. NASA CR-131. 1964

44. STOLLERY EL-EHWANY BURNS — An experimental study of the mixing of dissimilar gases with application to film cooling. Fluid Dynamic Trans. Vol. 4 (647-663). 1968

45. WYGANSKI — The effect of jet entrainment on loss of thrust for a two-dimensional symmetrical jet flap aerofoil. McGill University Report 64-13. 1964

46. FOLEY — An experimental study of jet flap thrust recovery. Ph.D. Thesis. Standford University. 1962

47. ECKERT — Heat and Mass Transfer. McGraw Hill. N.Y. 1954

LIST OF FIGURES

FIGURE	
2.1	schematic of wind-tunnel.
2.2	cut-away view of wind-tunnel.
2.3(a)	details of jet interior.
2.3(b)	details of slot reduction and throat.
2.4	plate of traverse gear.
2.5	distribution of turbulent intensities across jet.
2.6	distribution of turbulent intensities along jet centre-line.
2.7(a) 2.7(b)	internal and external boundary layer growth at slot exit.
2.8	details of Katharometer.
2.9	Katharometer calibrations.
3.1	jet exit profile.
3.2(a)	experimental velocity profiles: Series I
3.2(b)	experimental velocity profiles: Series II
3.2(c)	experimental velocity profiles: Series III
3.2(d)	experimental velocity profiles: Series IV
3.3(a)	experimental concentration profiles: Series II
3.3(b)	experimental concentration profiles: Series IV
3.4(a)	experimental temperature profiles: Series III
3.4(b)	experimental temperature profiles: Series IV
3.5(a)	momentum balance: Series I
3.5(b)	momentum balance: Series II

3.5(c)	momentum balance: Series III
3.5(d)	momentum balance: Series IV
3.6(a)	mass balance: Series II
3.6(b)	mass balance: Series IV
3.7(a)	heat balance: Series III
3.7(b)	heat balance: Series IV
5.1(a)	centre-line velocity decay: Series I
5.1(b)	centre-line velocity decay: Series II
5.1(c)	centre-line velocity decay: Series III
5.1(d)	centre-line velocity decay: Series IV
5.2	centre-line velocity decay: Burns results.
5.3(a)	centre-line concentration decay: Series II
5.3(b)	centre-line concentration decay: Series IV
5.4	centre-line concentration decay: Burns results
5.5(a)	centre-line temperature decay: Series III
5.5(b)	centre-line temperature decay: Series IV
5.6(a)	velocity spread: Series I
5.6(b)	velocity spread: Series II
5.6(c)	velocity spread: Series III
5.6(d)	velocity spread: Series IV
5.7(a)	concentration spread: Series II
5.7(b)	concentration spread: Series IV
5.8(a)	temperature spread: Series III
5.8(b)	temperature spread: Series IV
5.9(a)	comparison of centre-line velocity decays
5.9(b)	comparison of centre-line concentration and temperature decays

5.9(c)	comparison of spread of velocity, concentration and temperature
5.10(a)	Sc_t along axis: simple theory
5.10(b)	Sc_t along axis: Forstall & Shapiro
5.10(c)	Sc_t along axis: Zakkay et al
5.10(d)	Sc_t along axis: Morkovin
5.11(a)	Pr_t along axis: simple theory
5.11(b)	Pr_t along axis: Forstall and Shapiro
5.11(c)	Pr_t along axis: Zakkay et al
5.11(d)	Pr_t along axis: Morkovin
5.12	Sc_t against velocity ratio
5.13	Pr_t against velocity ratio
5.14	Percentage of mass flow entrained to jet mass flow downstream of slot for $u_j / u_m = 2.83$
5.15	Percentage of mass flow entrained to jet mass flow against velocity ratio.

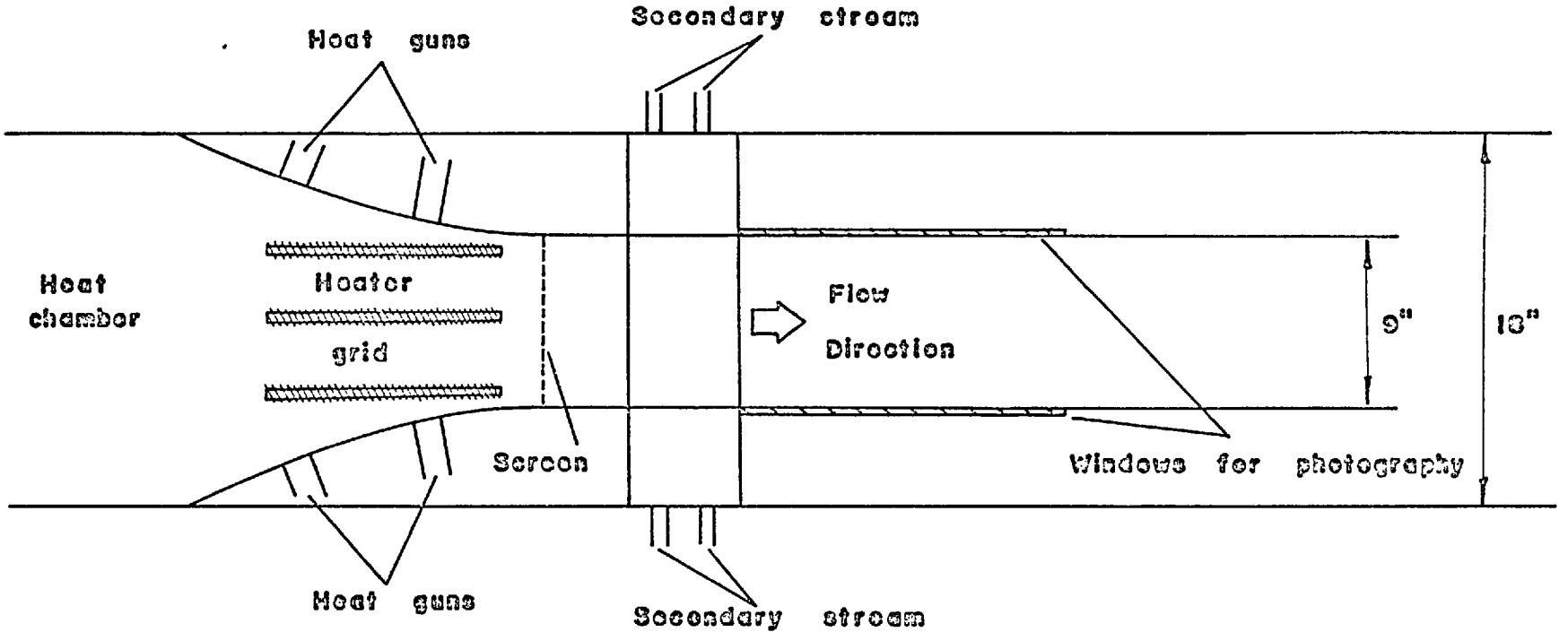


Fig. 2.1 Schematic of wind tunnel

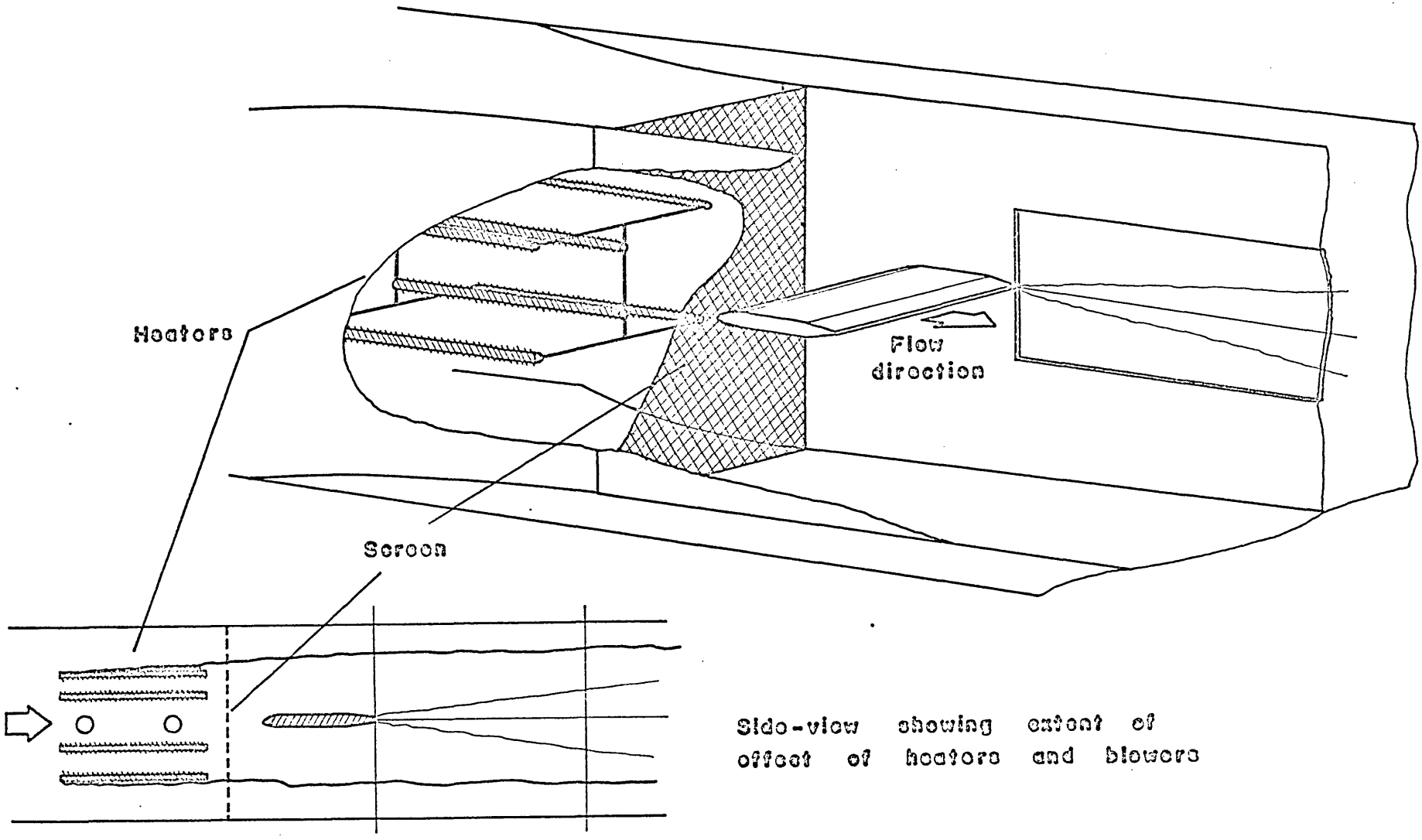


Fig. 2.2 Cut-away of tunnel working section

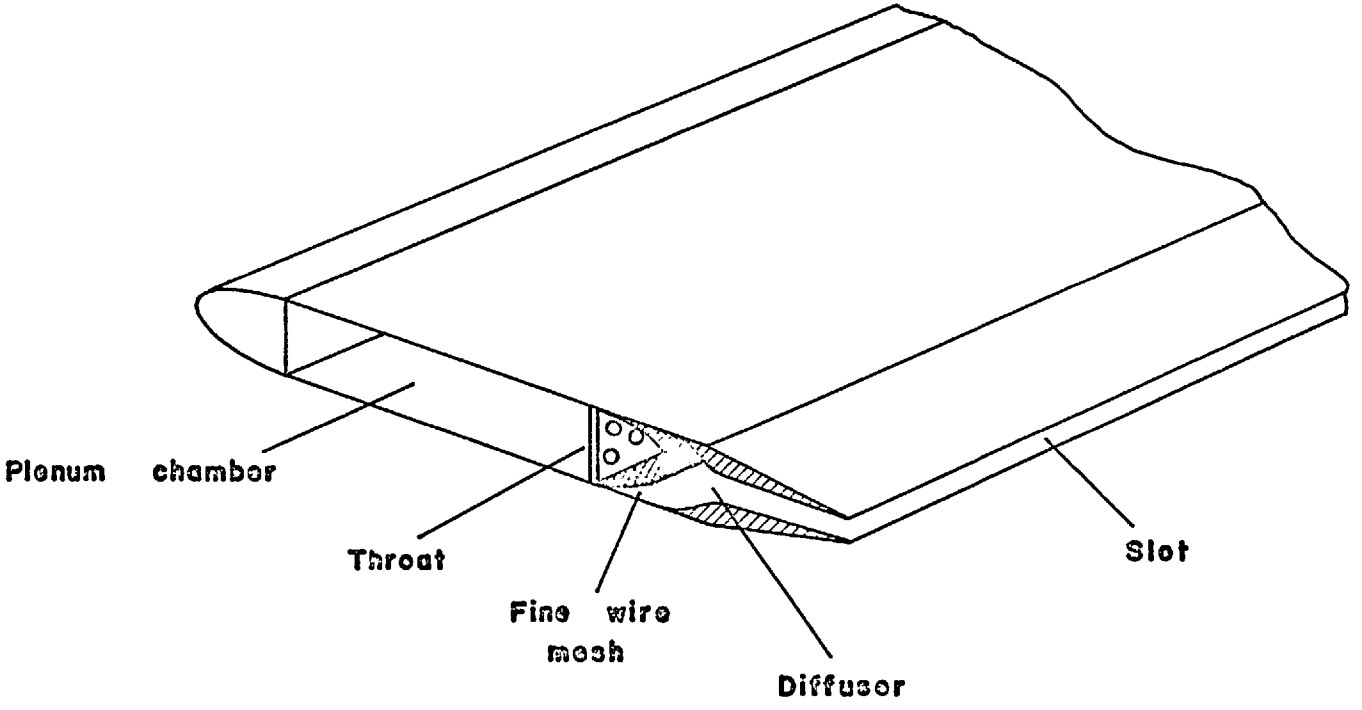


Fig. 2.3(a) Details of jet interior

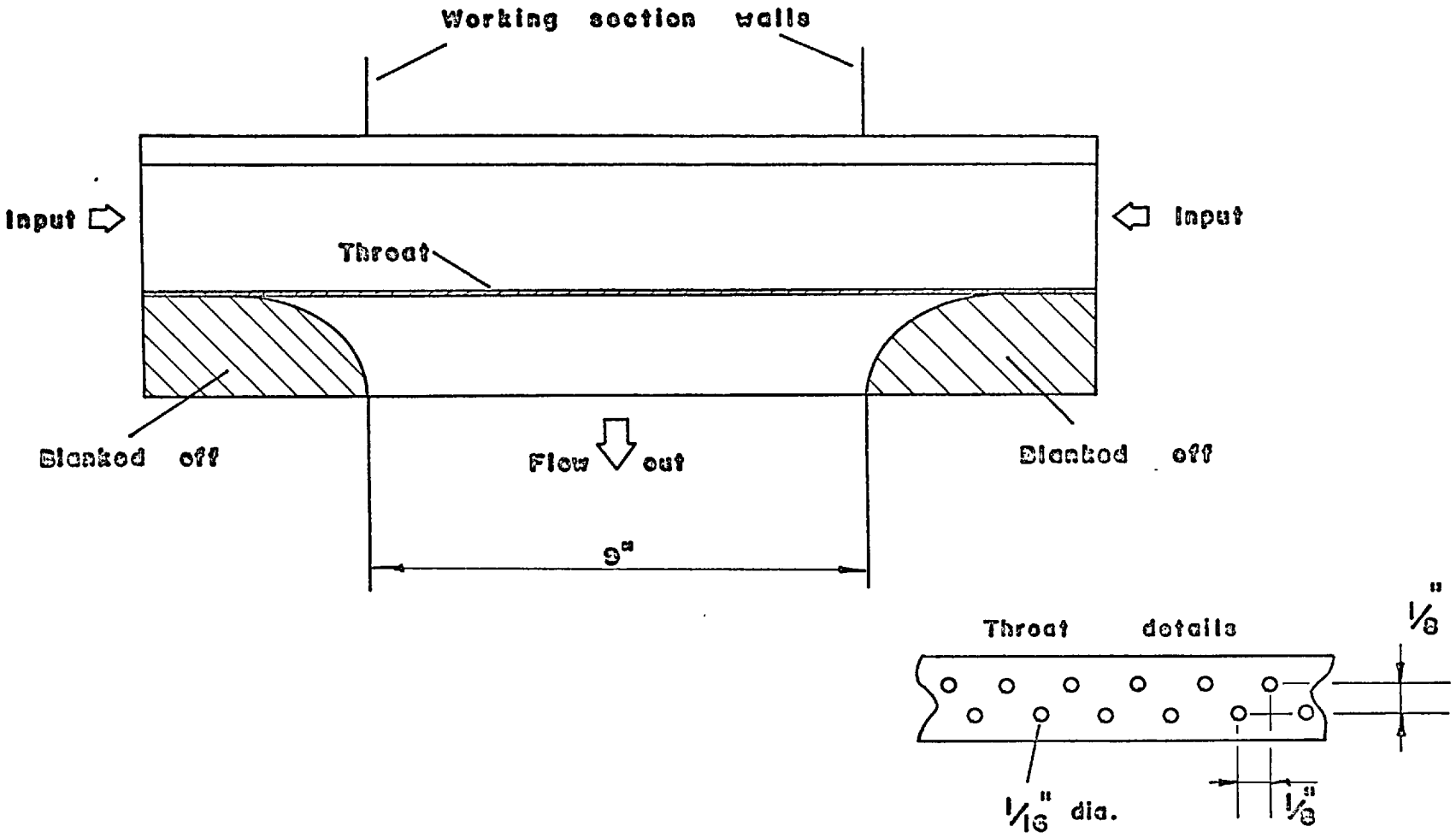


Fig. 2.3(b) Details of slot reduction and throat

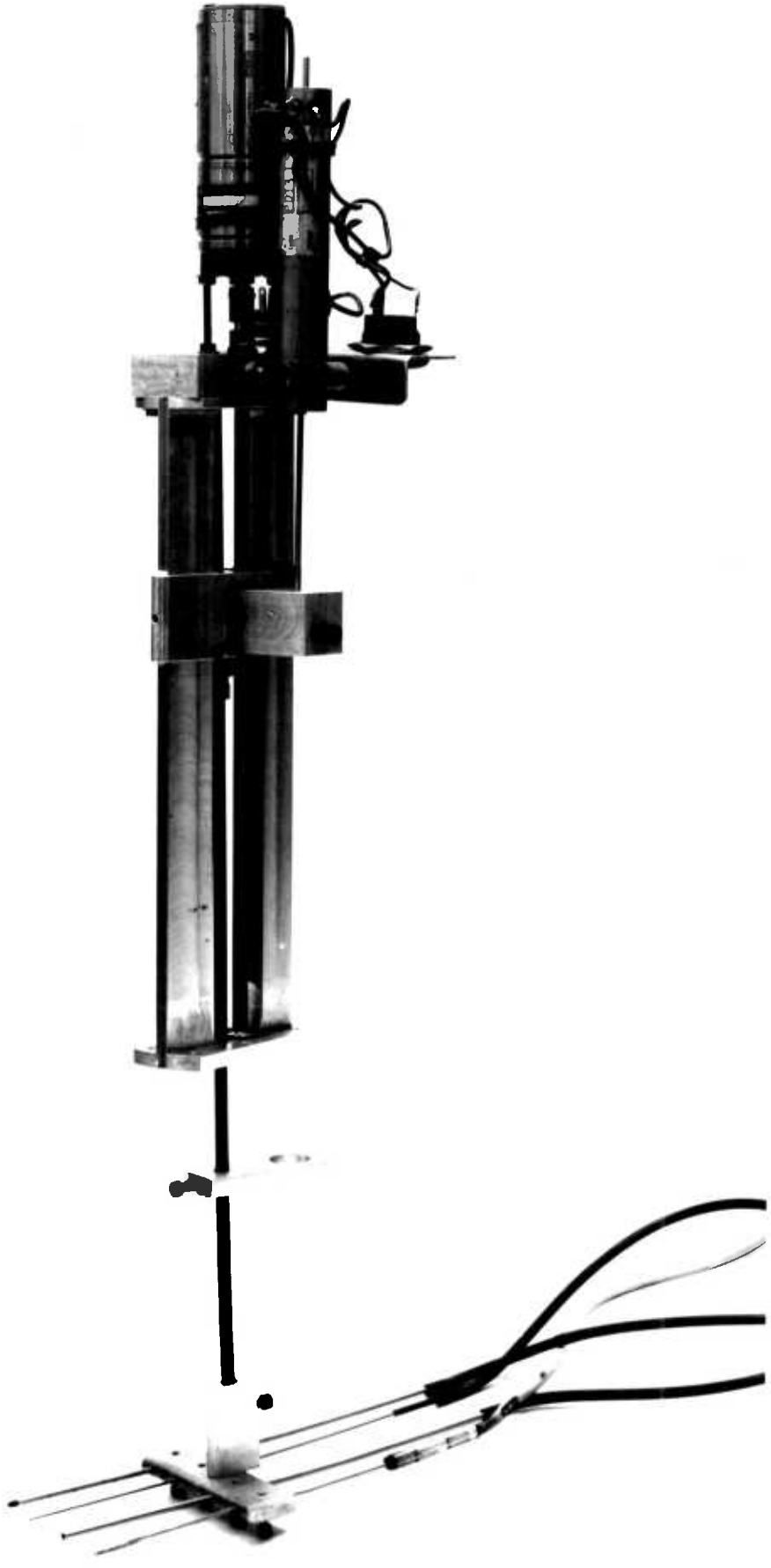


Fig . 2.4 Traverse gear

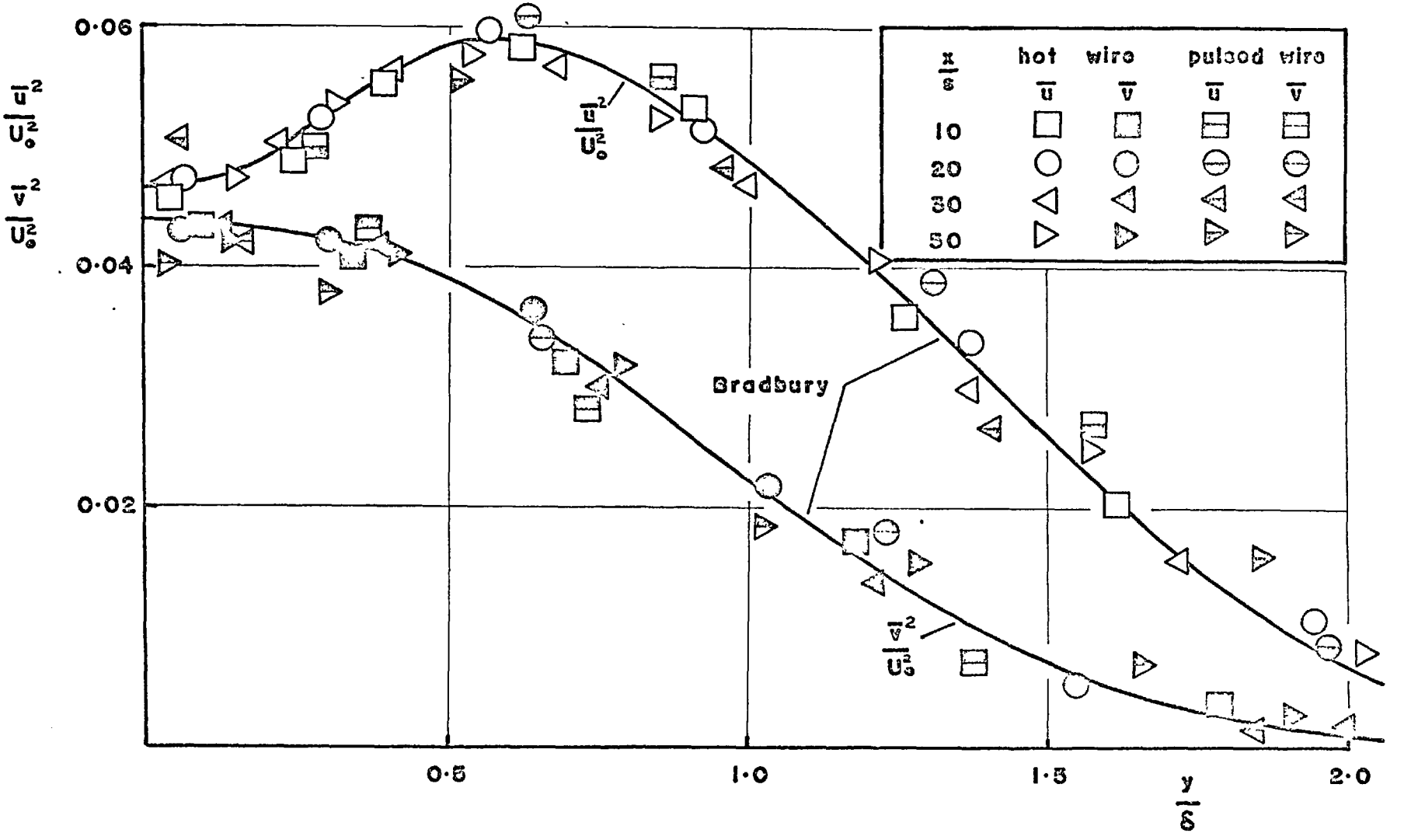


Fig. 2.5 Distribution of turbulent intensities across jet

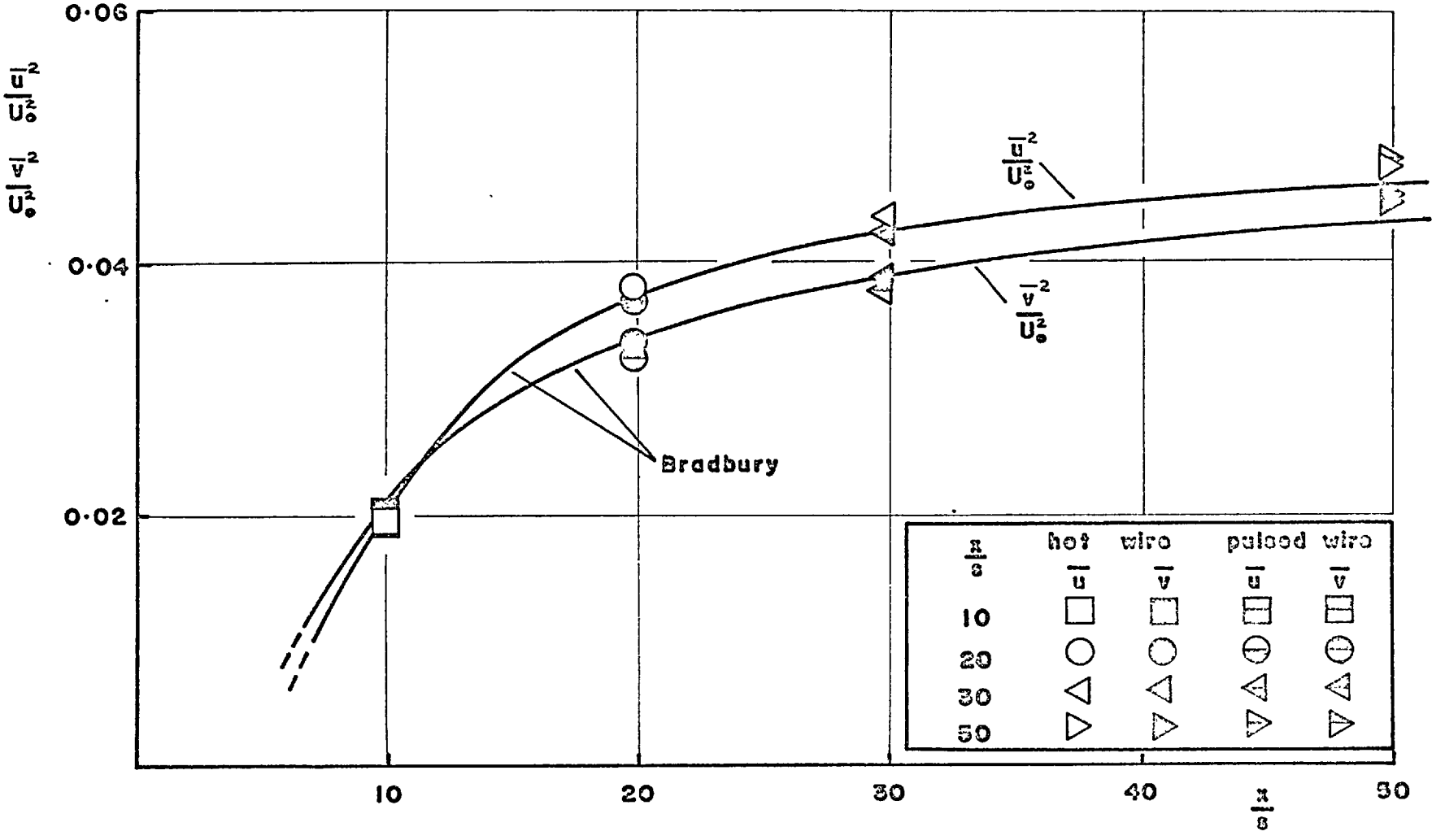


Fig. 2.6 Distribution of turbulent intensities along jet centre-line

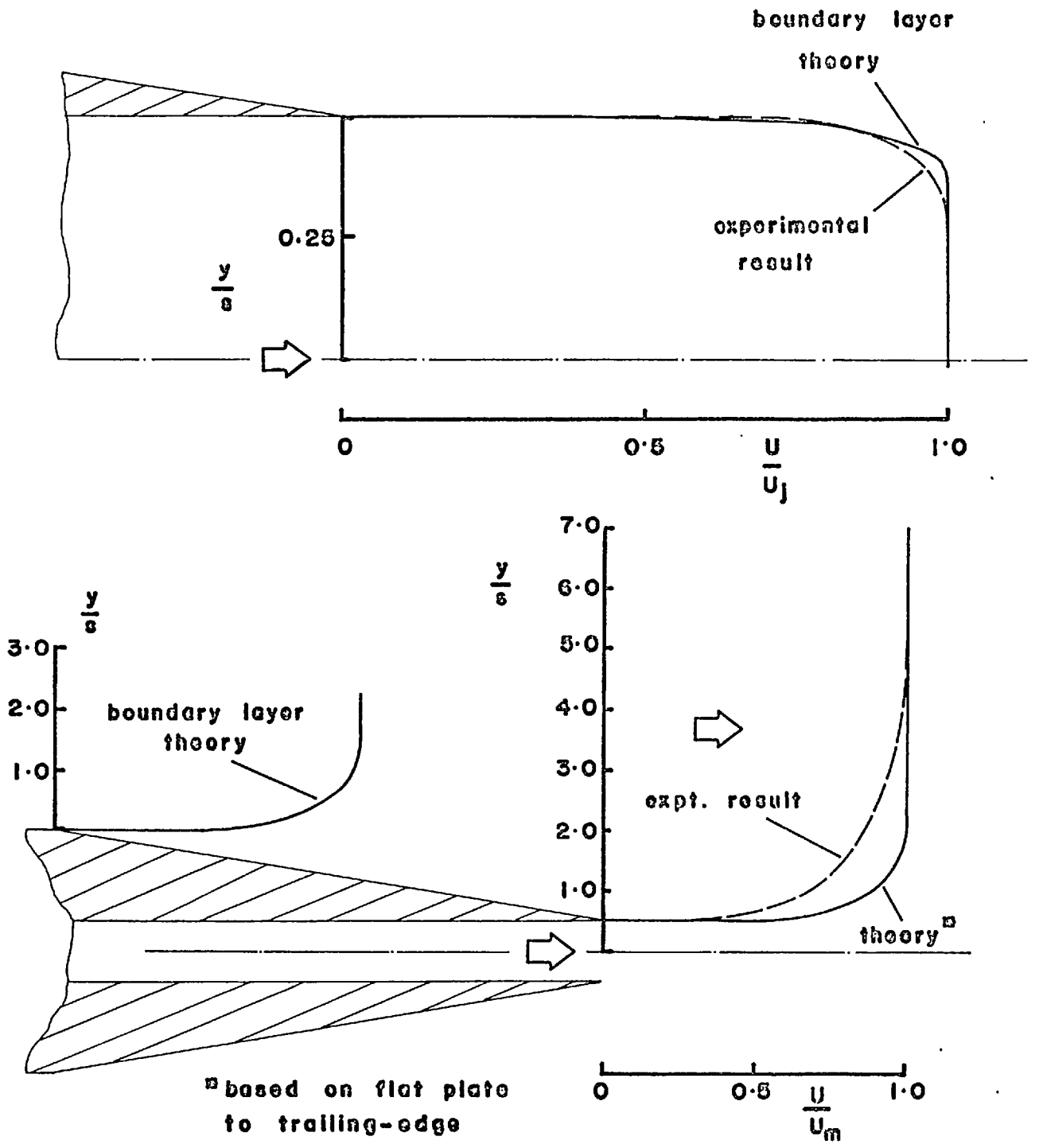


Fig. 2.7(a) Internal and external boundary layers at the slot exit.

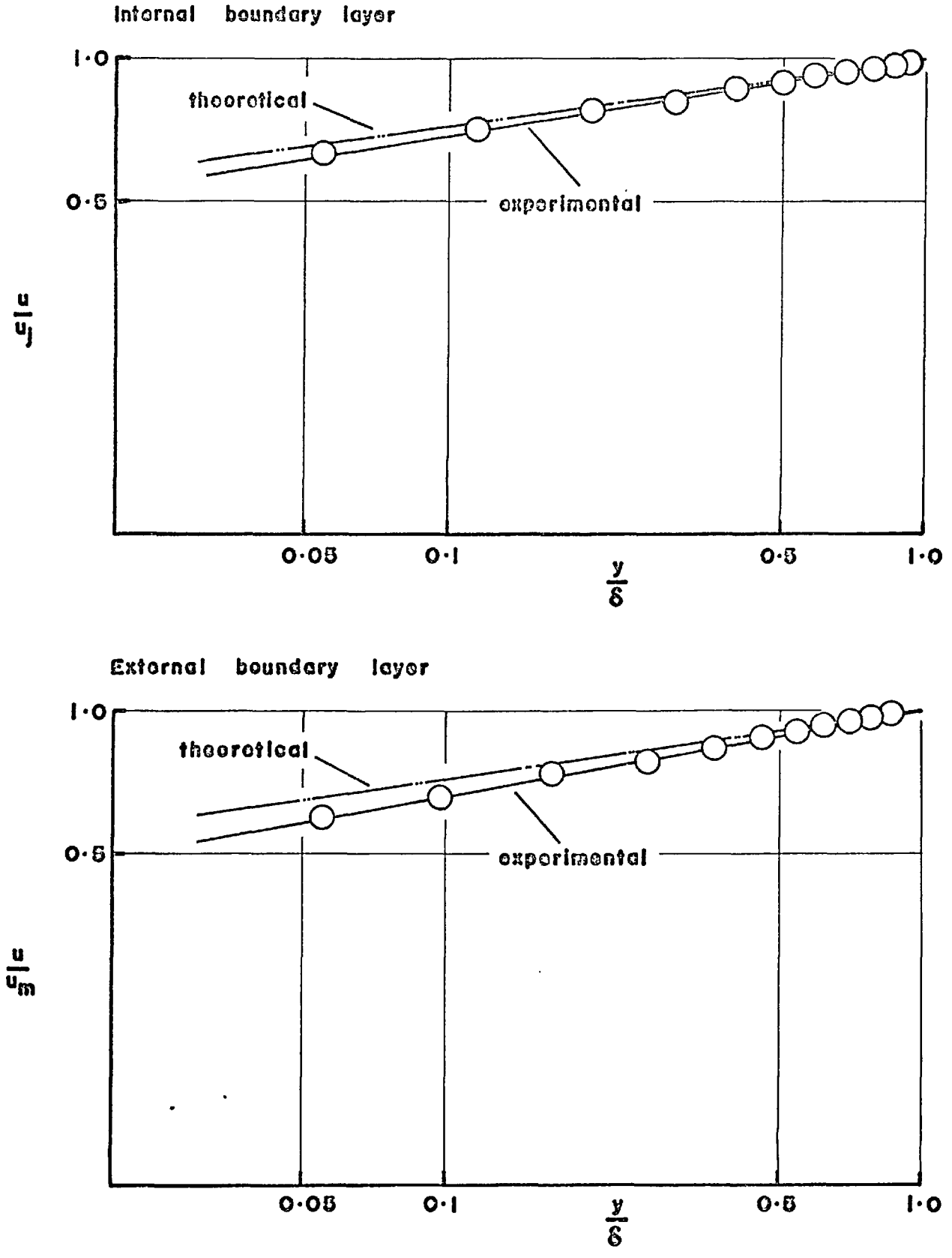
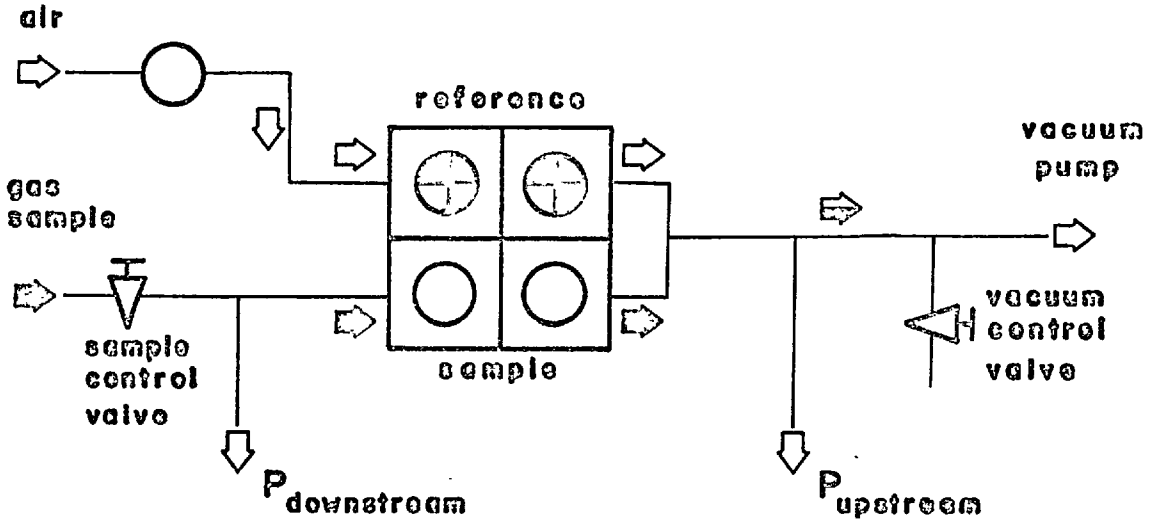


Fig. 2.7(b) Internal and external boundary layers at the slot exit

Gas flow diagram.



Electrical circuit.

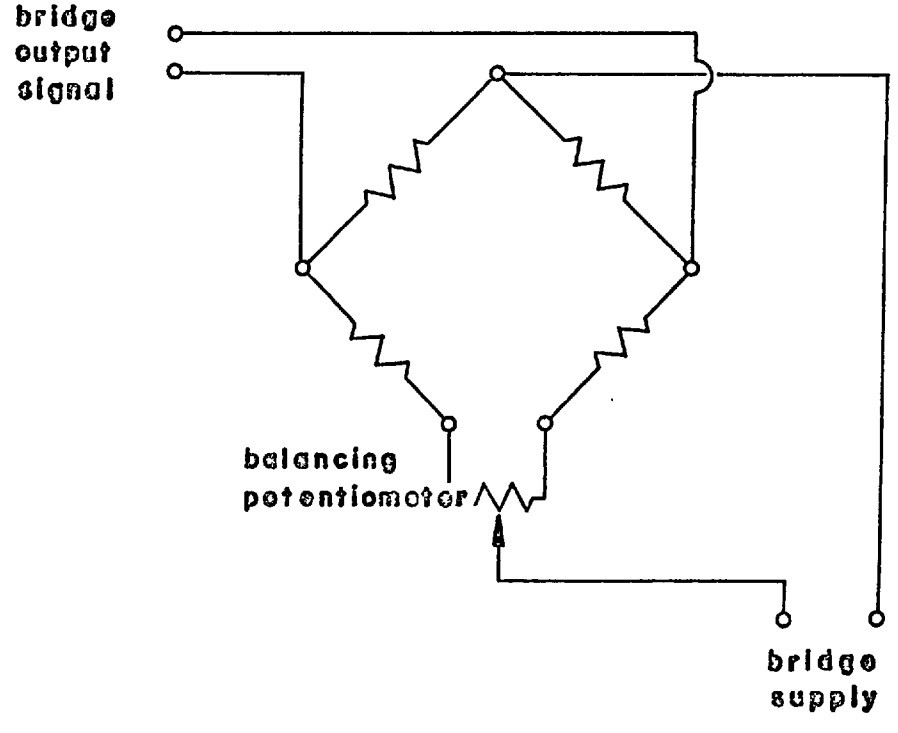


Fig. 2.8 Katharometer details.

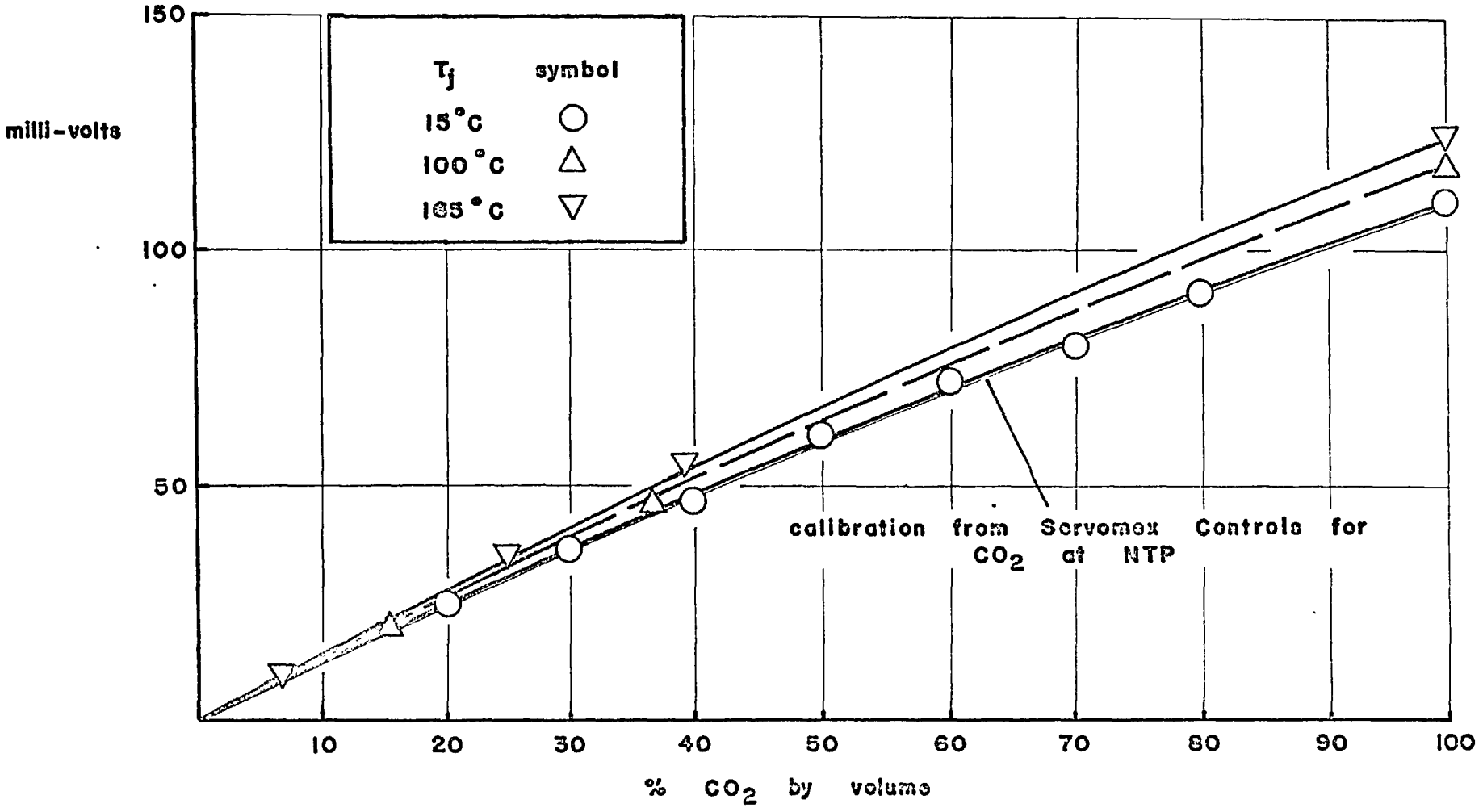


Fig. 2.9 Katharometer calibrations

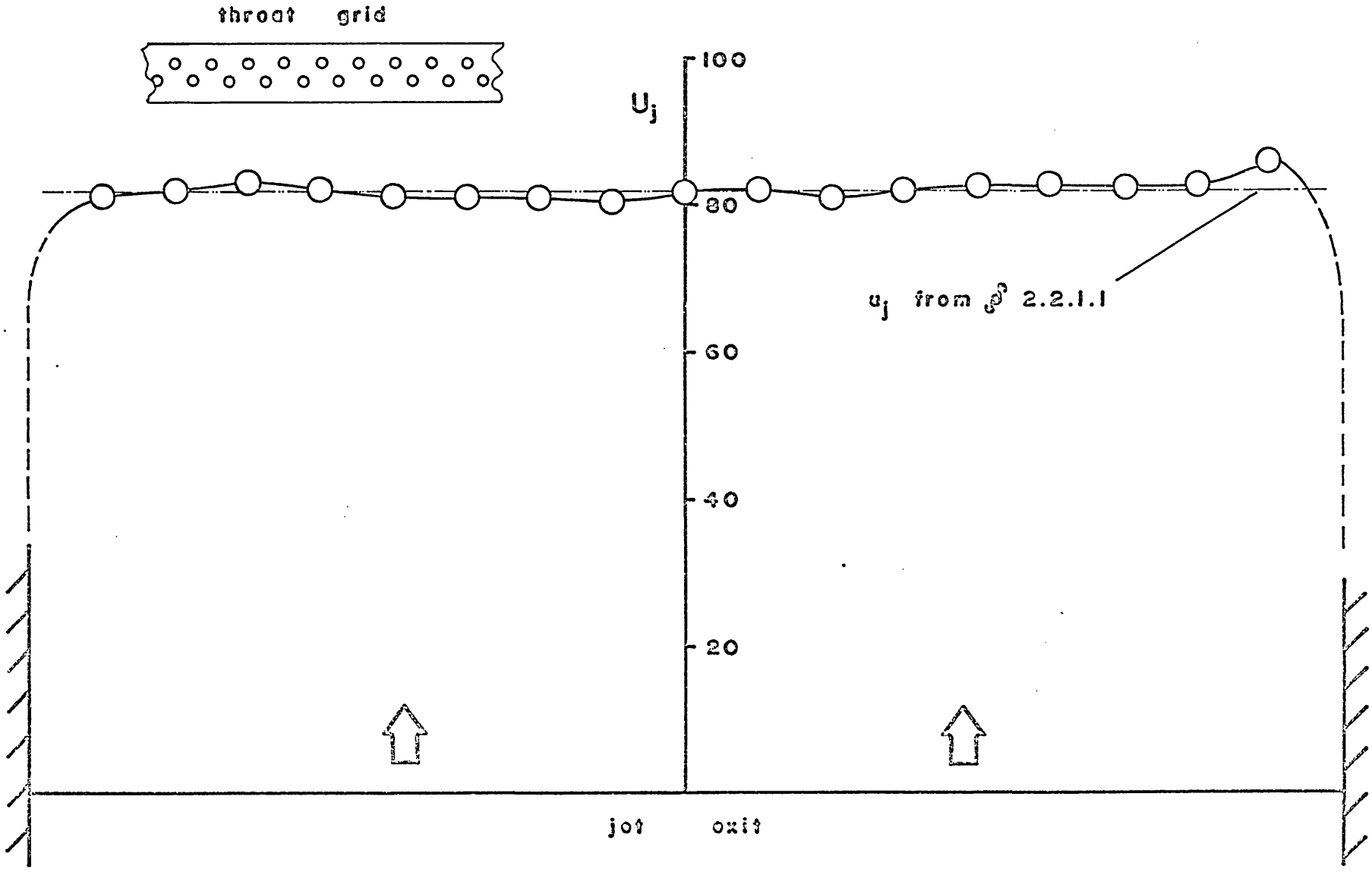


Fig. 3.1 Jet exit profile,

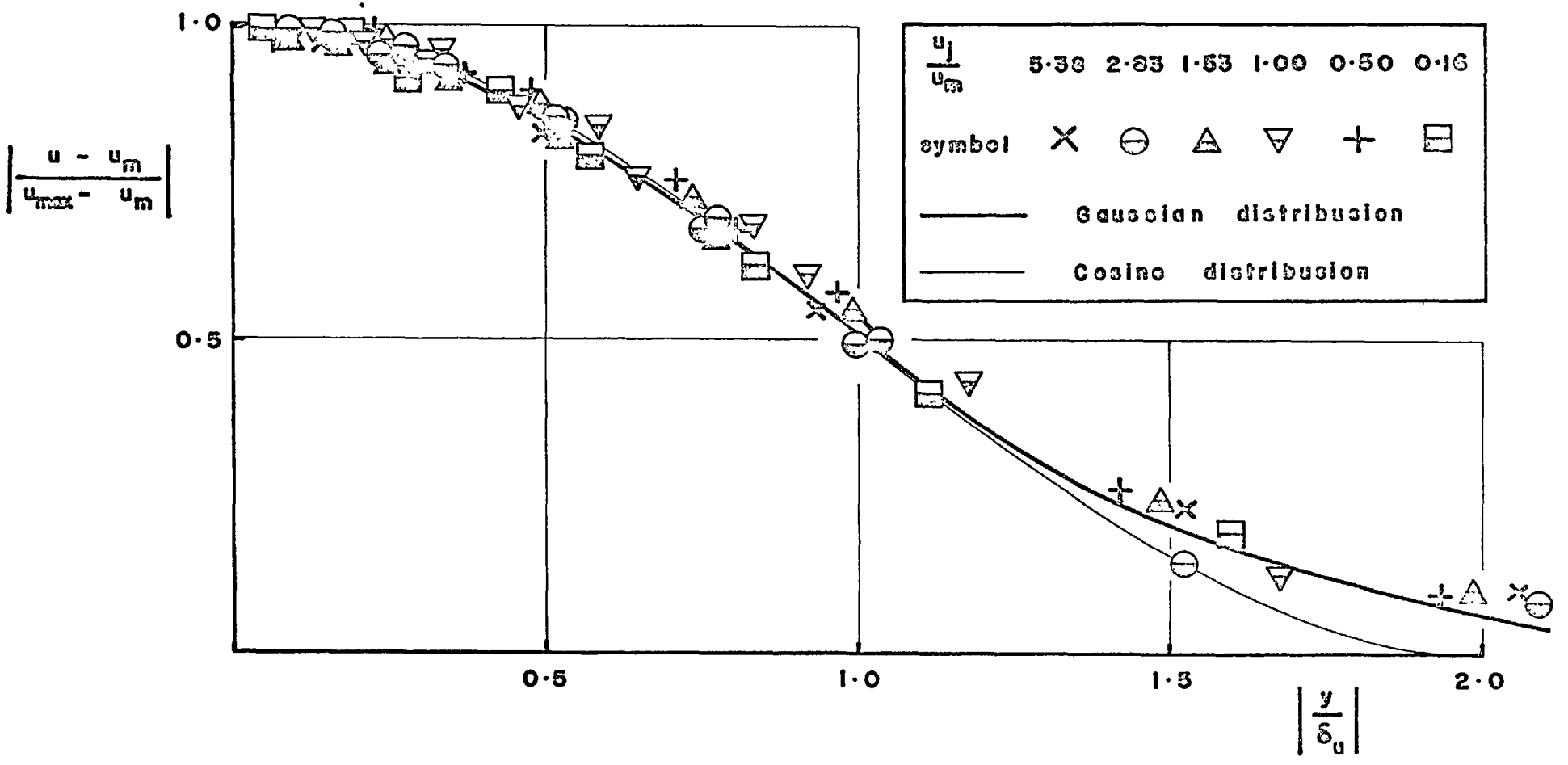


Fig. 3.2 (a) Experimental velocity profile : Series I

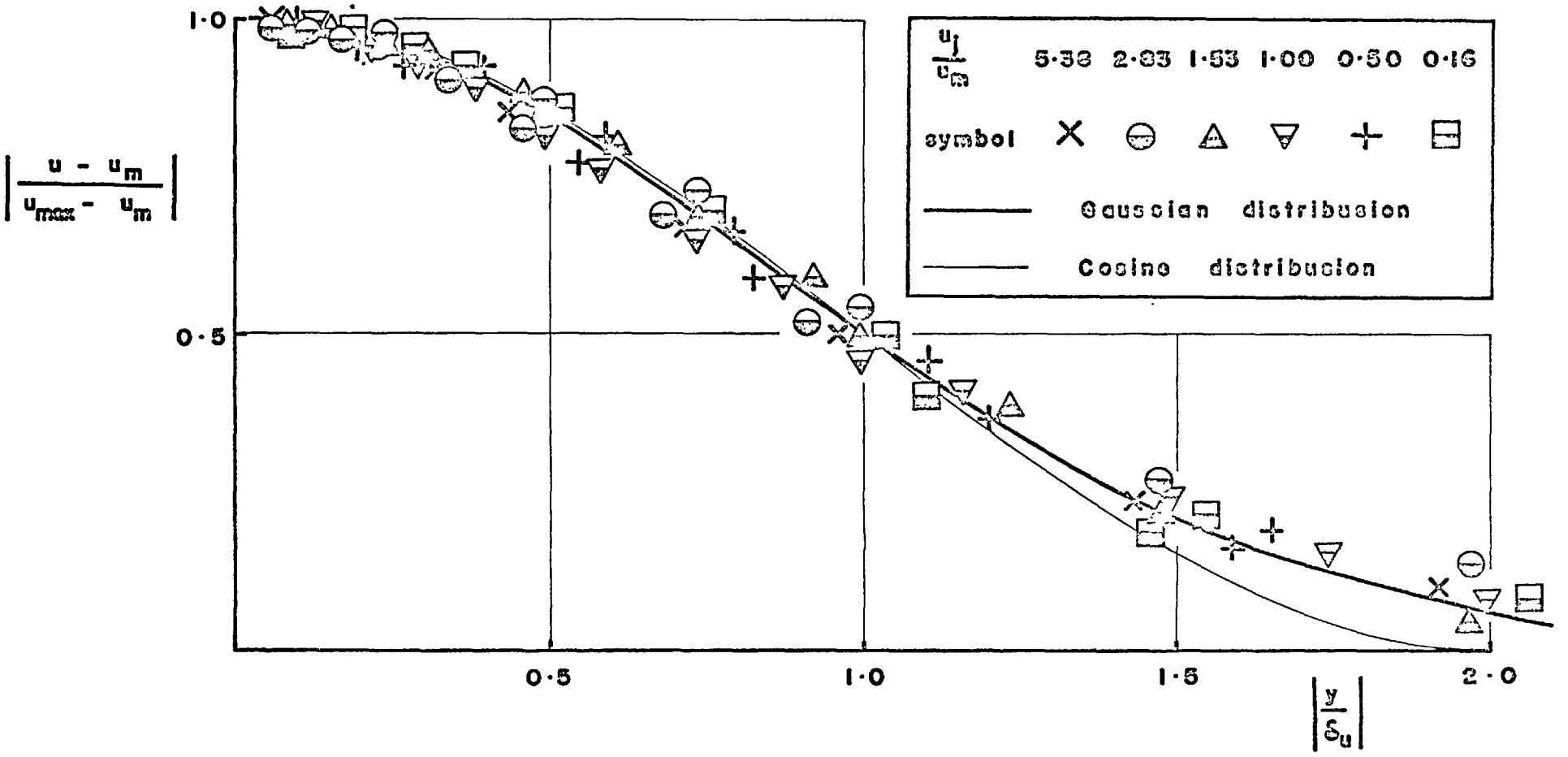


Fig. 3.2 (b) Experimental velocity profile : Series II

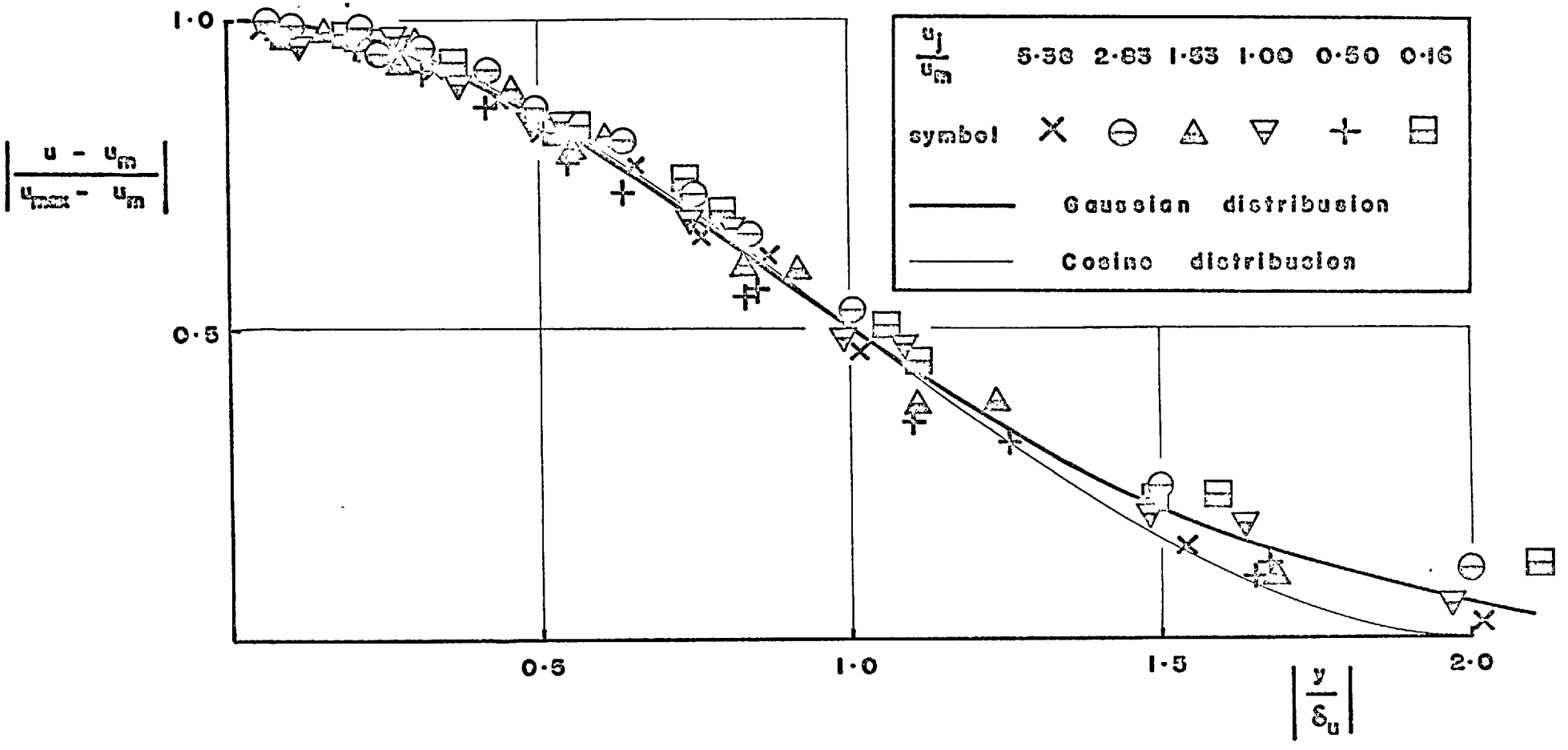


Fig. 3.2 (c) Experimental velocity profile : Series III

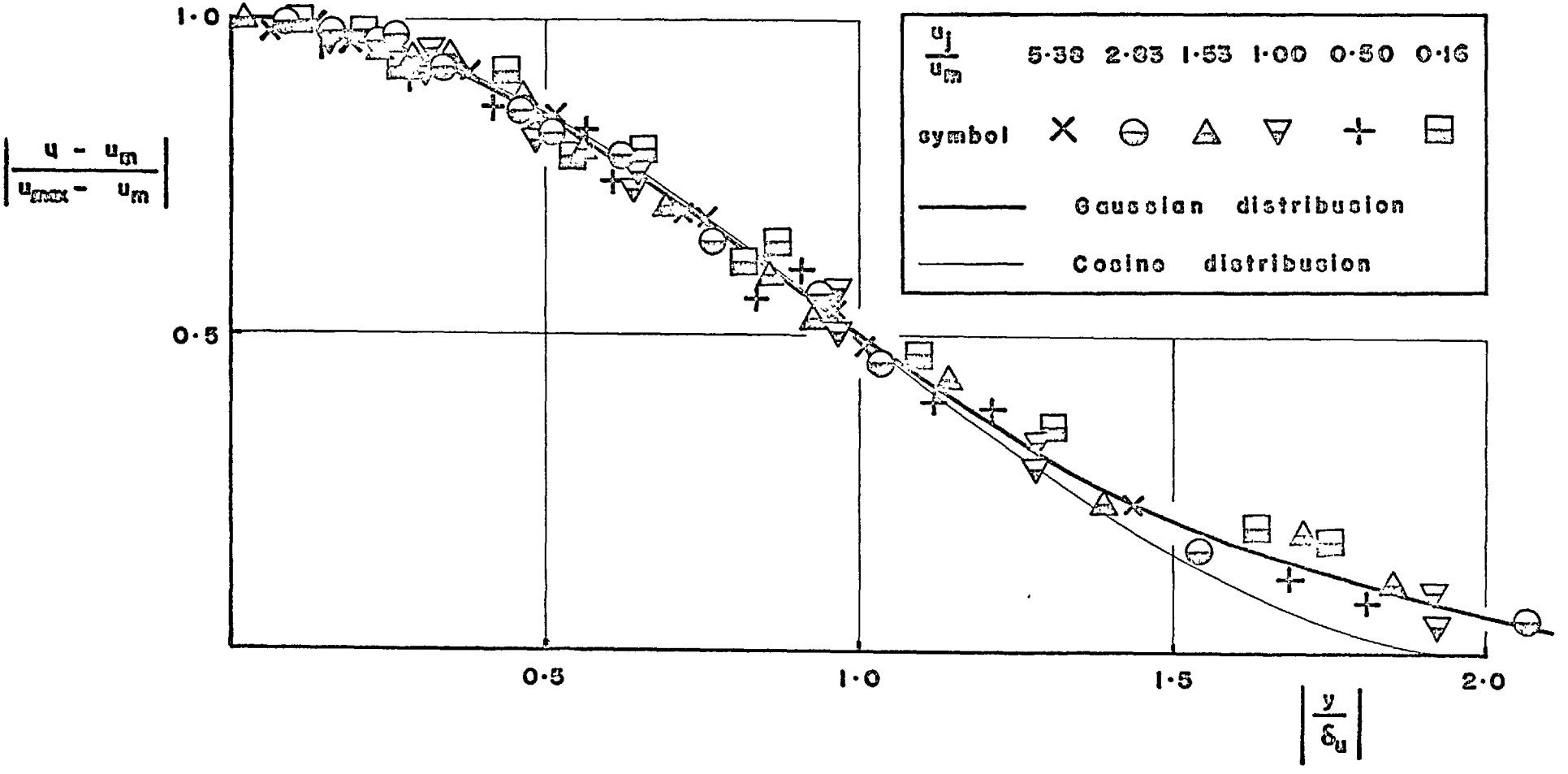


Fig. 3.2(d) Experimental velocity profile : Series IV

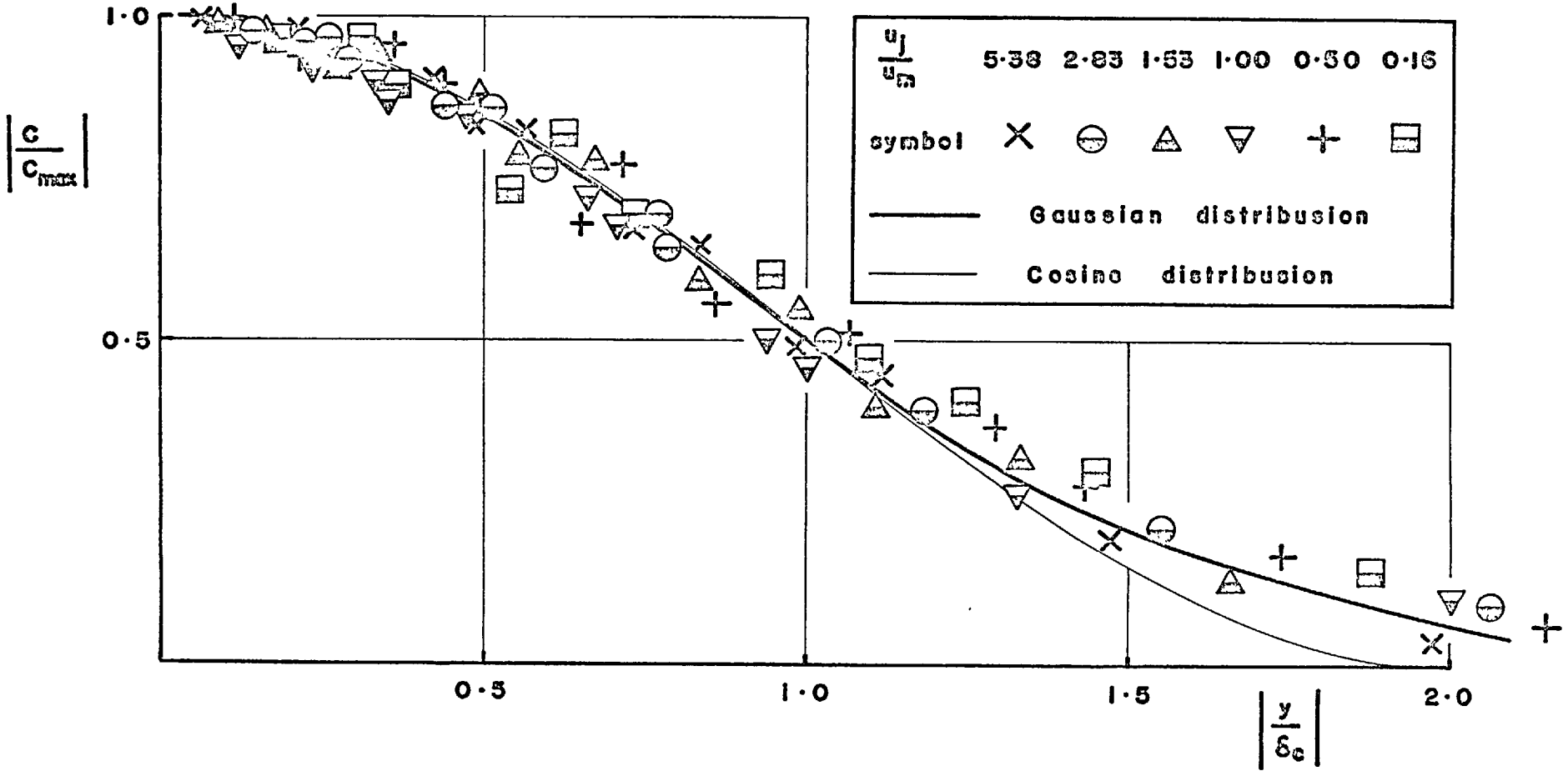


Fig. 3.3(a) Experimental concentration profile : Series II

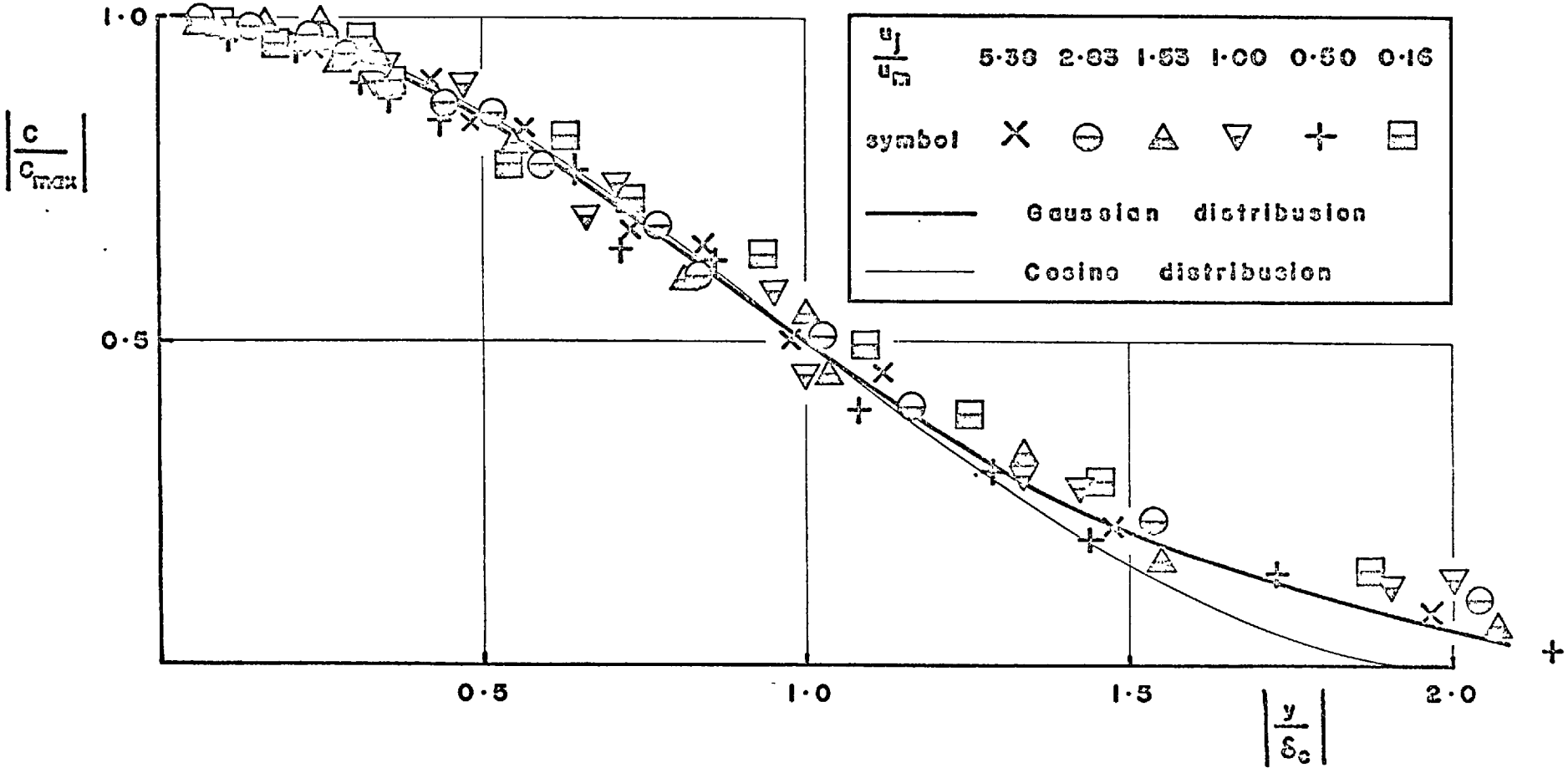


Fig. 3.3(b) Experimental concentration profile : Series IV

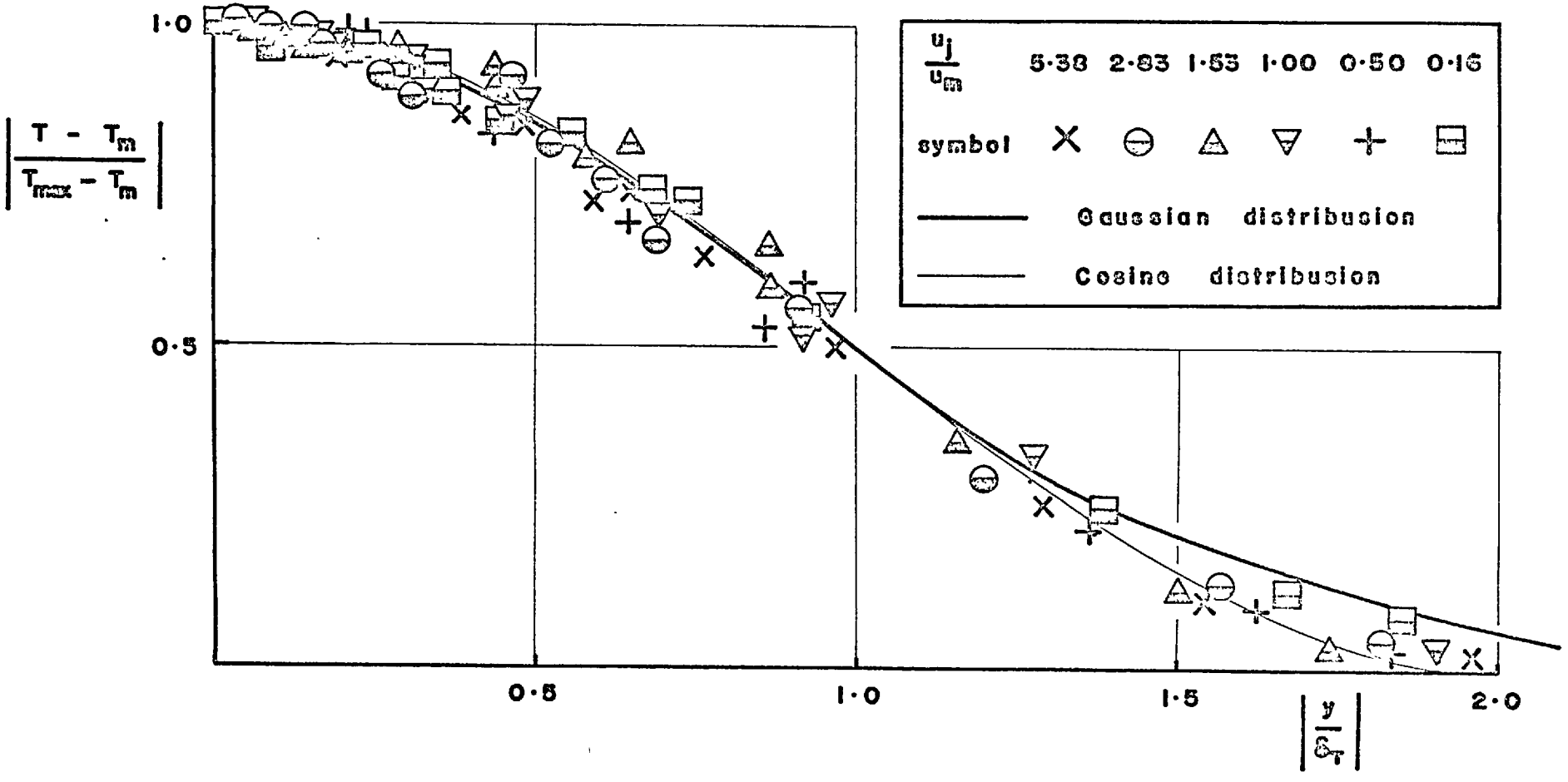


Fig. 3.4 (a) Experimental temperature profile : Series III

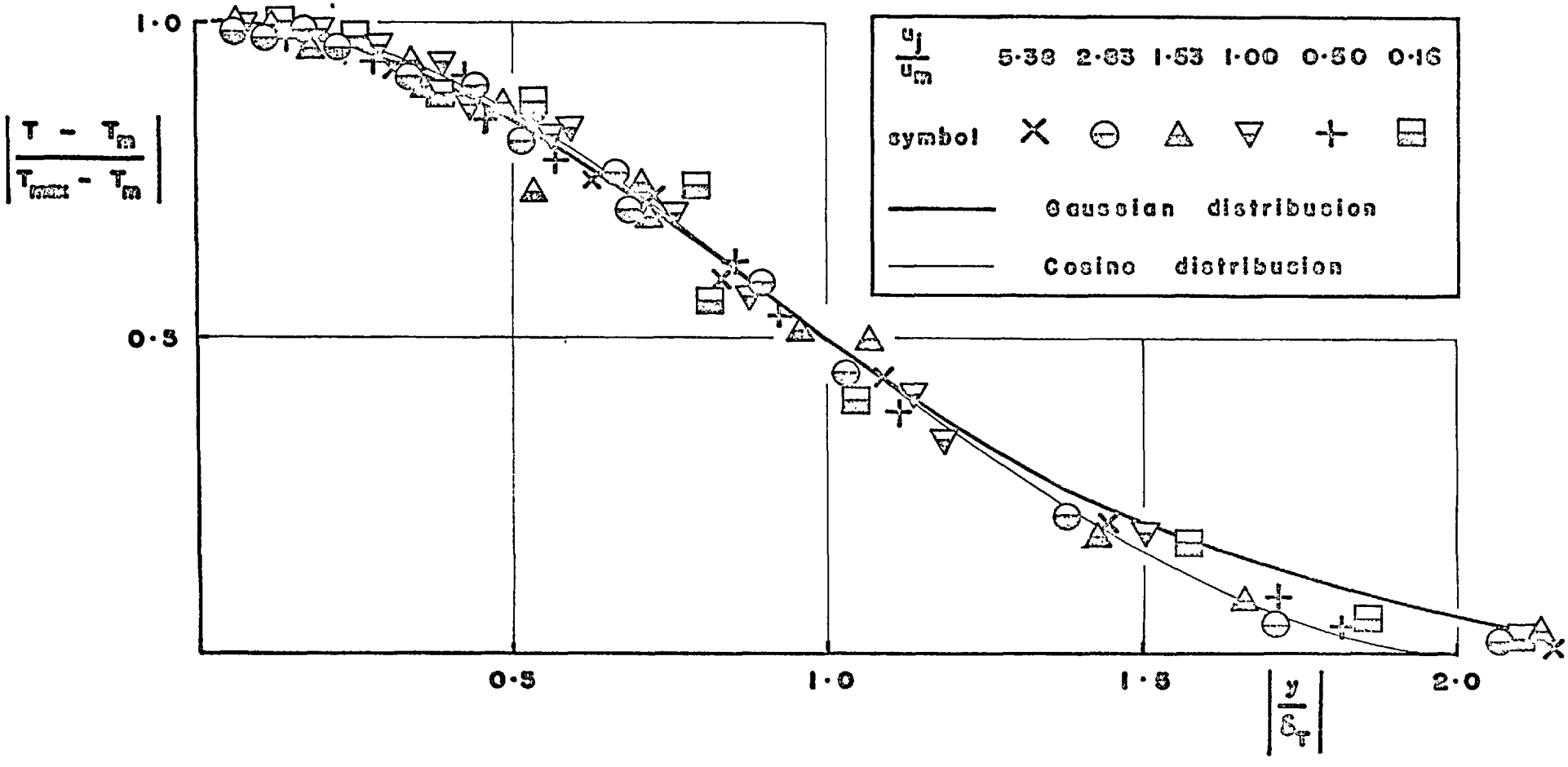
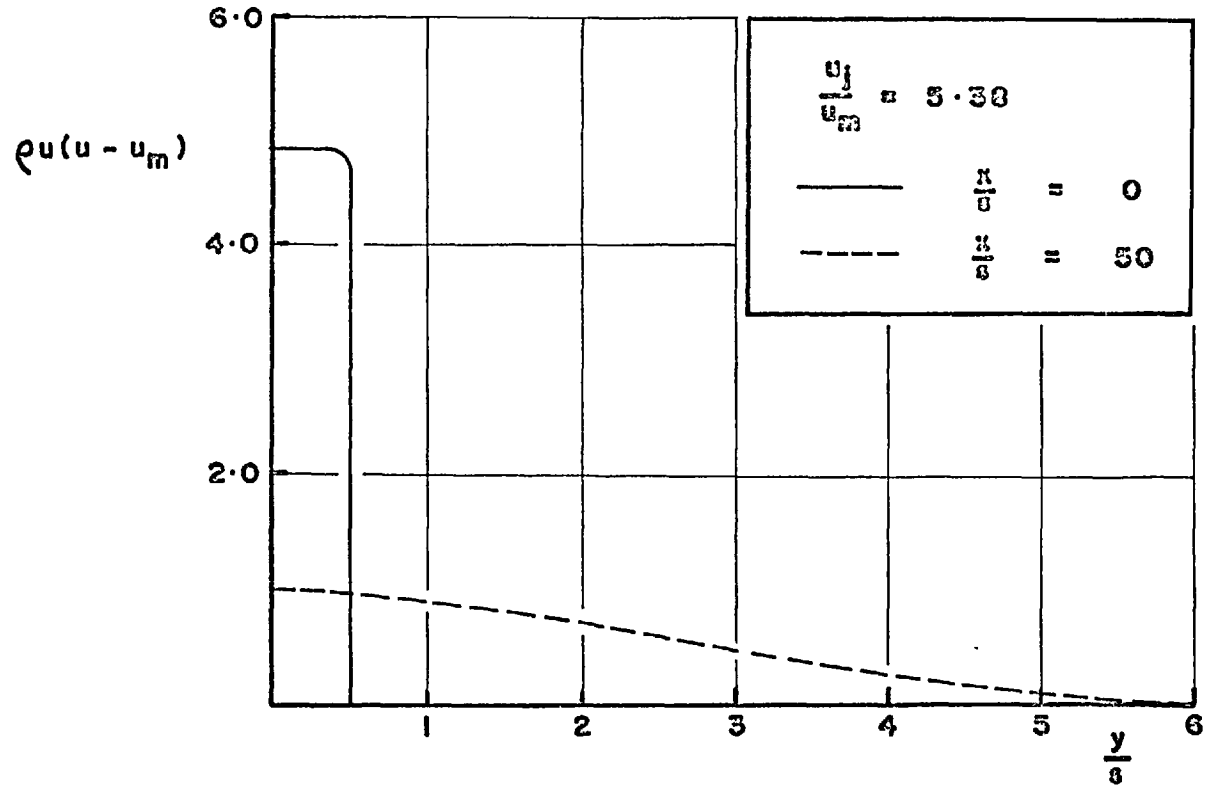


Fig. 3.4 (b) Experimental temperature profile : Series IV



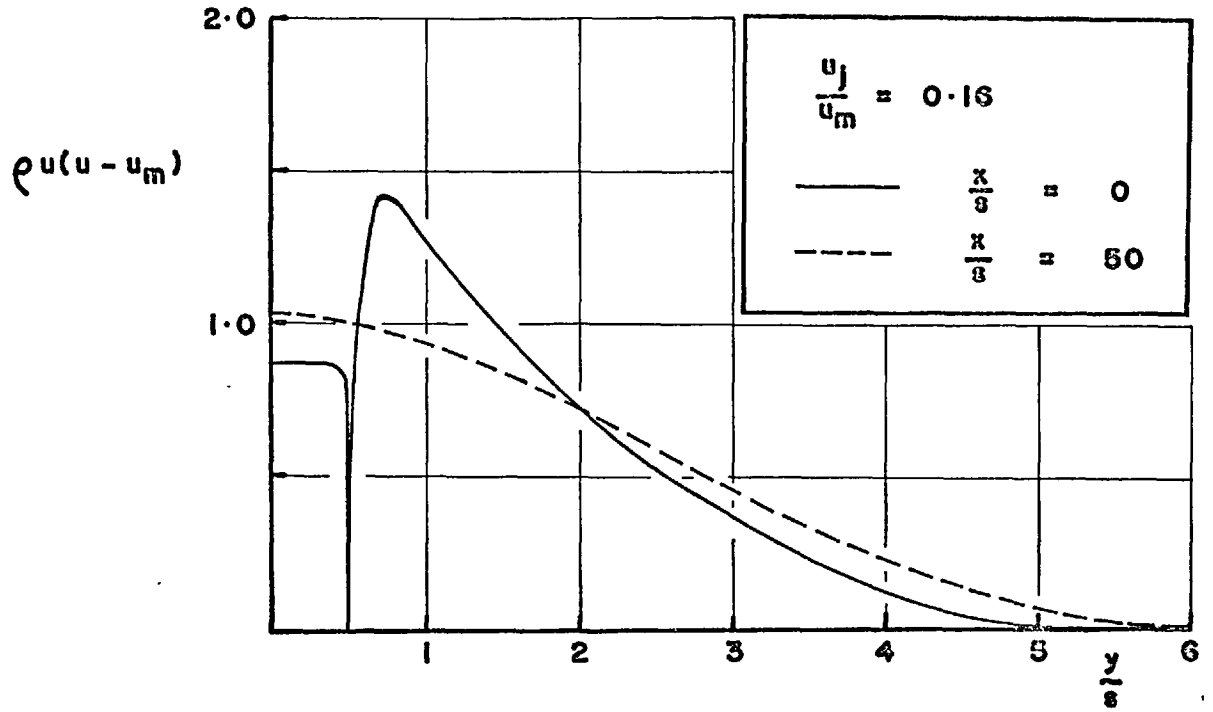
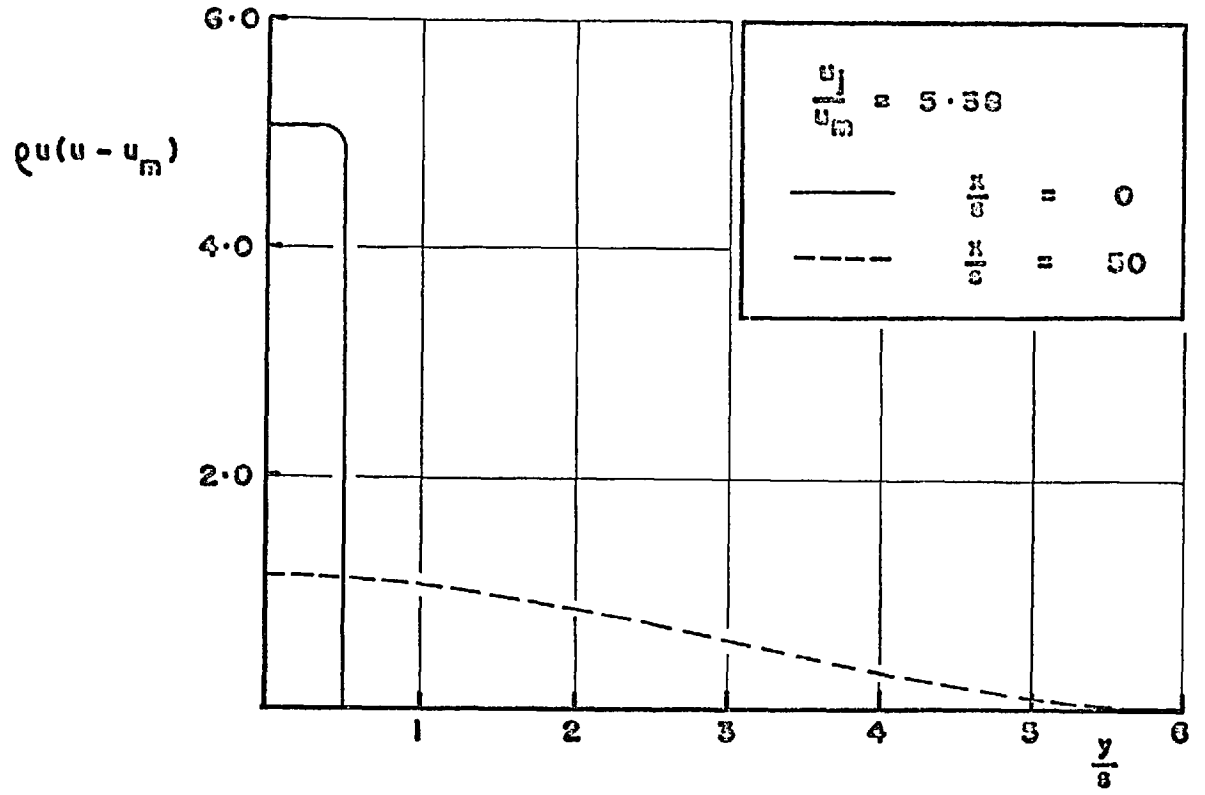


Fig. 3.5(a) Momentum balance : Series I



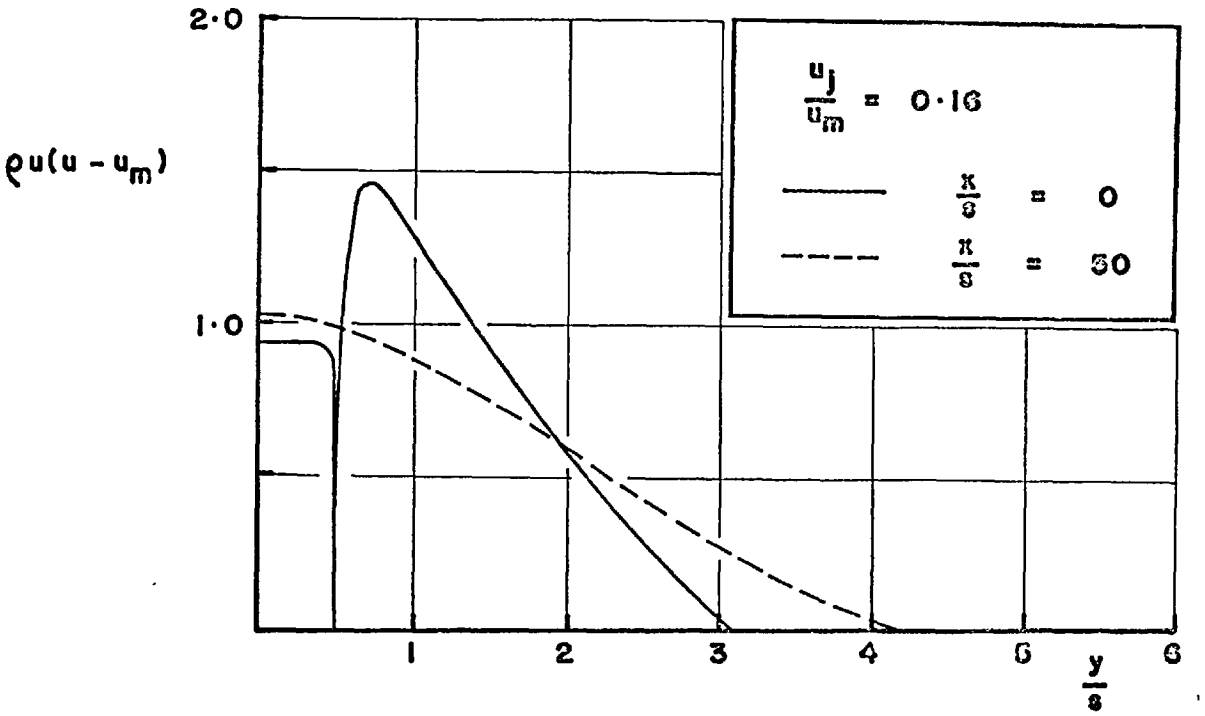
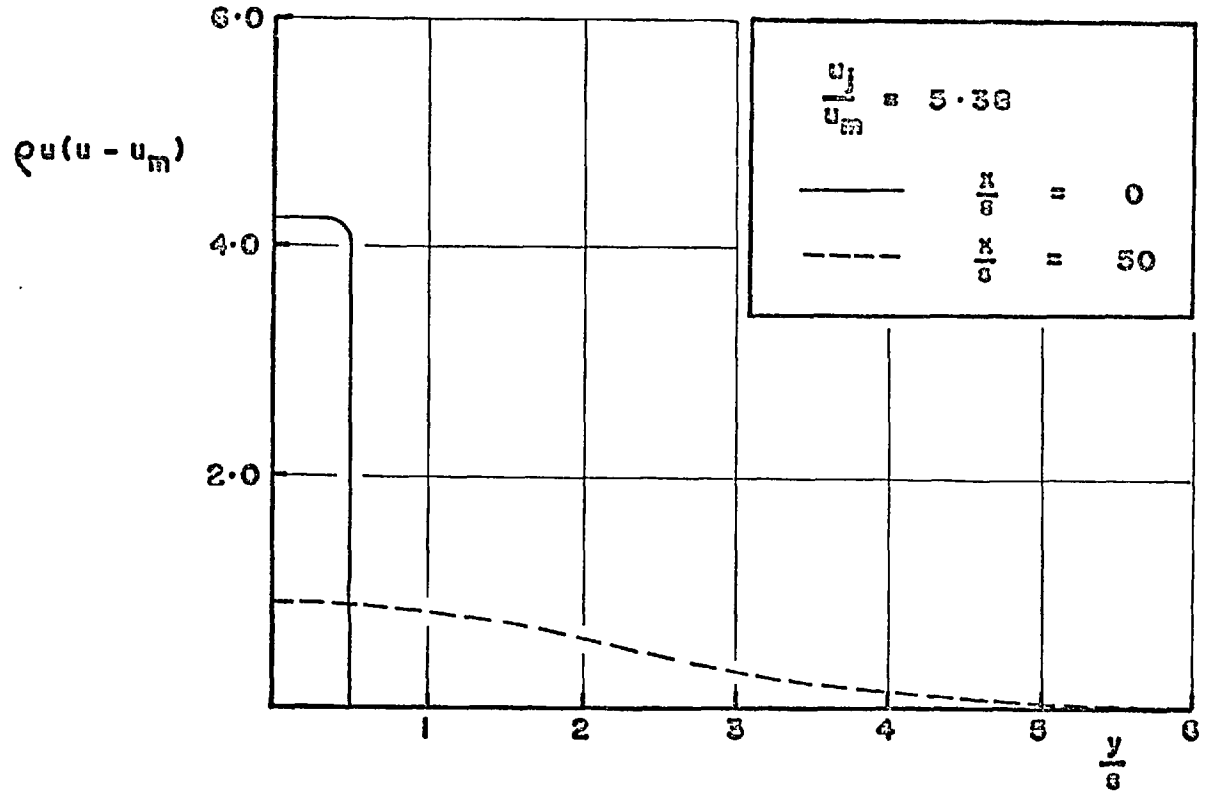


Fig. 3.5(b) Momentum balance : Series II



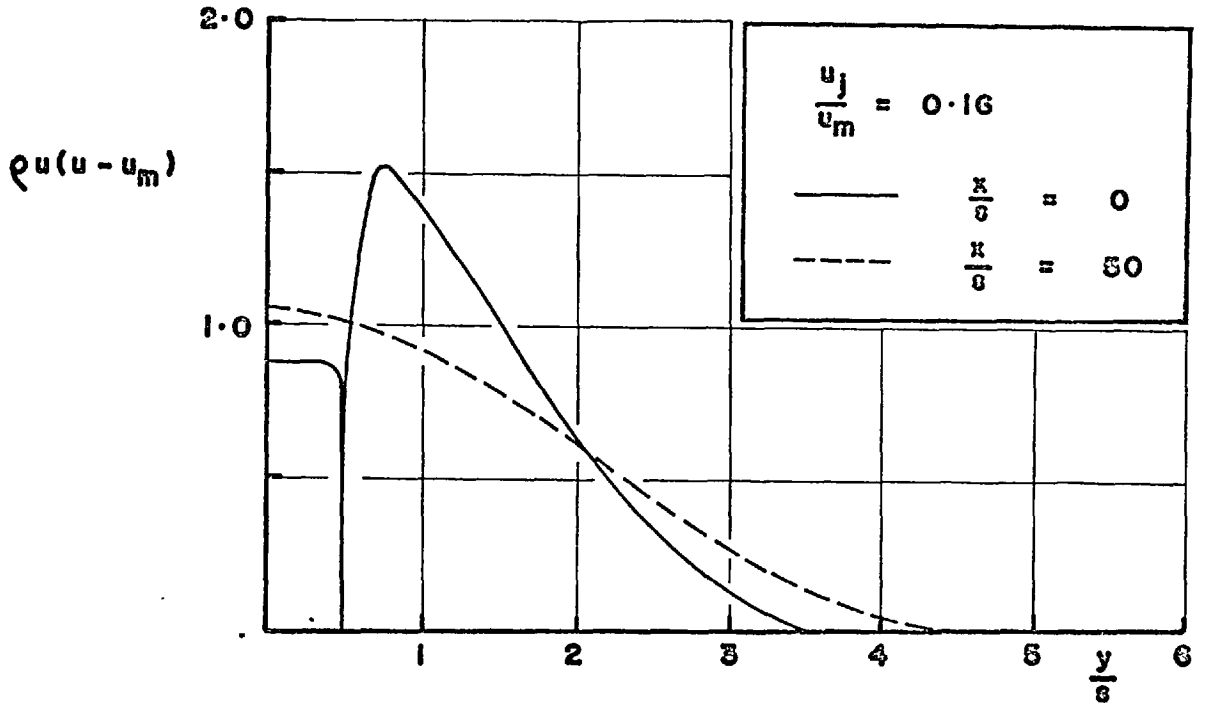
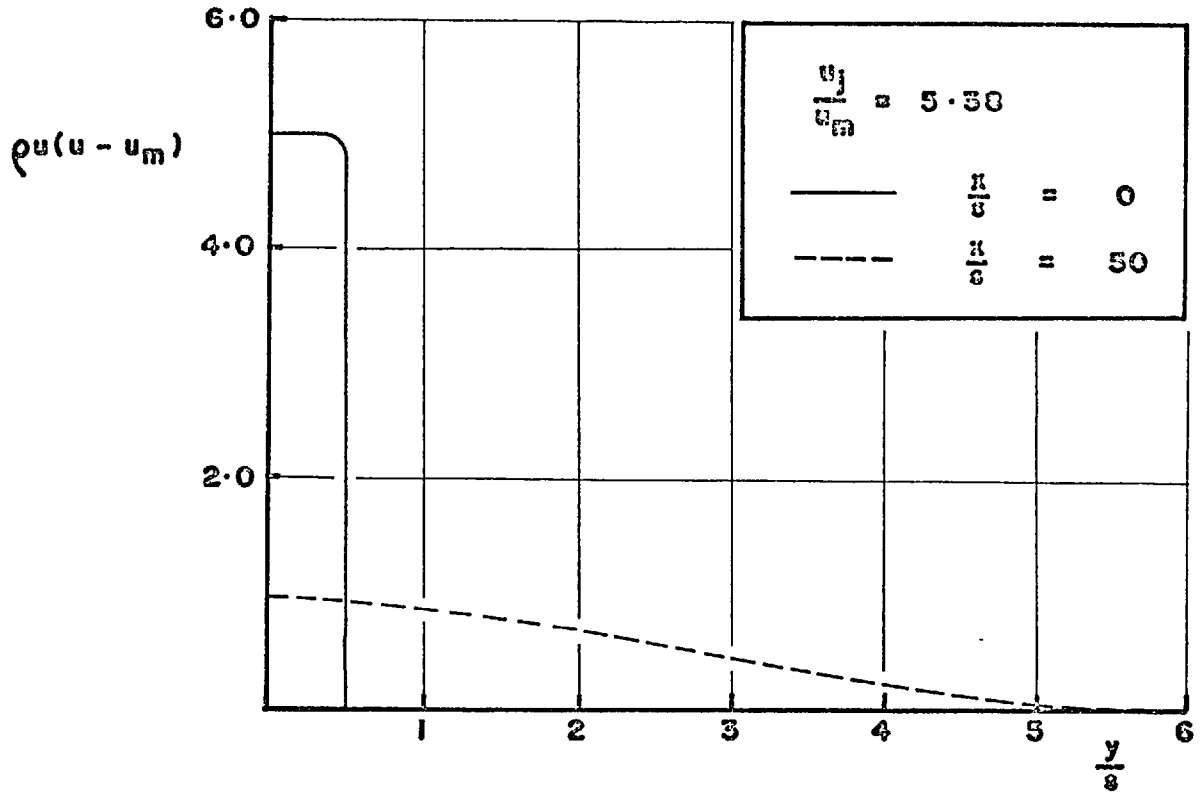


Fig. 3.5(c) Momentum balance : Series III



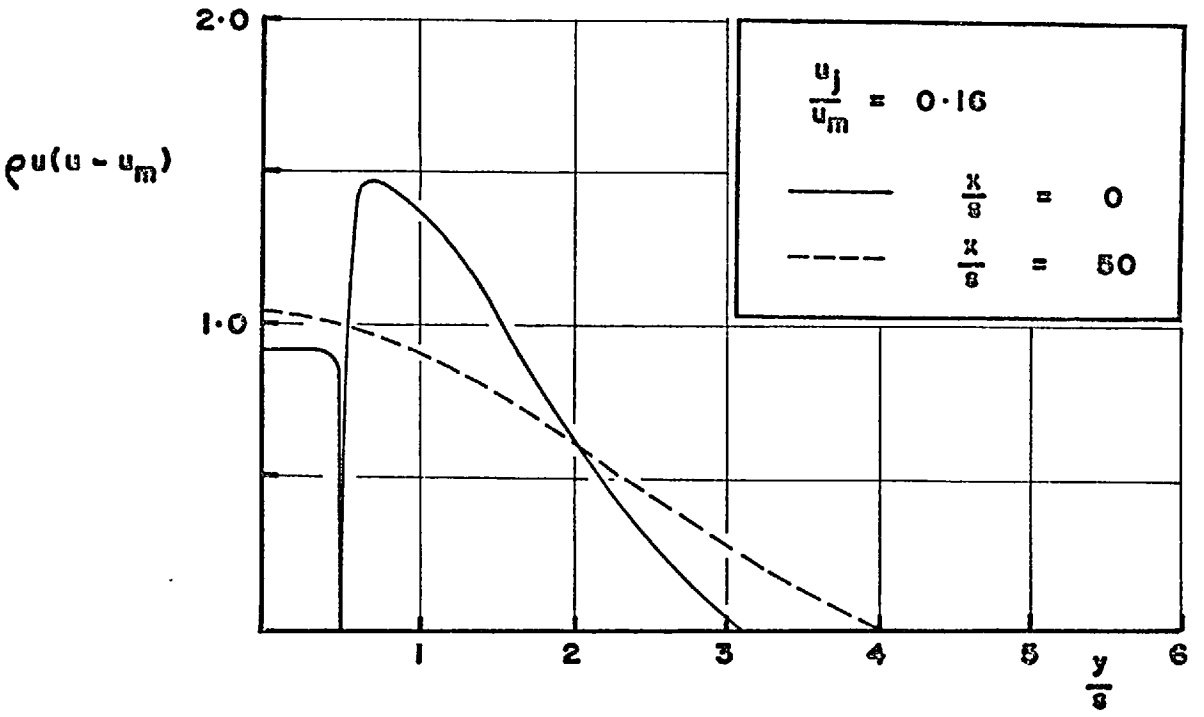
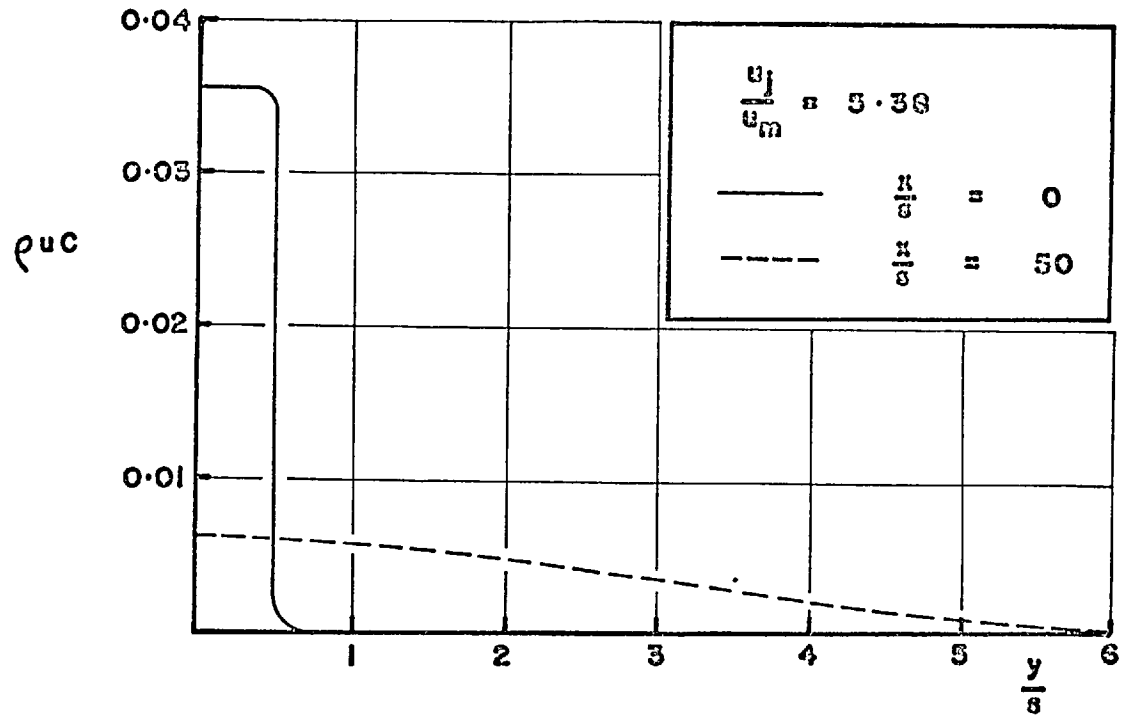


Fig. 3.5(d) Momentum balance : Series IV



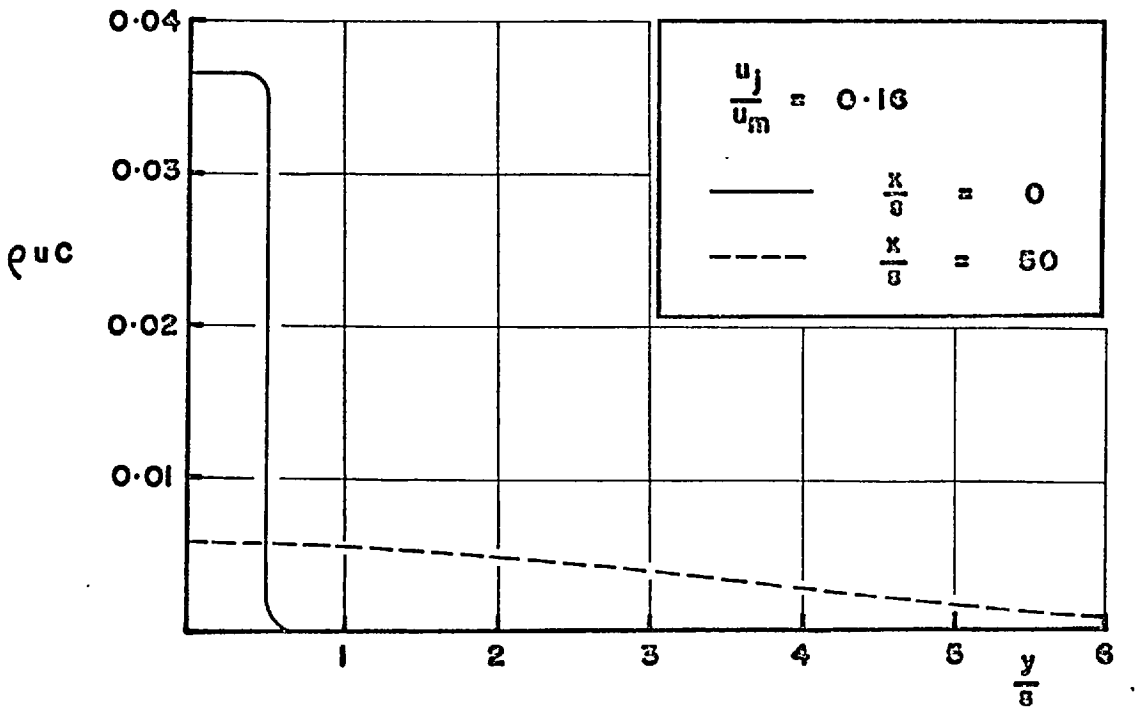
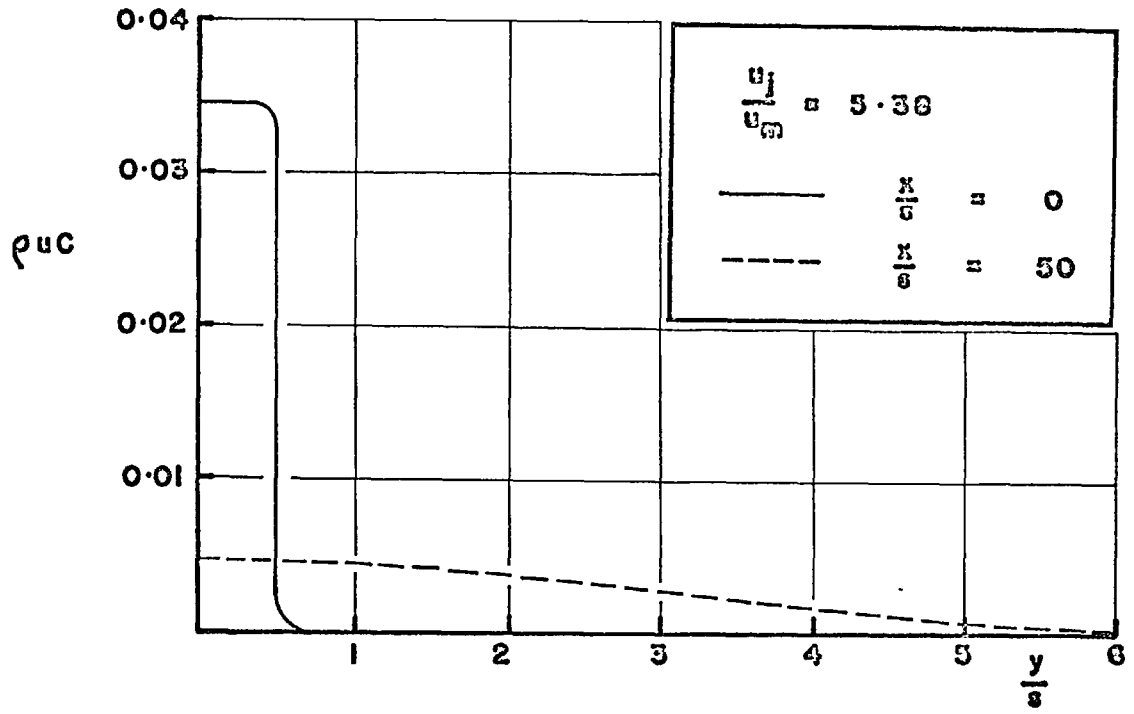


Fig. 3.6(a) Mass balance : Series II



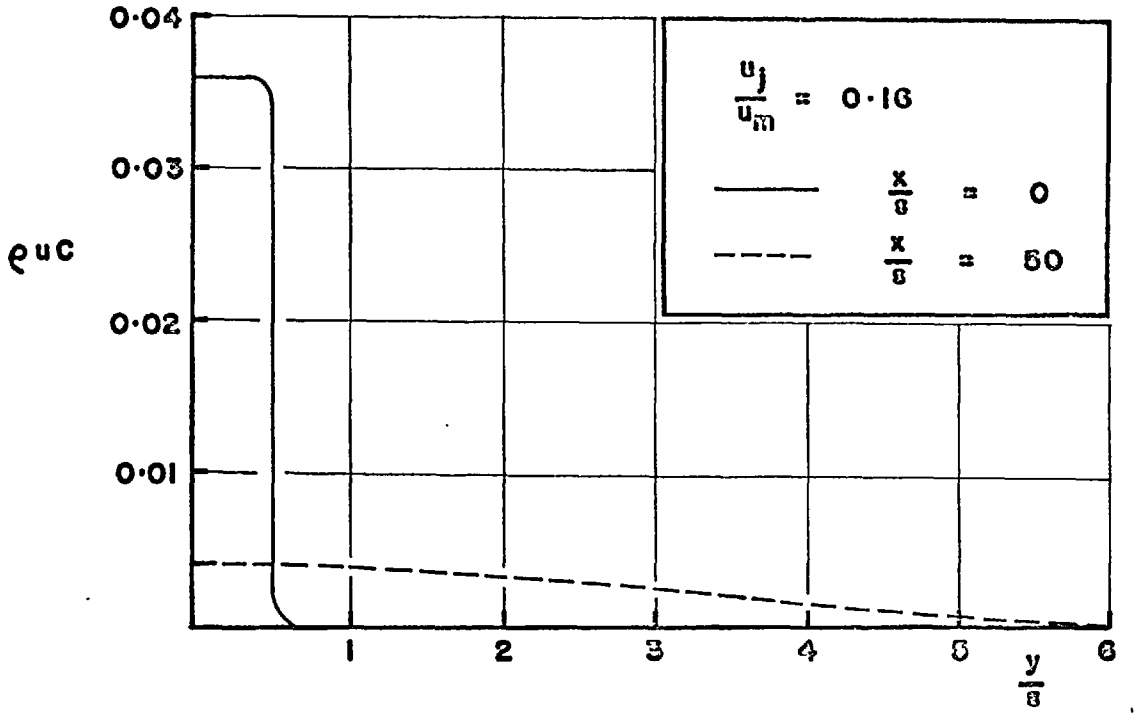


Fig. 3.6(b) Mass balance : Series IV

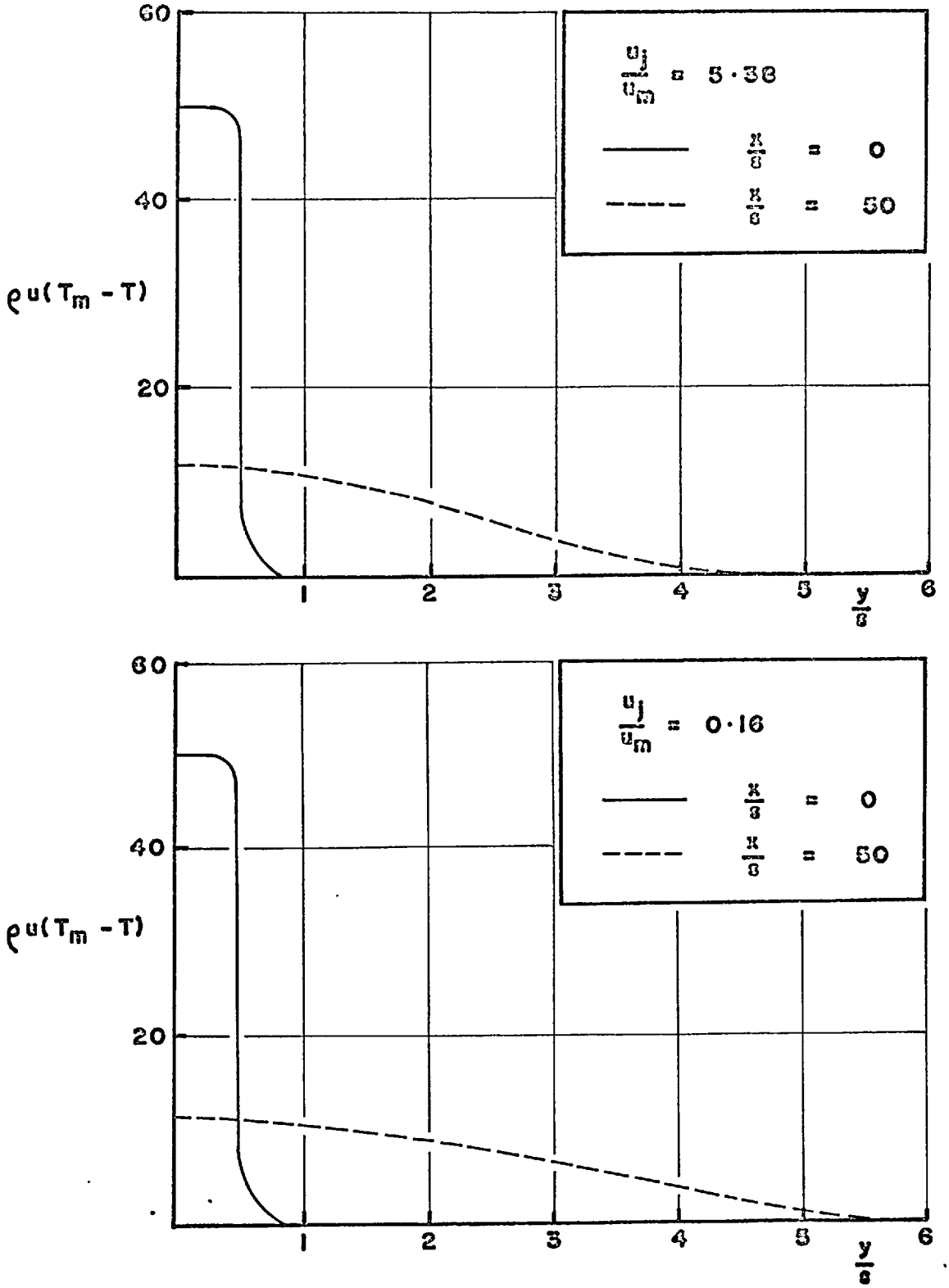
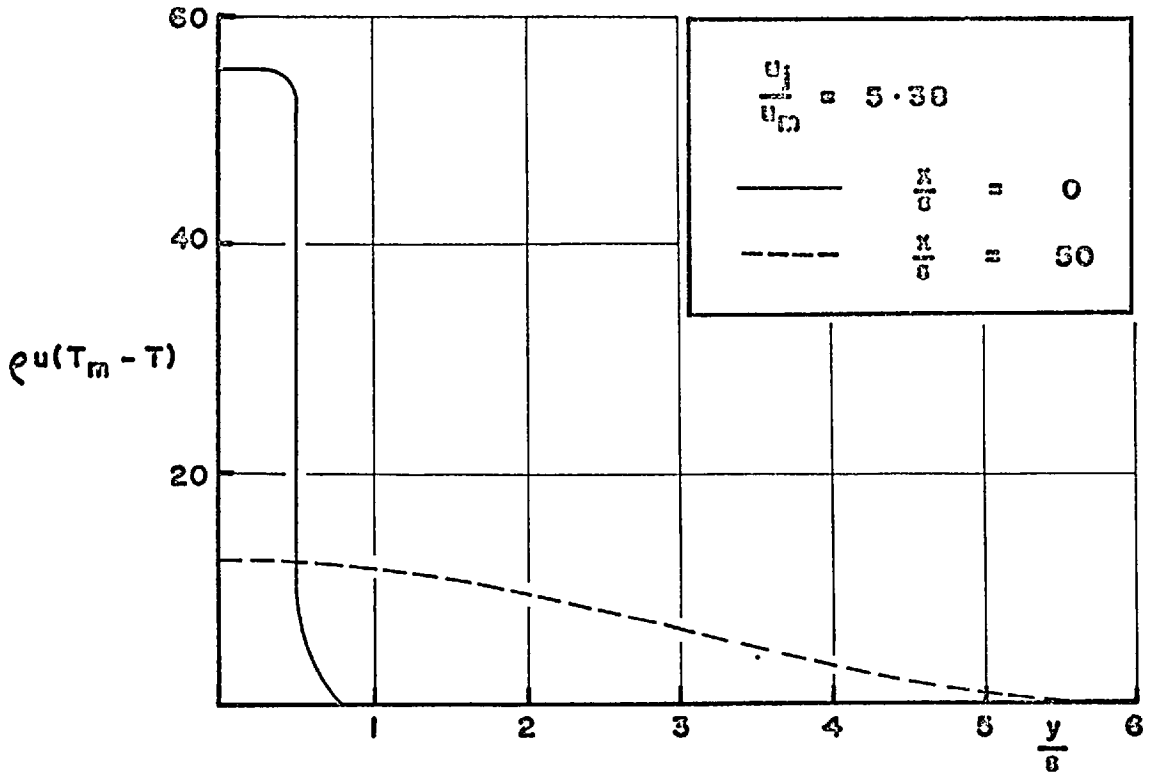


Fig. 3.7 (a) Heat balance : Series III



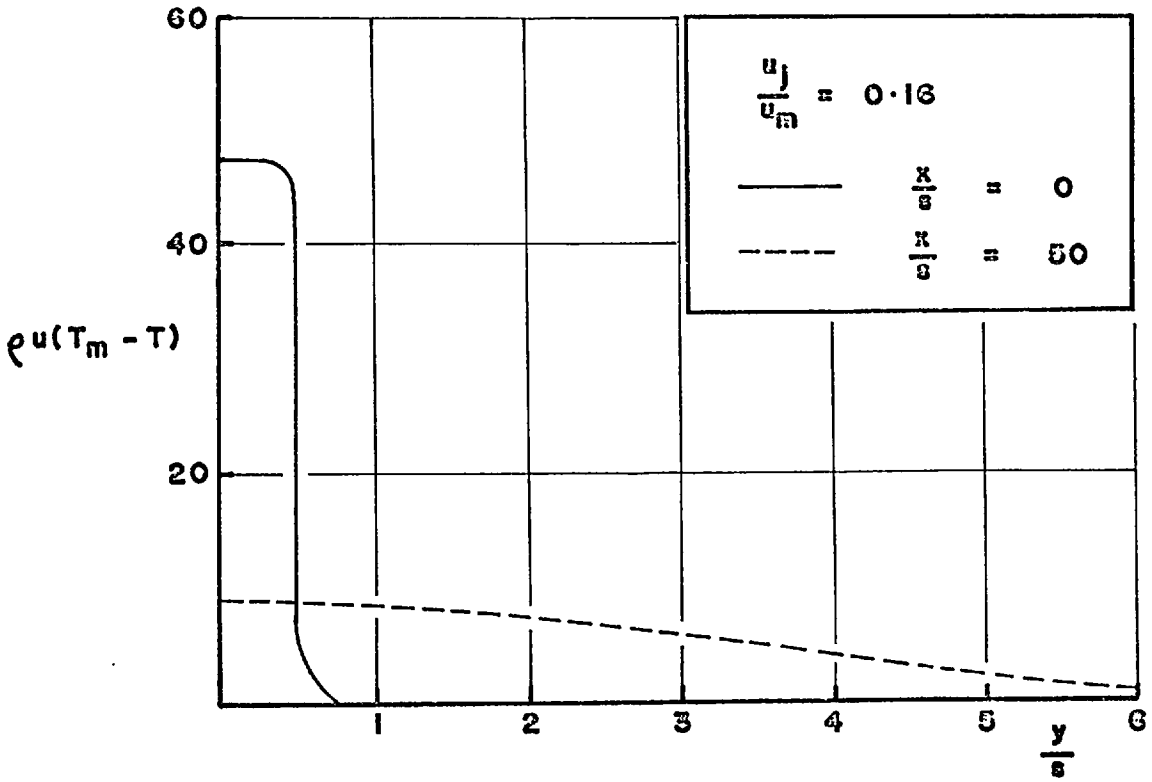


Fig. 3.7 (b) Heat balance : Series IV

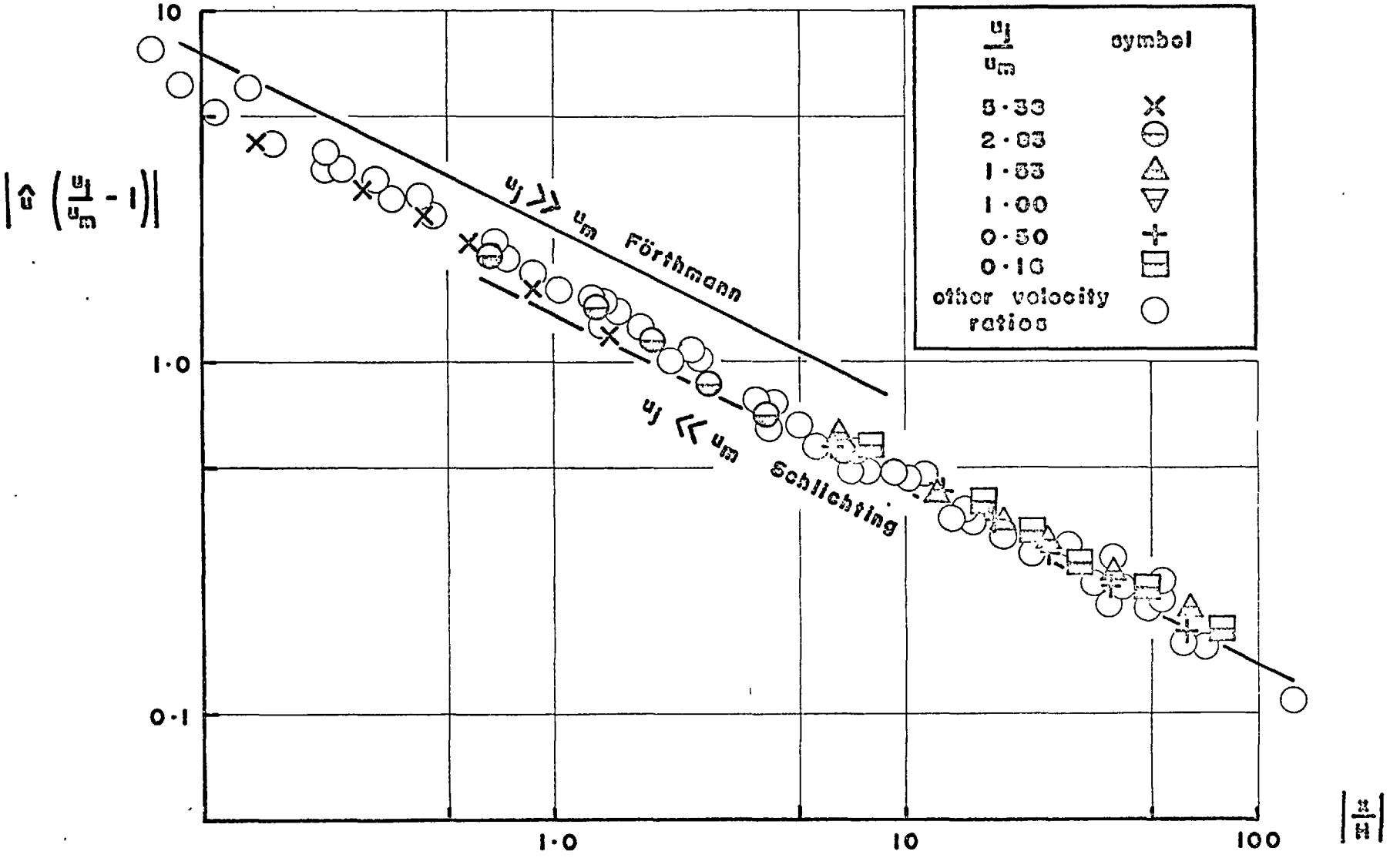


Fig. 5.1(a) Centre-line velocity decay : Series I

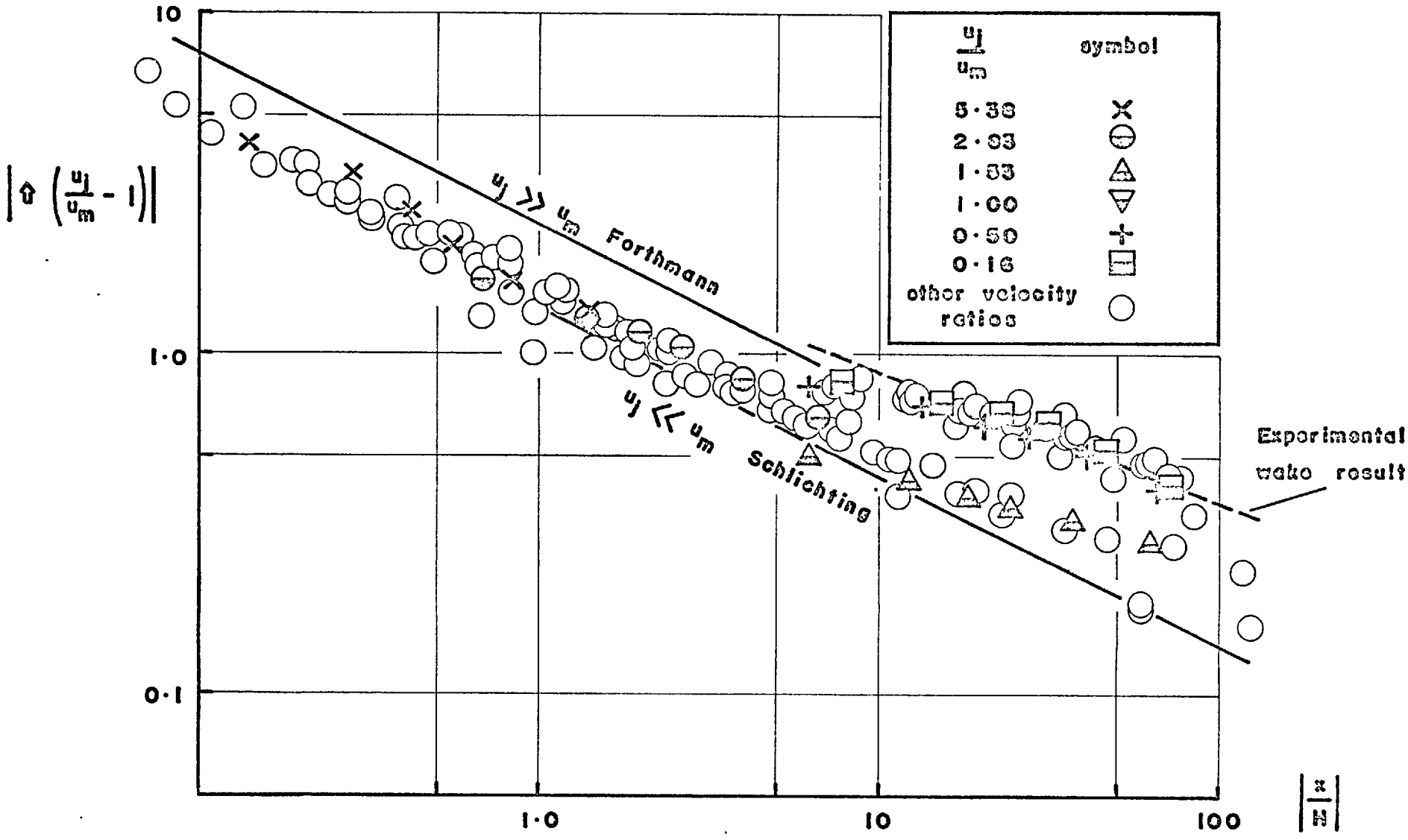


Fig. 5.1(b) Centre-line velocity decay : Series II

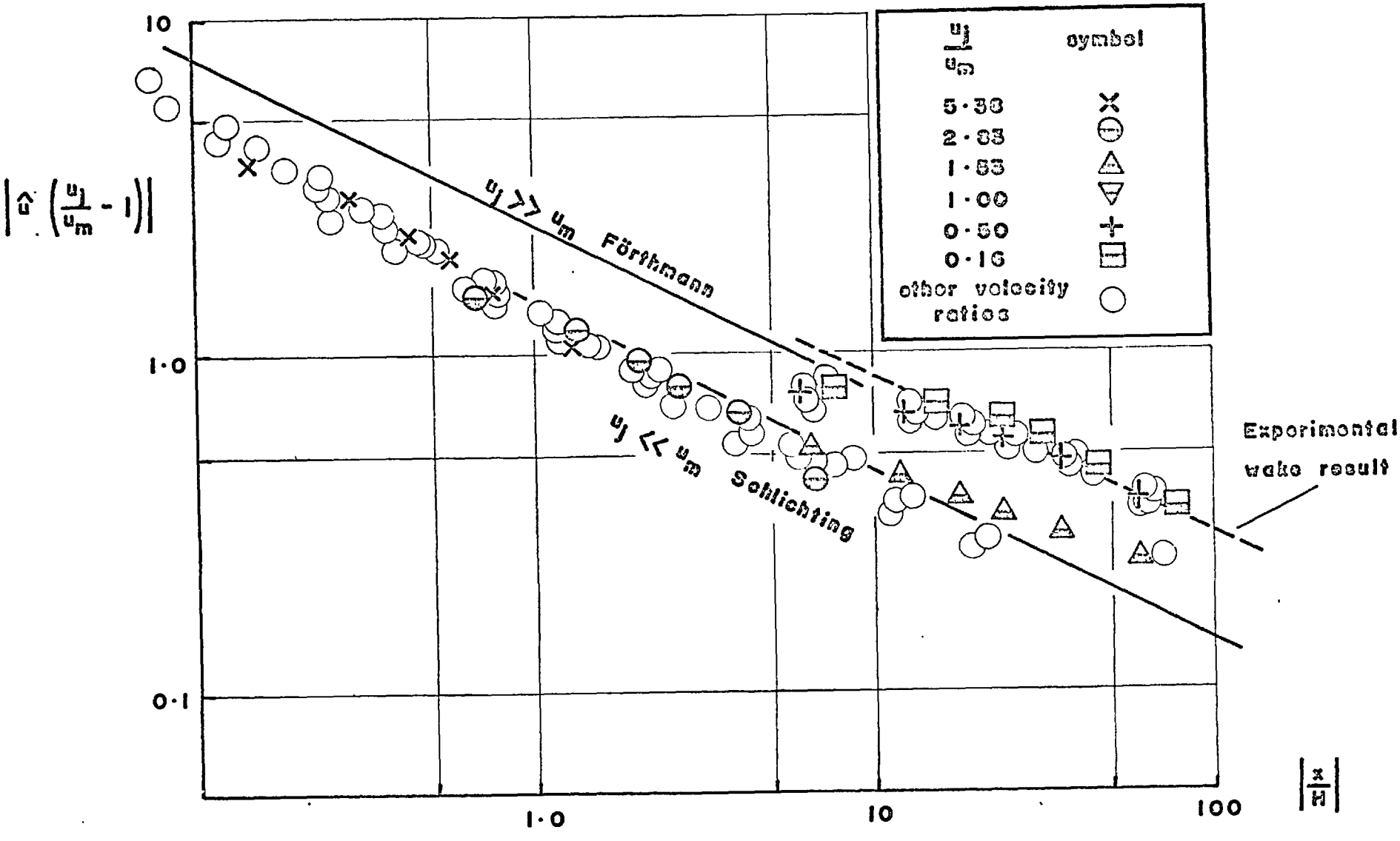


Fig. 5.1(c) Centre-line velocity decay : Series III

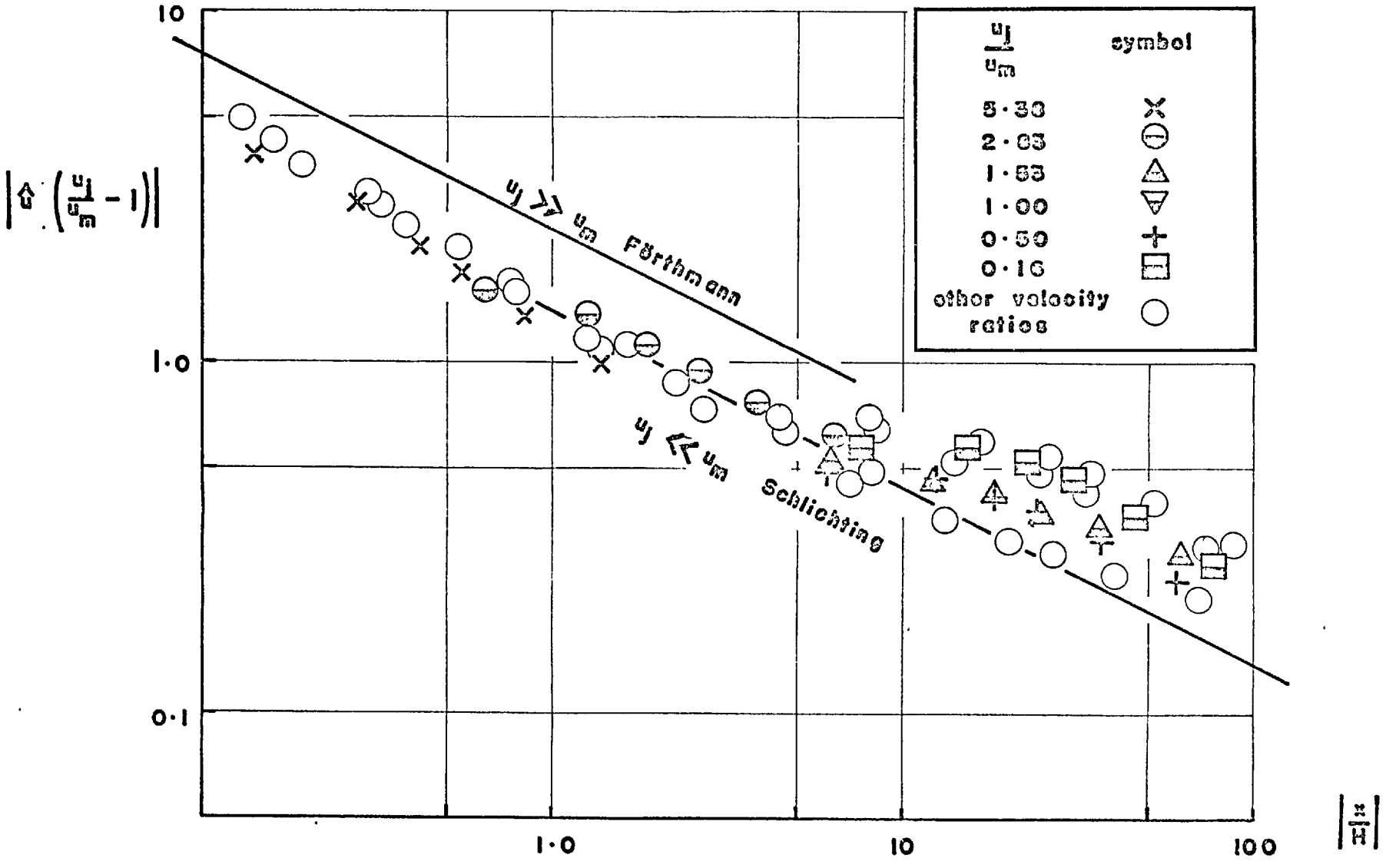


Fig. 5.1(d) Centre-line velocity decay : Series IV

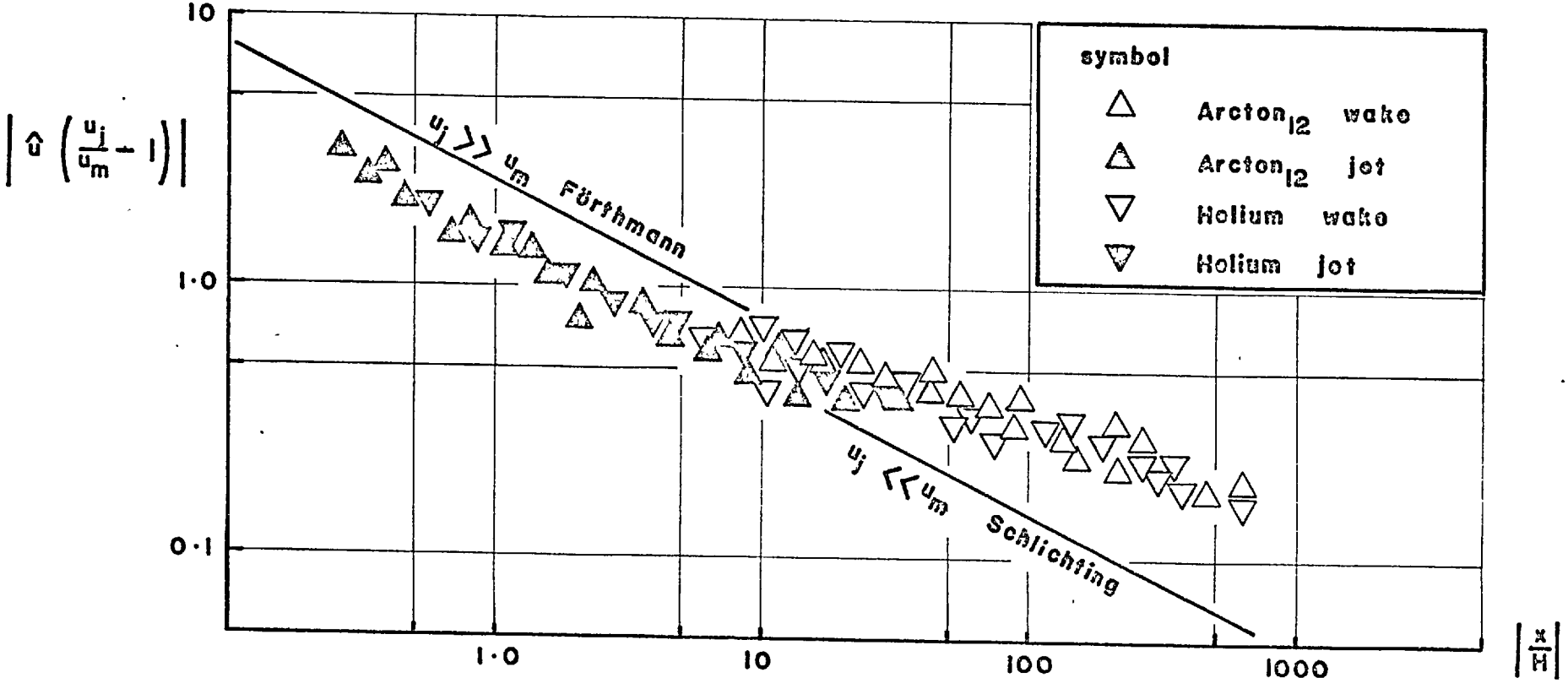


Fig. 5.2 Results of Burns

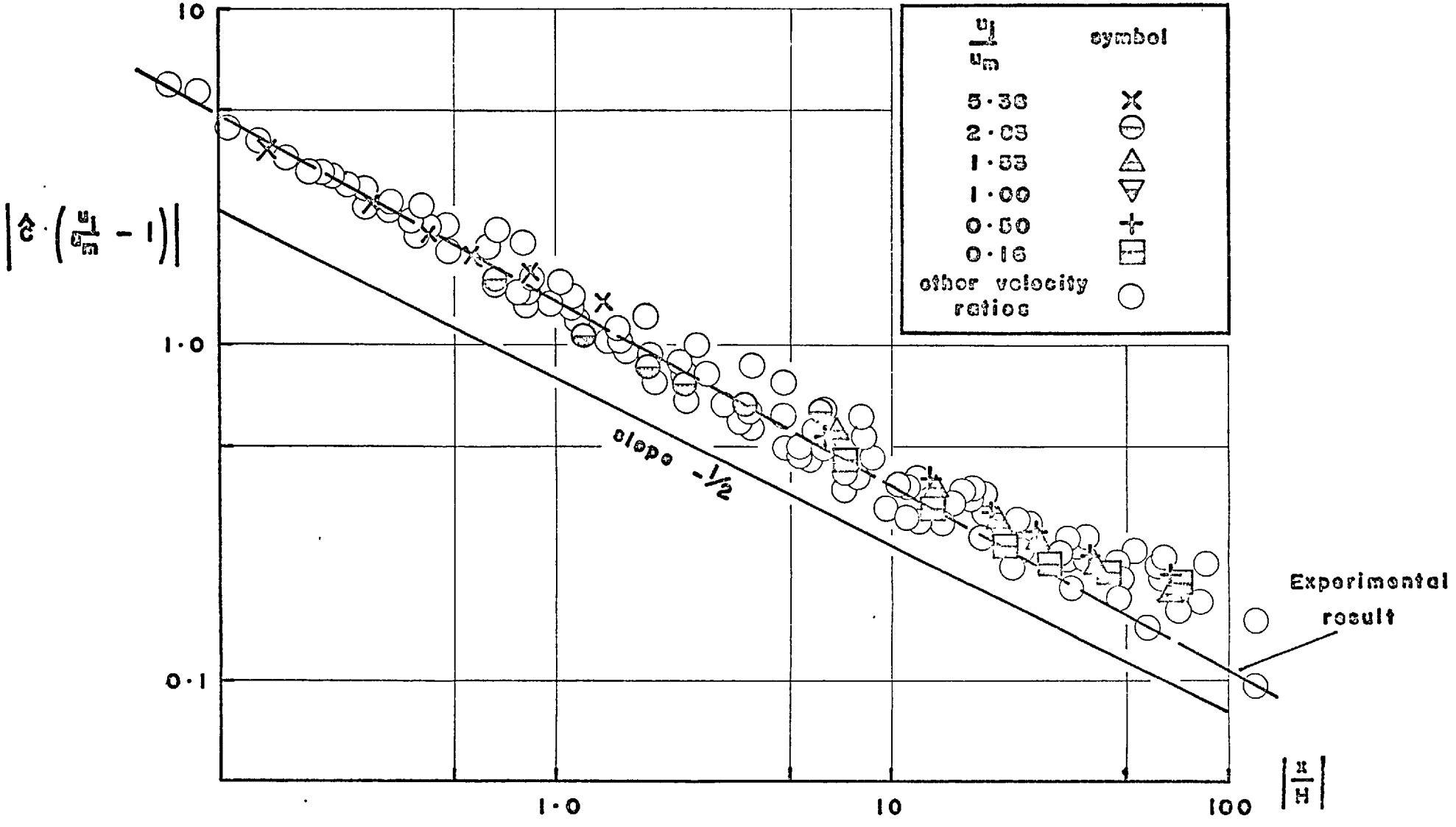


Fig. 5.3(a) Centre-line concentration decay : Series II

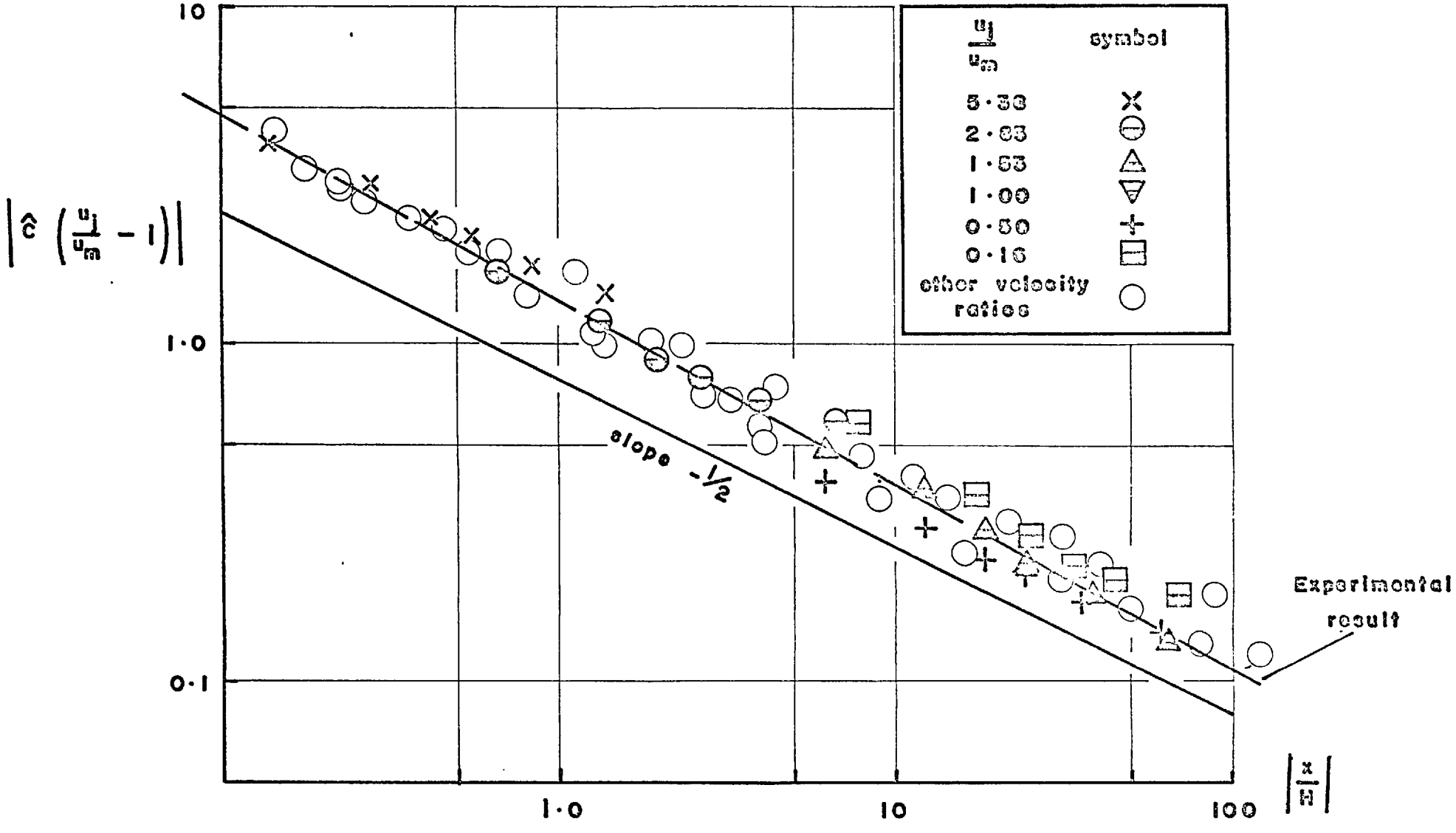


Fig. 5.3 (b) Centre-line concentration decay : Series IV.

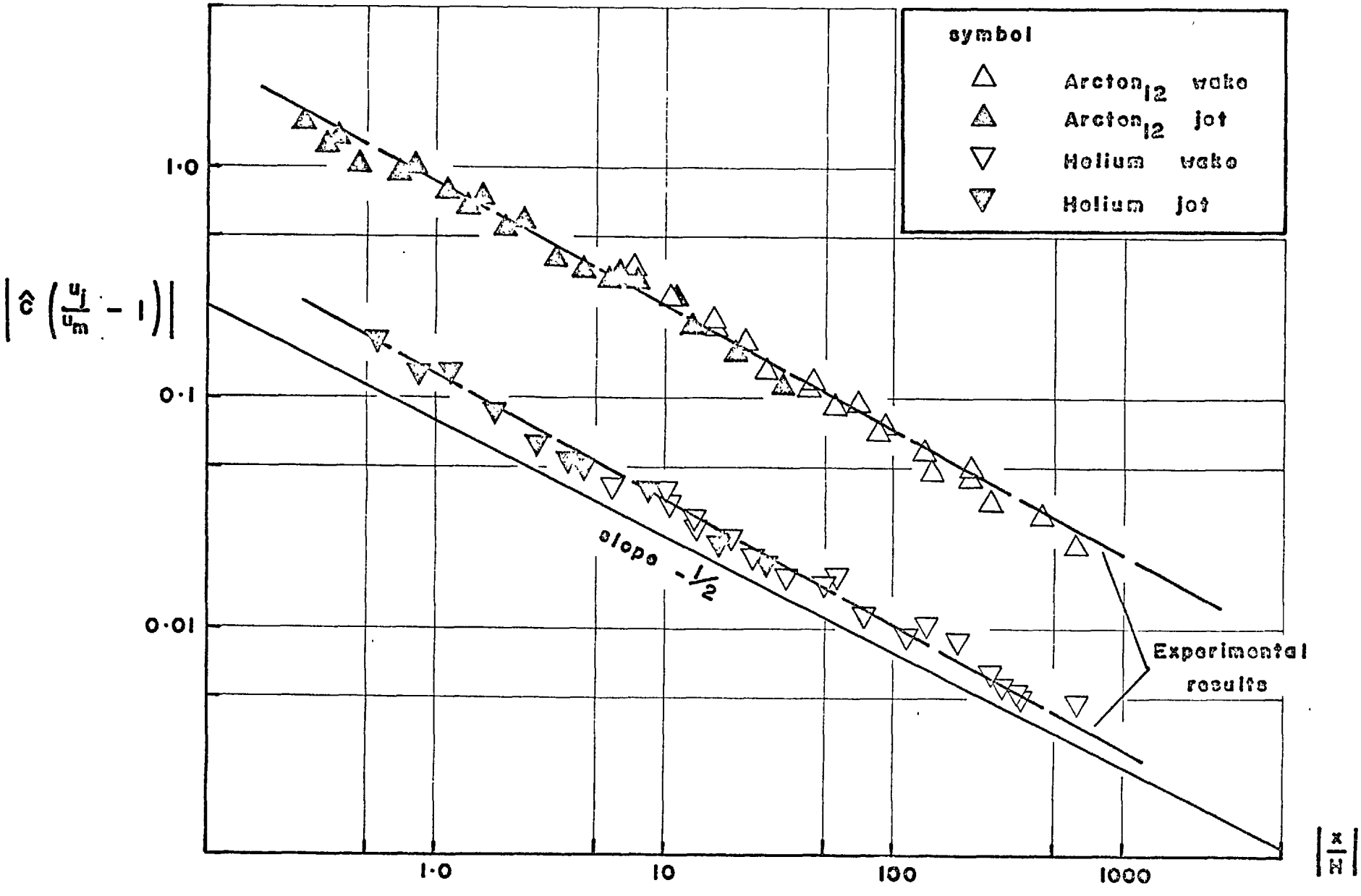


Fig. 5.4 Results of Burns

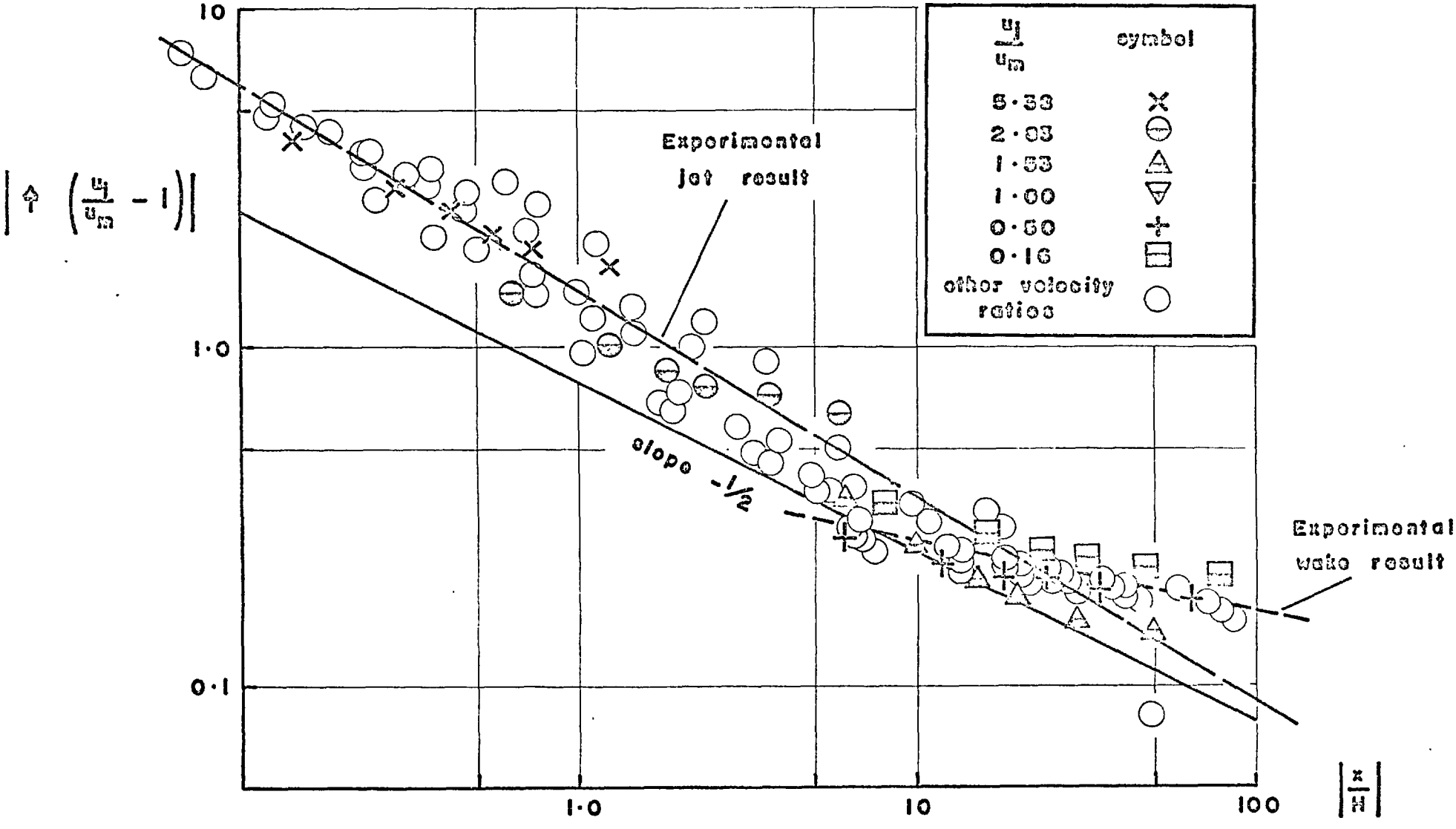


Fig. 5.5 (a) Centre-line temperature decay : Series III

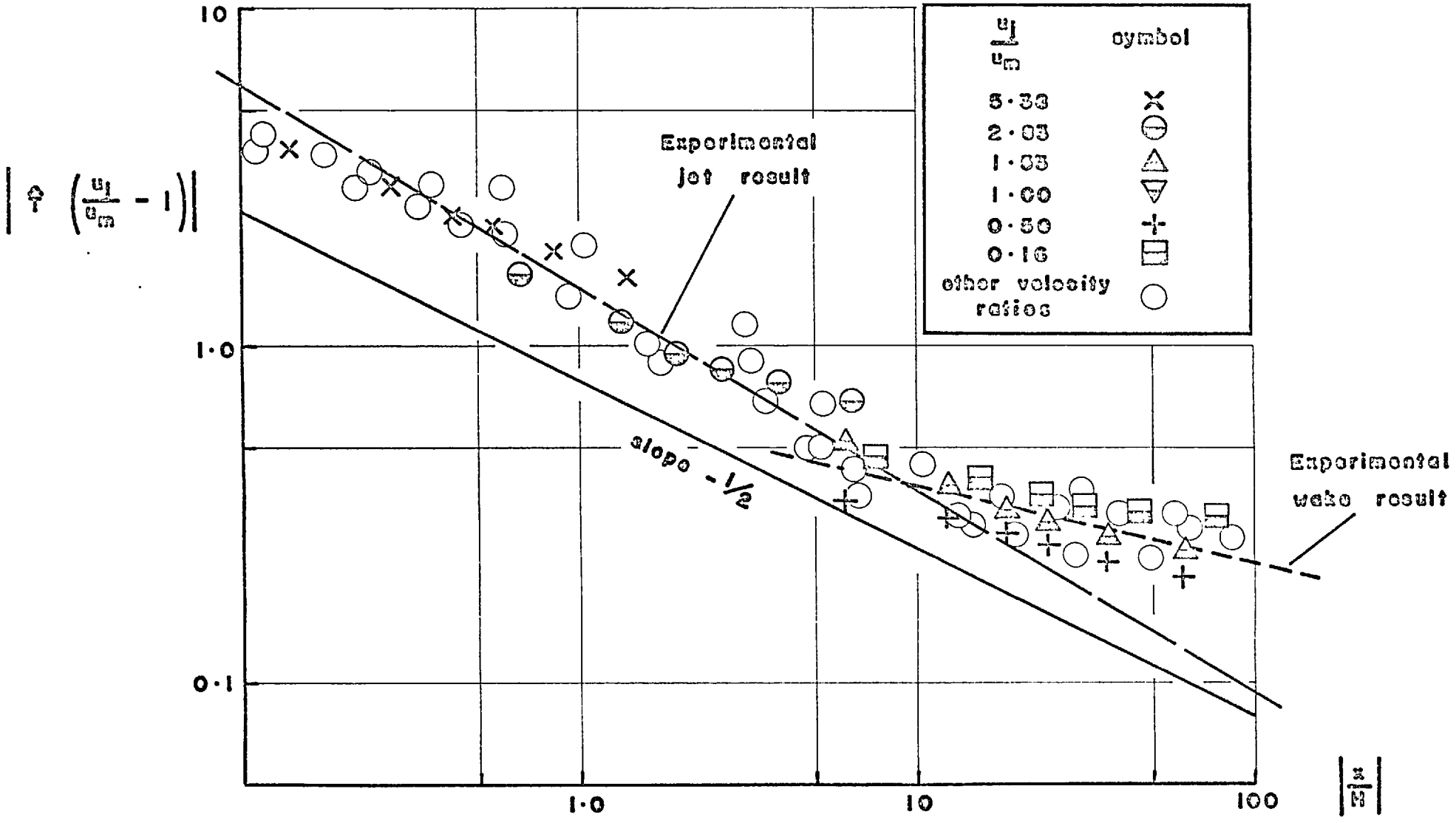


Fig. 5.5 (b) Centre-line temperature decay : Series IV

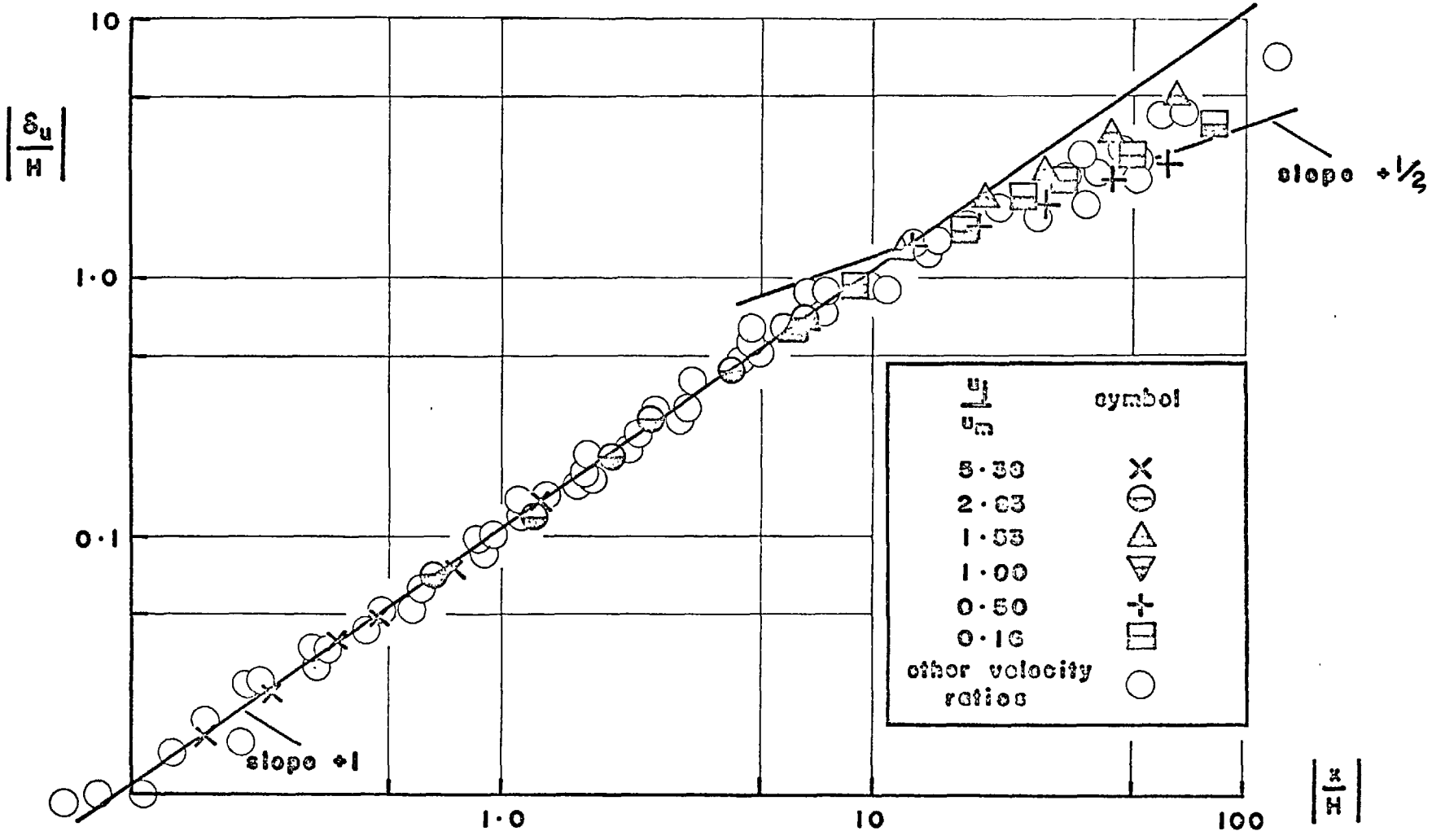


Fig. 5.6 (a) Velocity spread : Series I

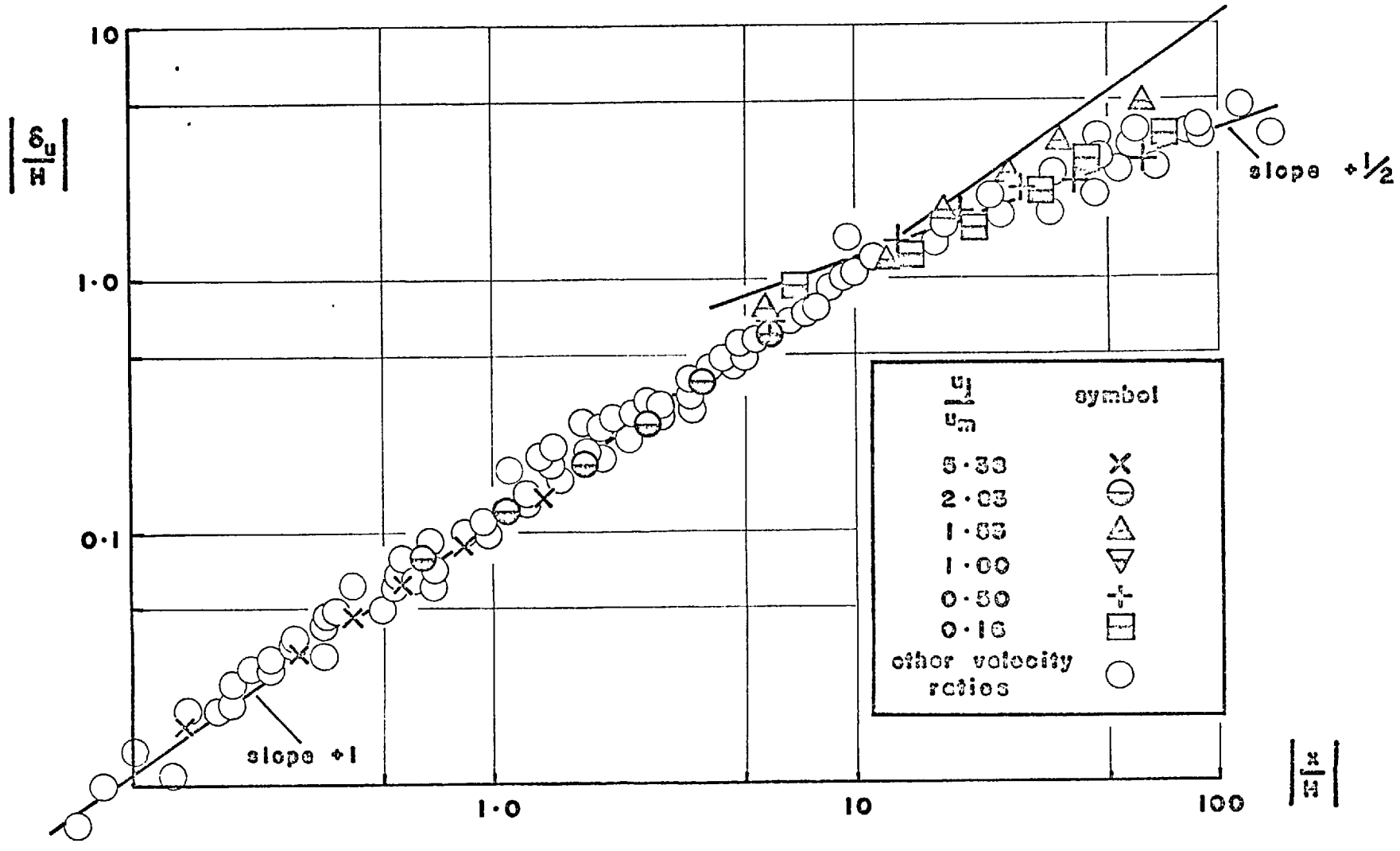


Fig. 5.6 (b) Velocity spread : Series II

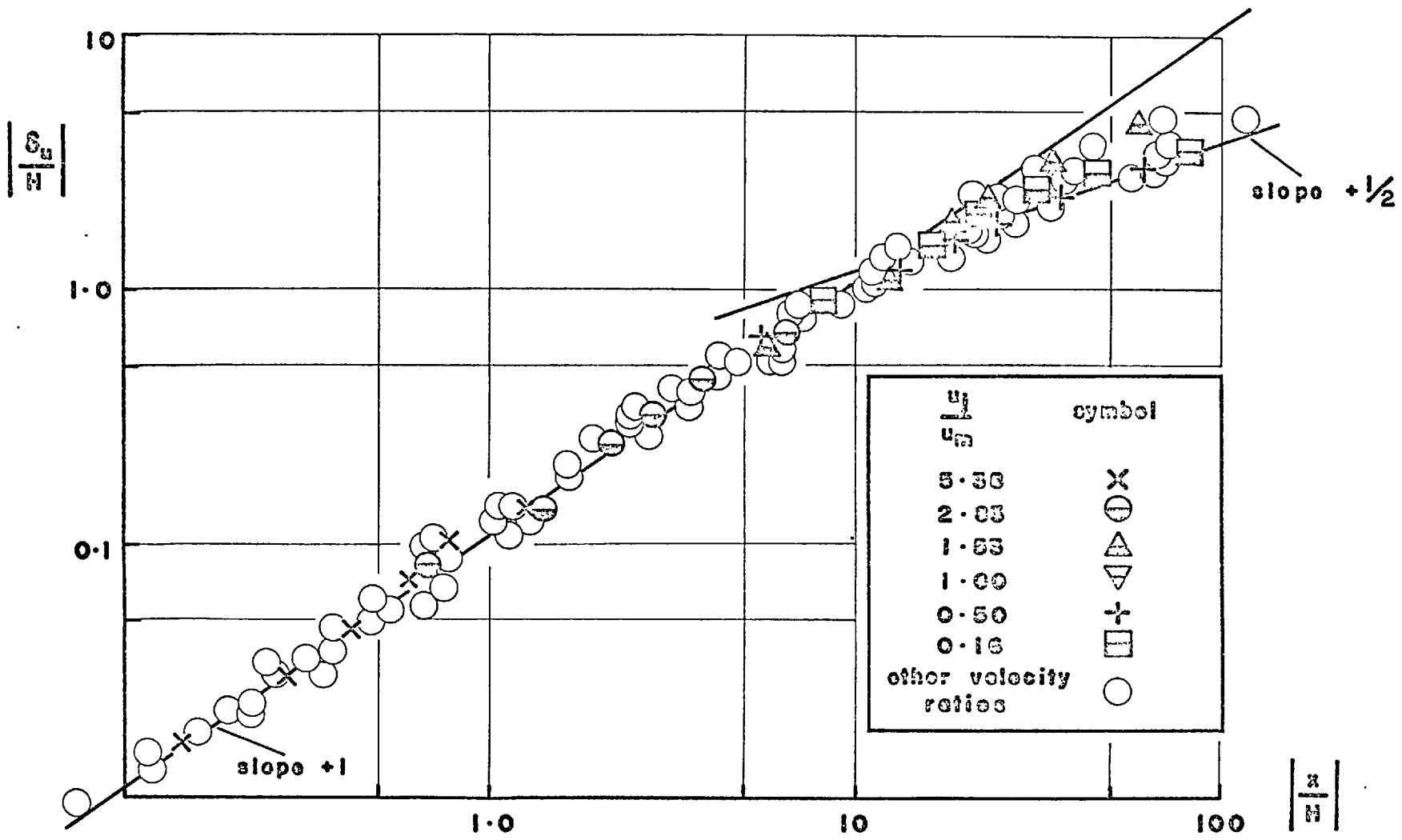


Fig. 5.6 (c) Velocity spread : Series III

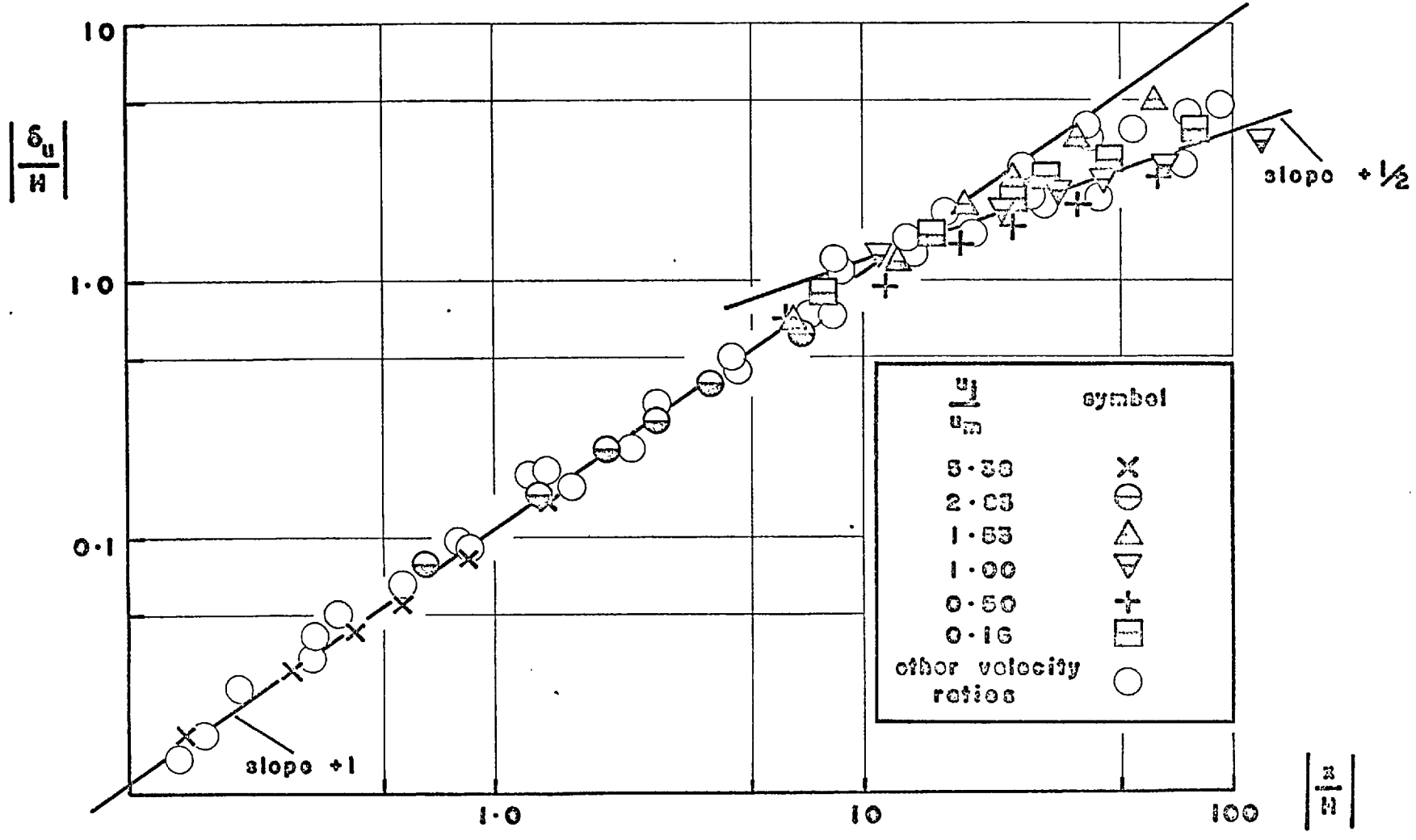


Fig. 5.6 (d) Velocity spread : Series IV

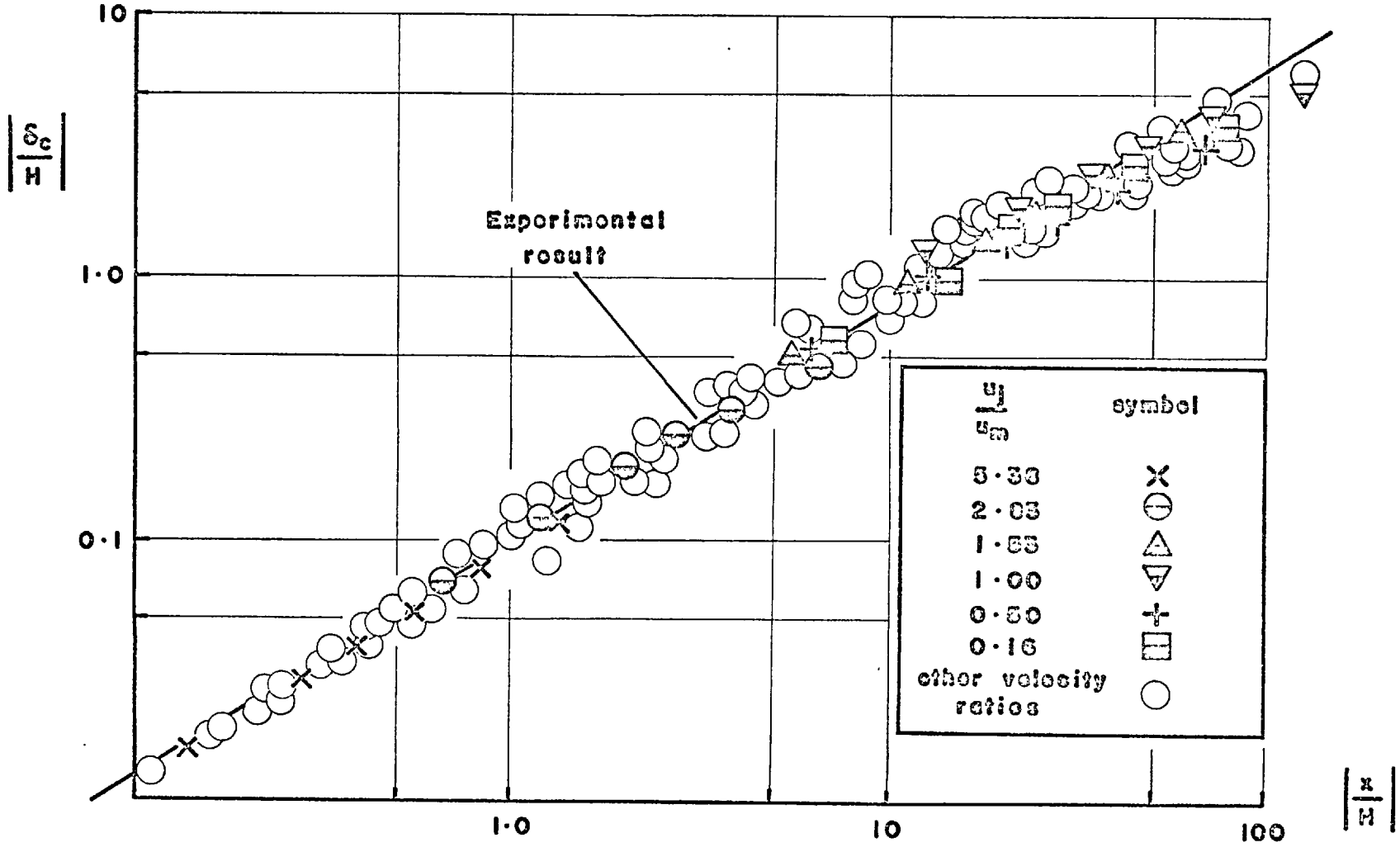


Fig. 5.7 (a) Concentration spread : Series II

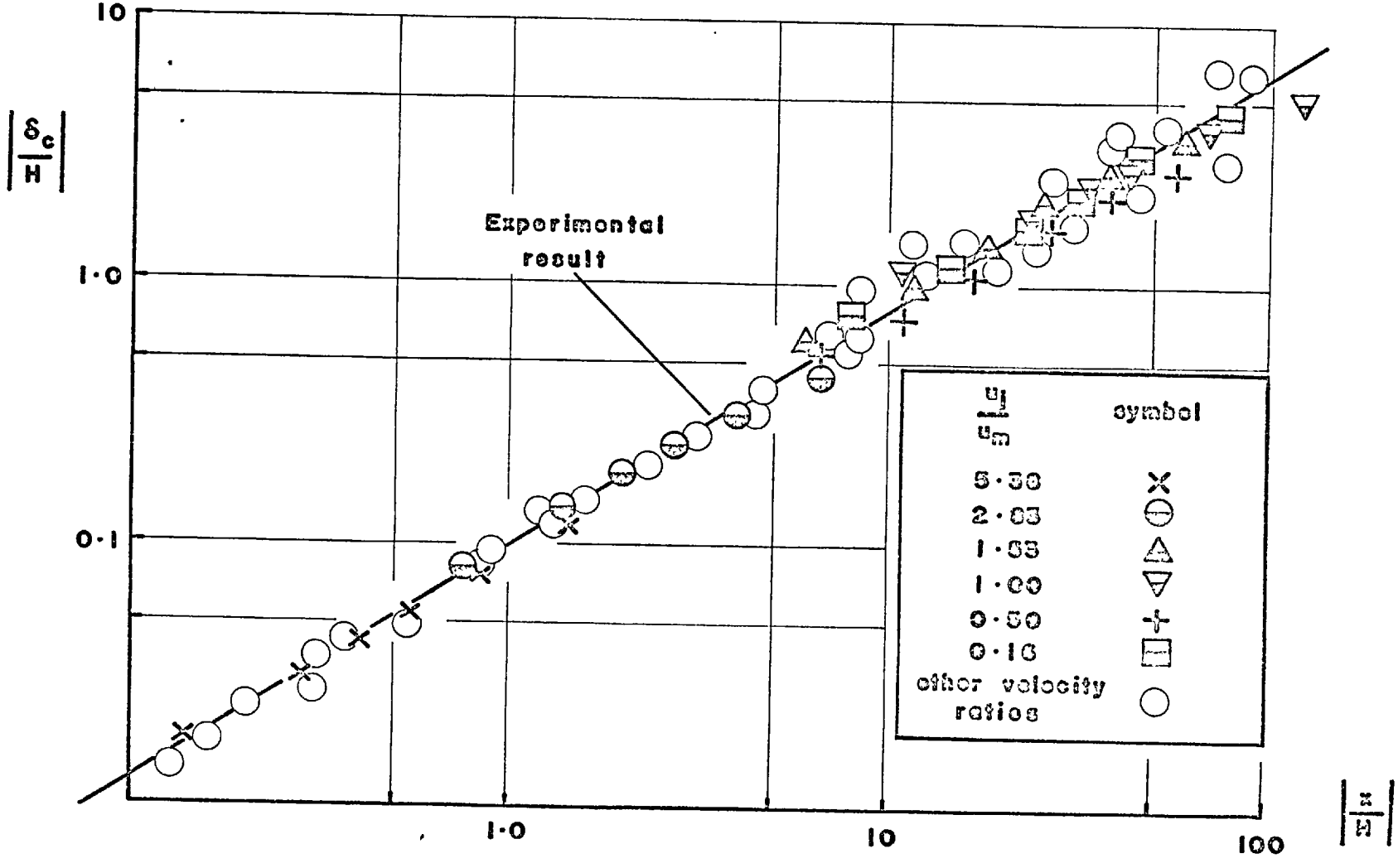


Fig. 5.7 (b) Concentration spread : Series IV

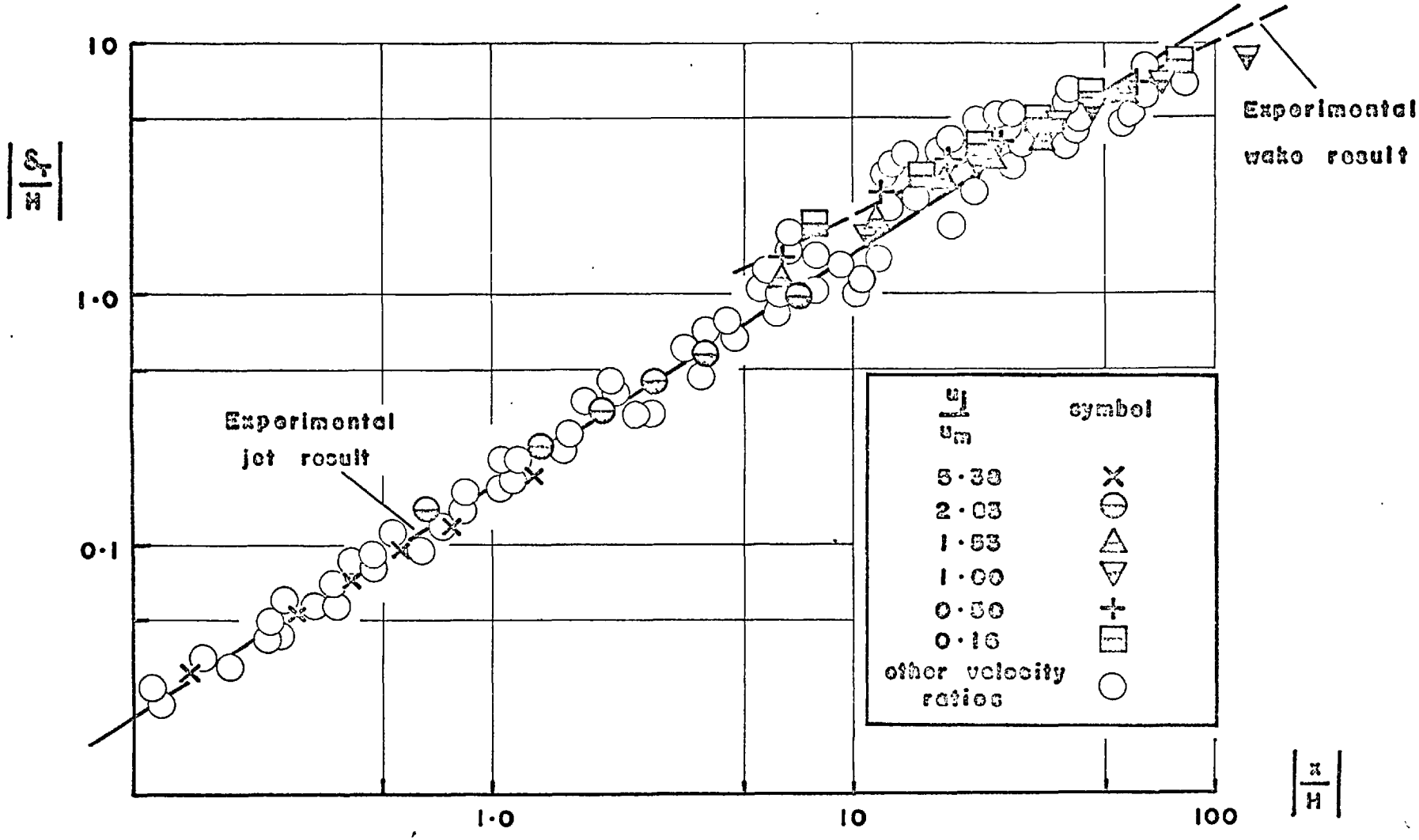


Fig. 5.8 (a) Temperature spread : Series III

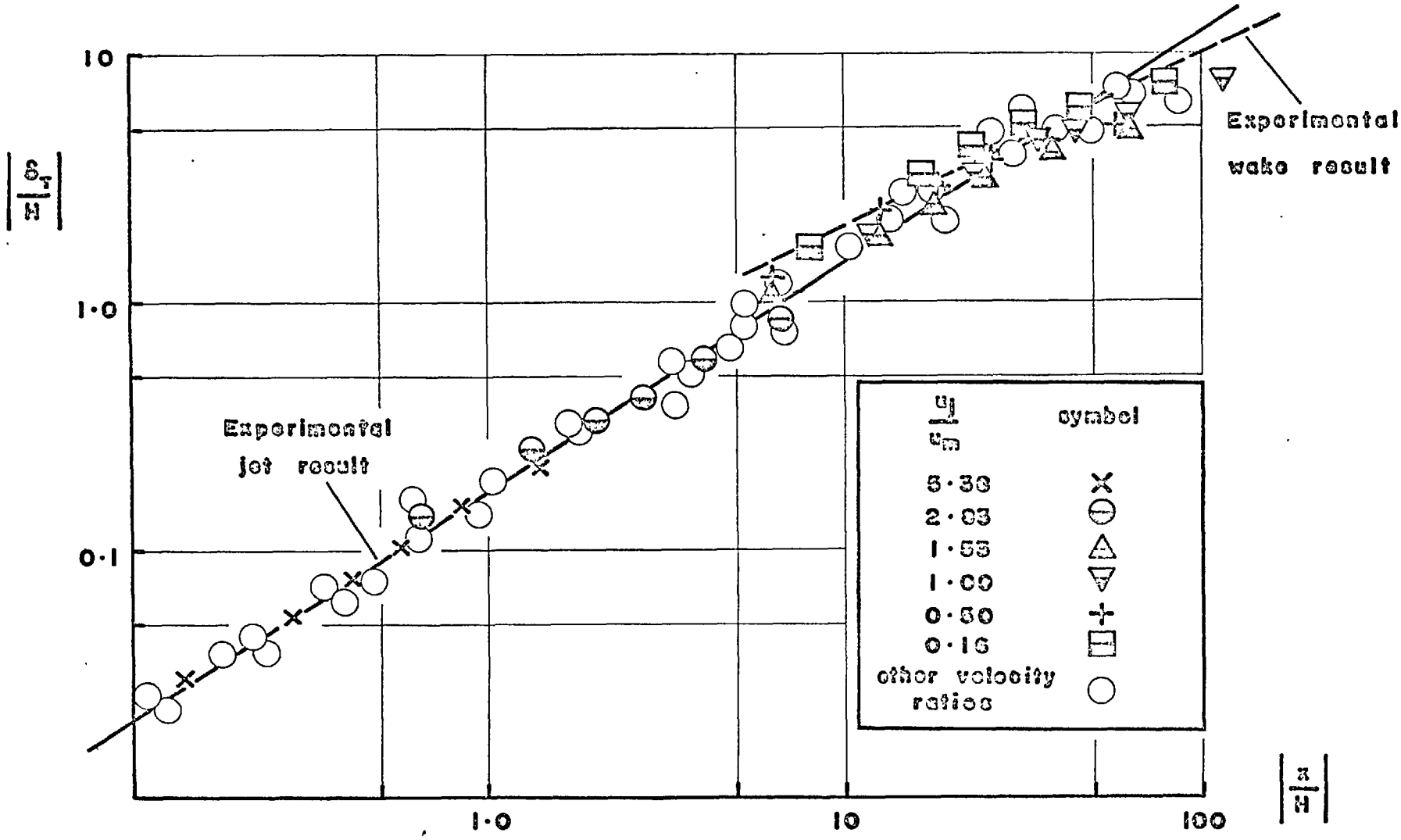


Fig. 5.8 (b) Temperature spread : Series IV

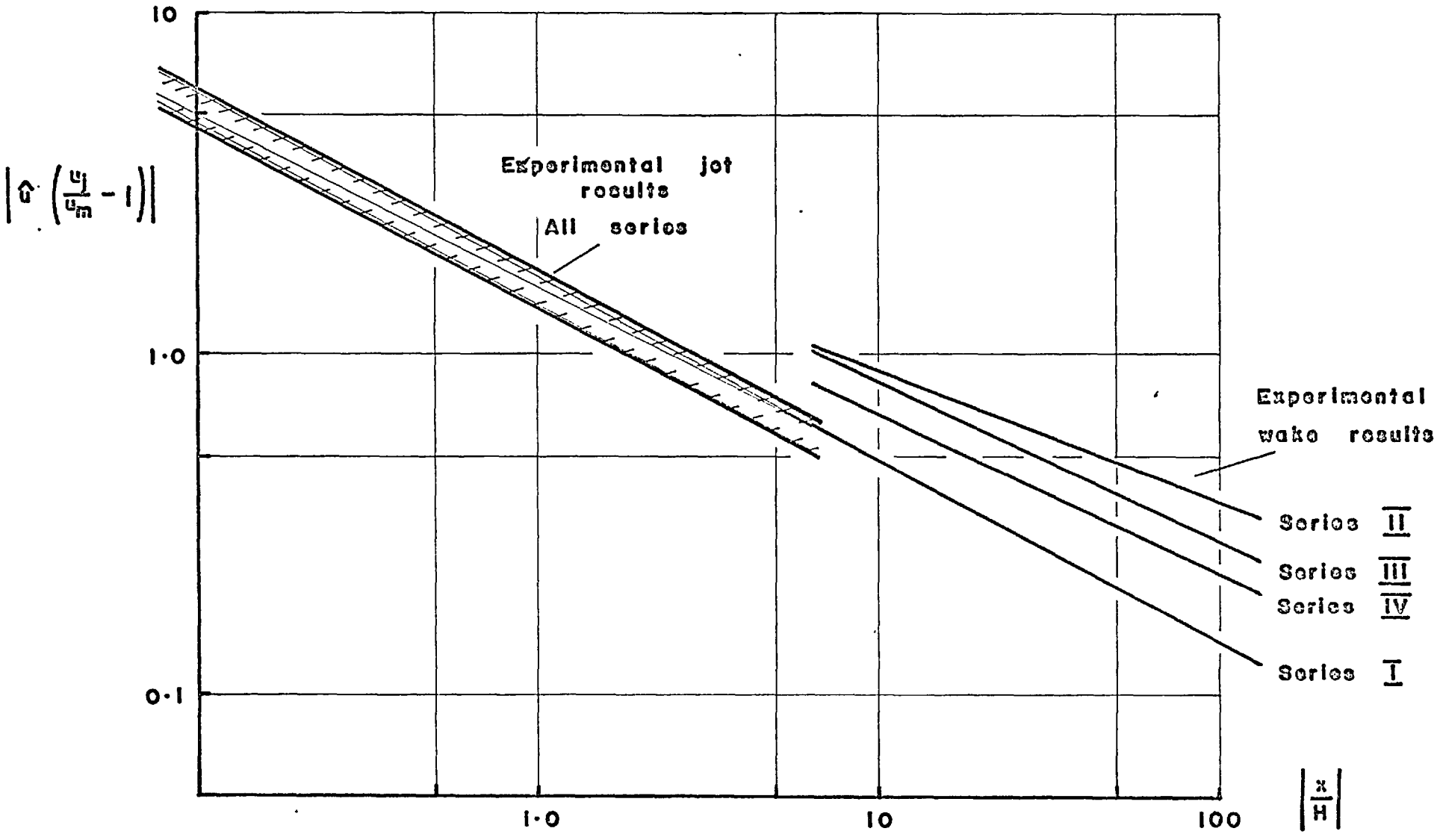


Fig. 5.9(a) Summary of centre-line velocity decays

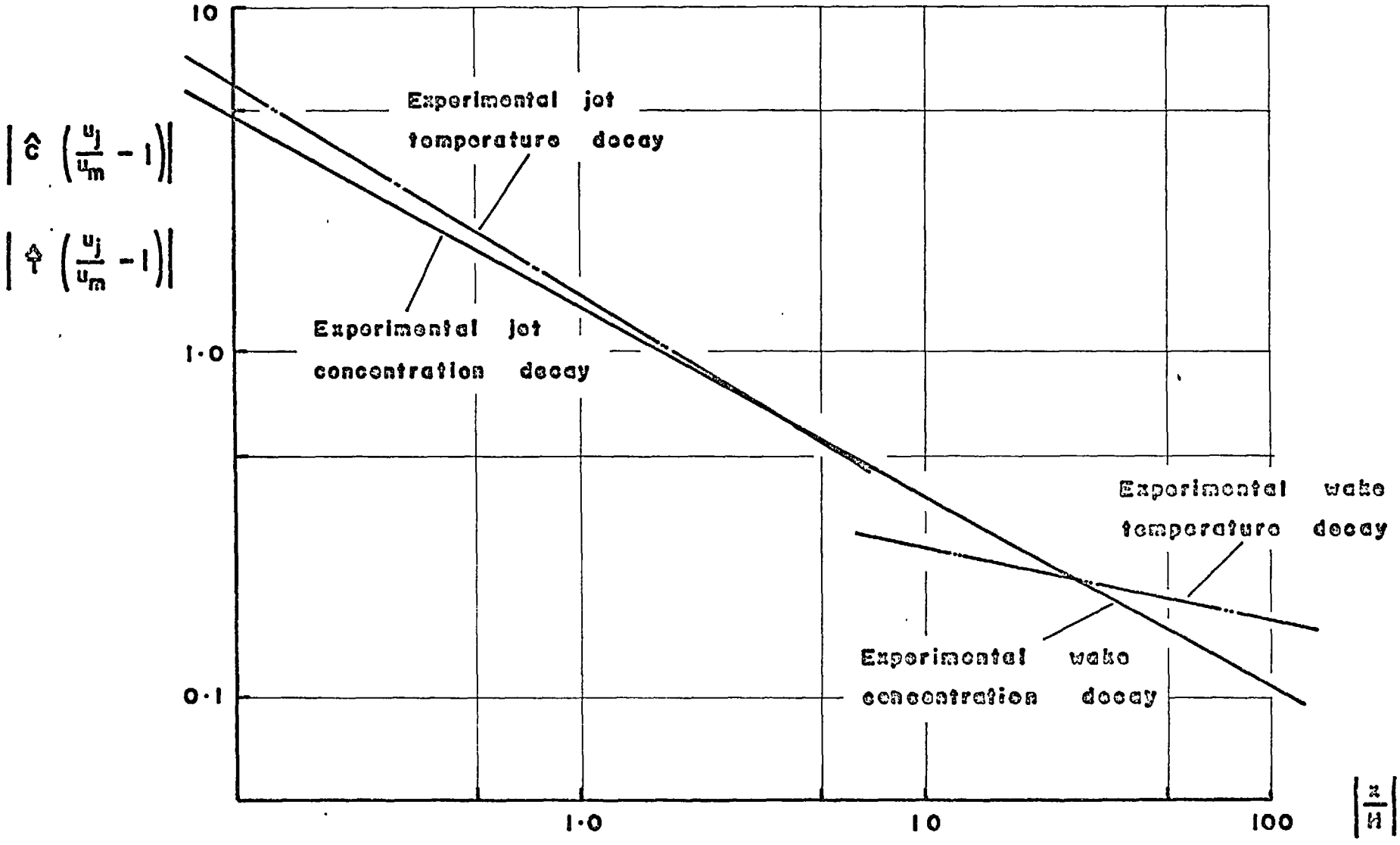


Fig. 5.9 (b) Comparison of concentration and temperature decays

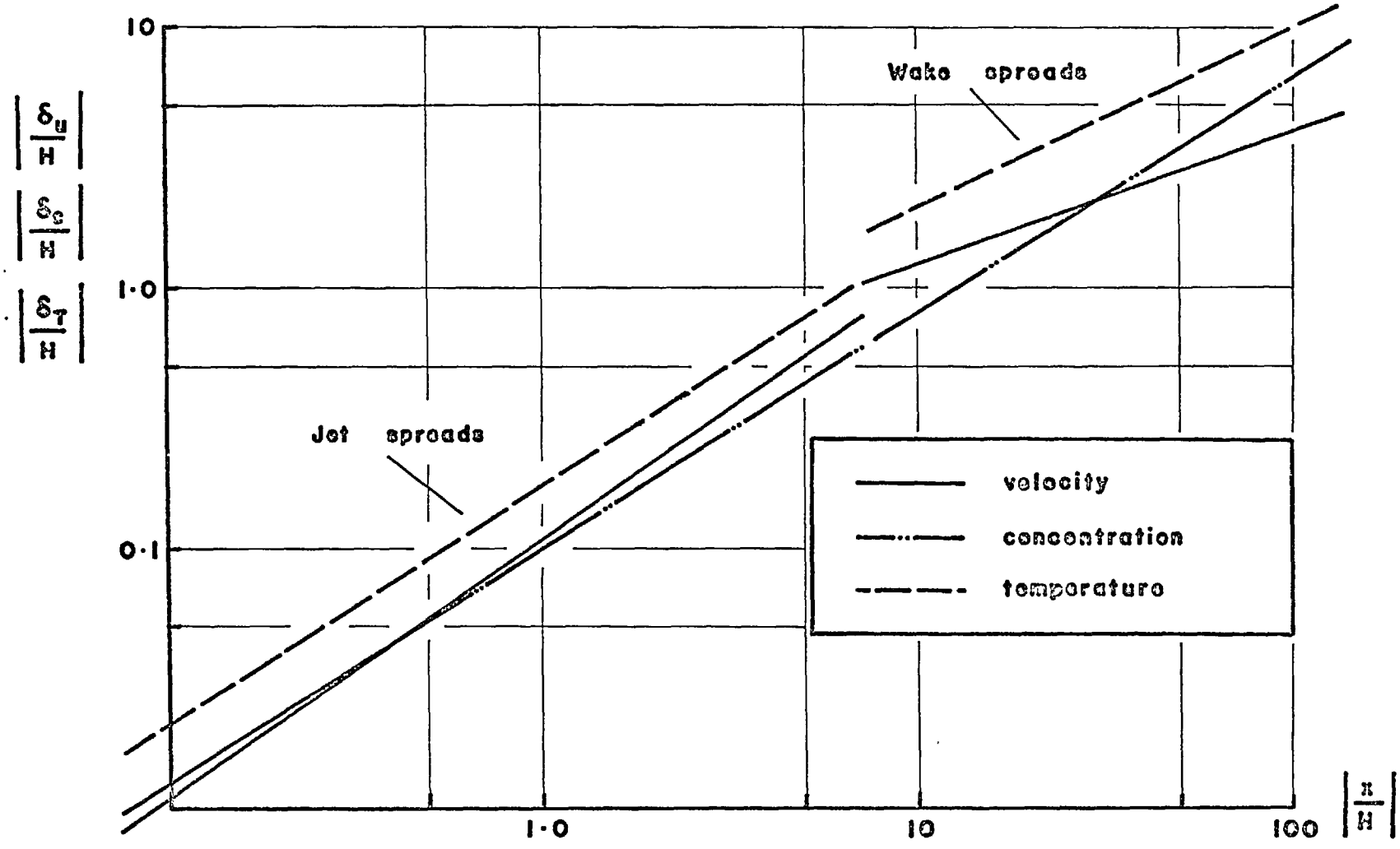


Fig. 5.9 (c) Comparison of jet and wake spreads of velocity , concentration and temperature

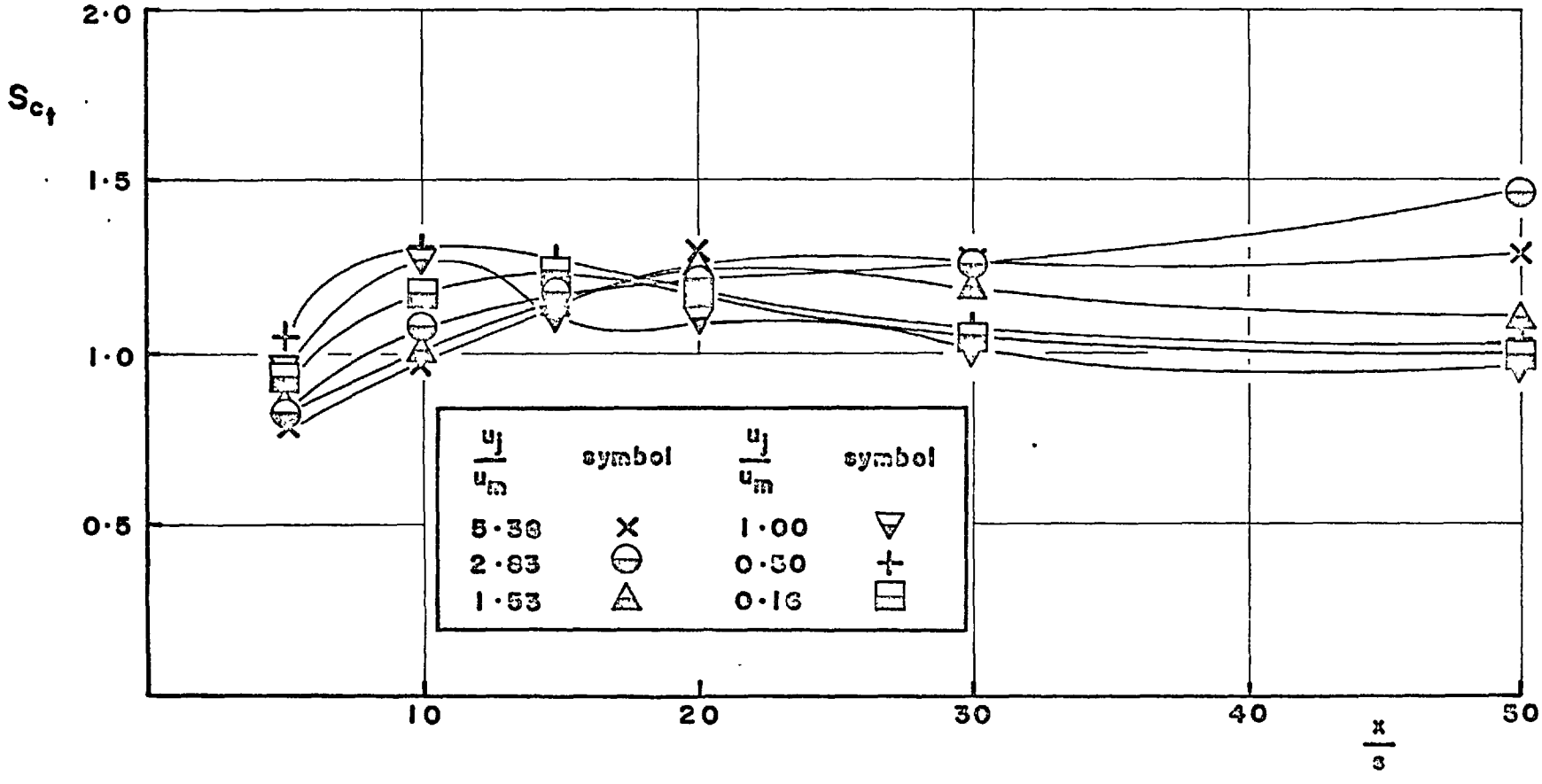


Fig. 5.10 (a) Turbulent Schmidt number along axis : Simple theory

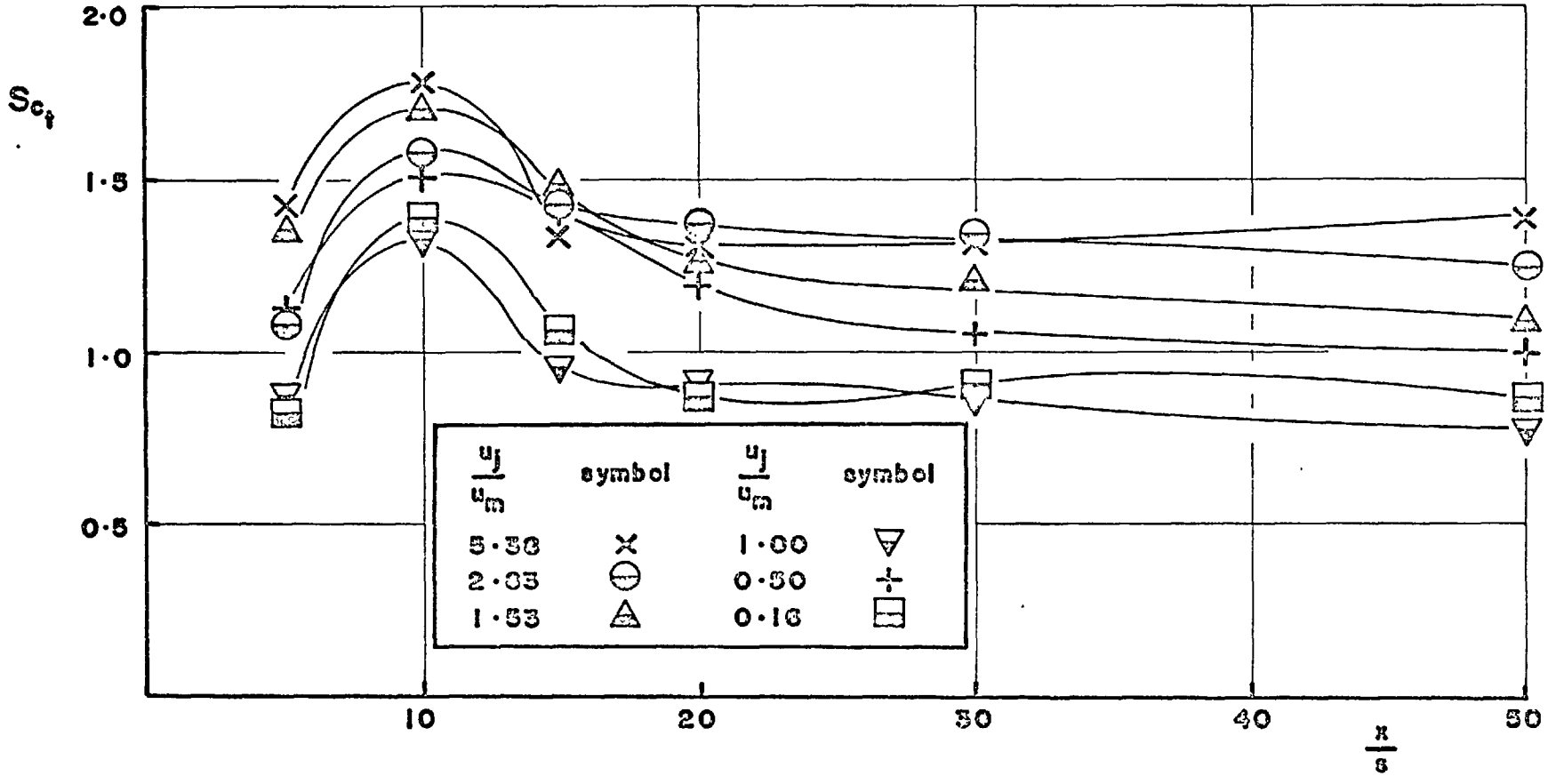


Fig. 5.10 (b) Turbulent Schmidt number along axis : Forstall & Shapiro

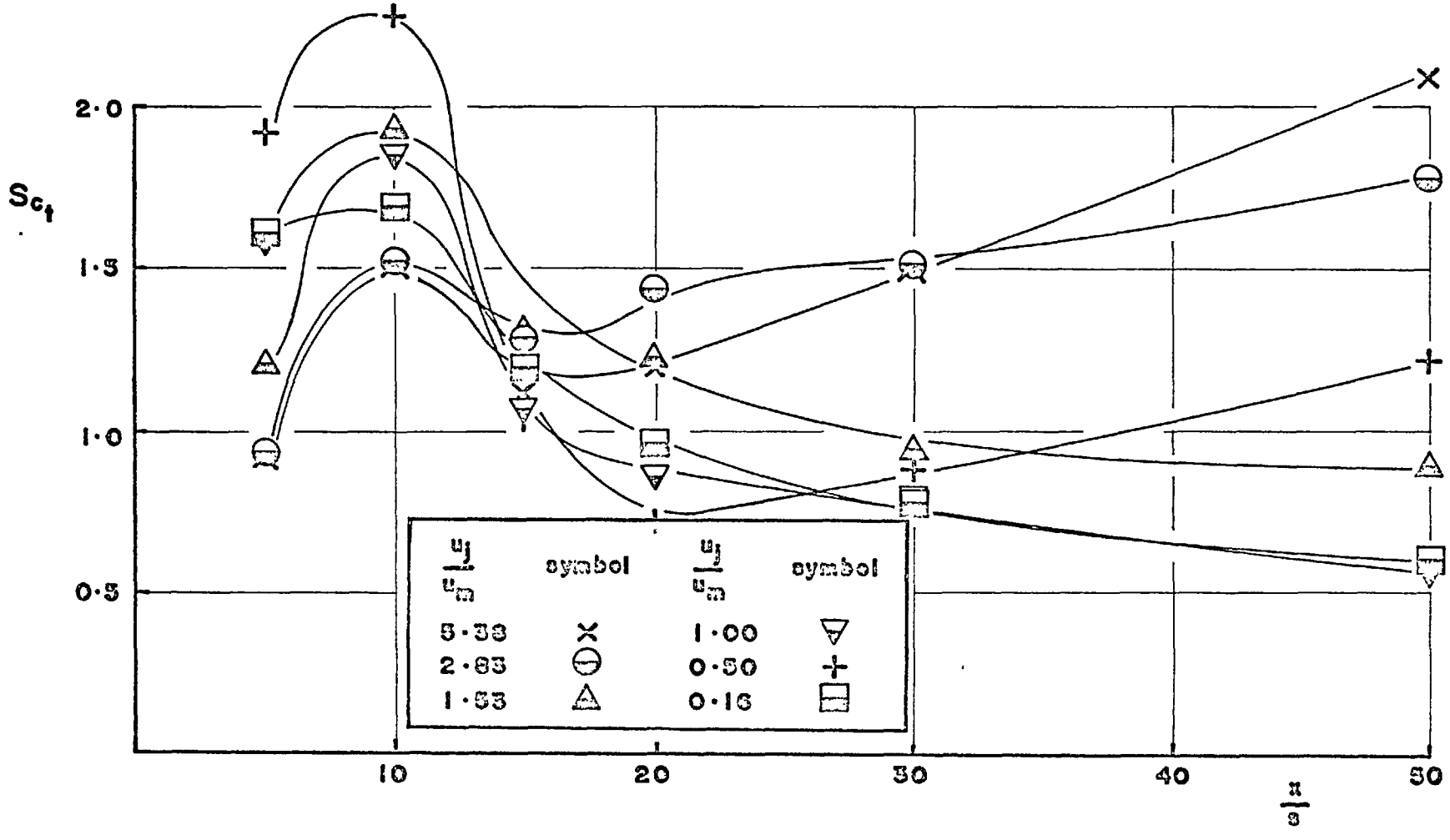


Fig. 5.10 (c) Turbulent Schmidt number along axis : Zakkay et al

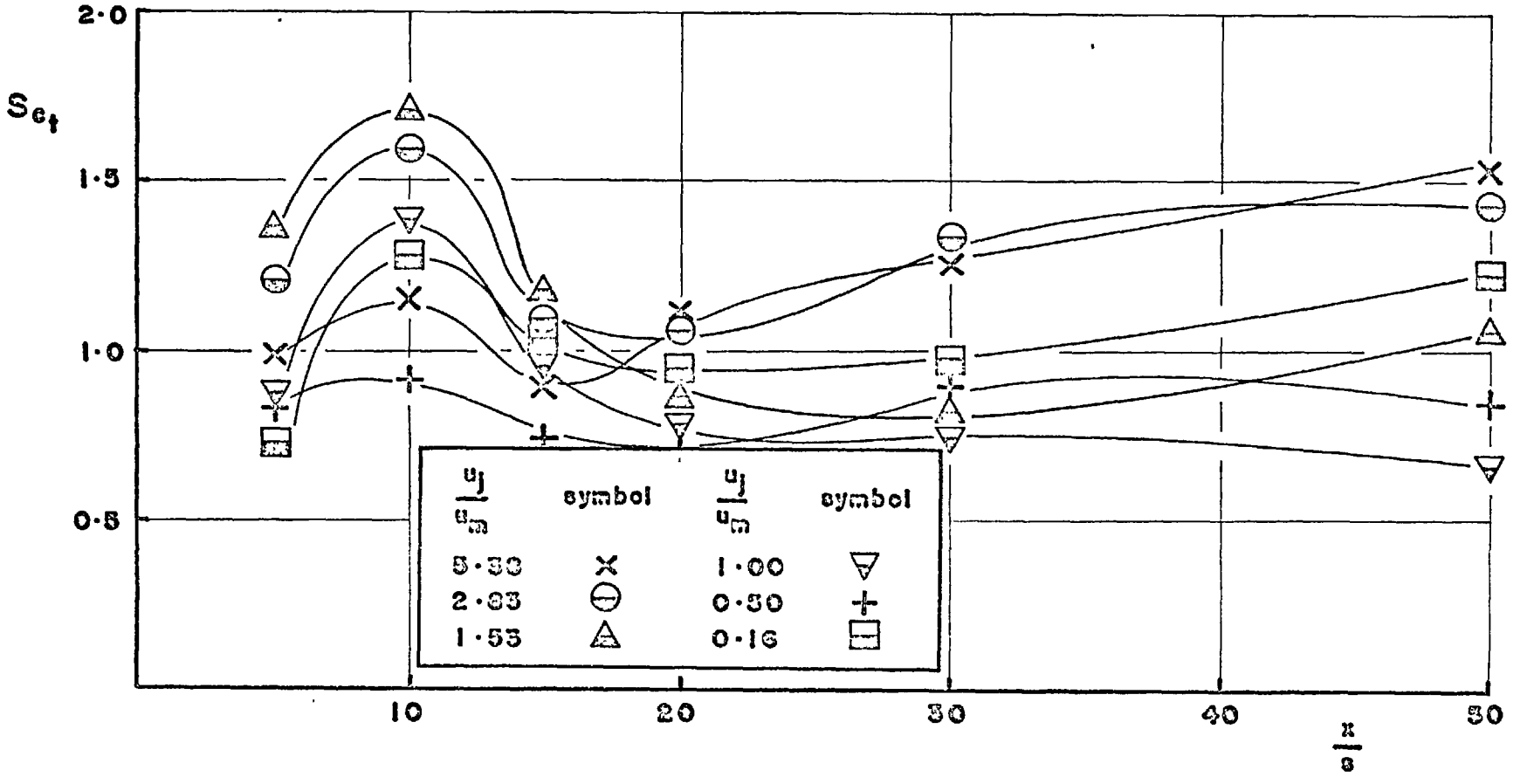


Fig. 5.10(d) Turbulent Schmidt number along axis : Morkovin

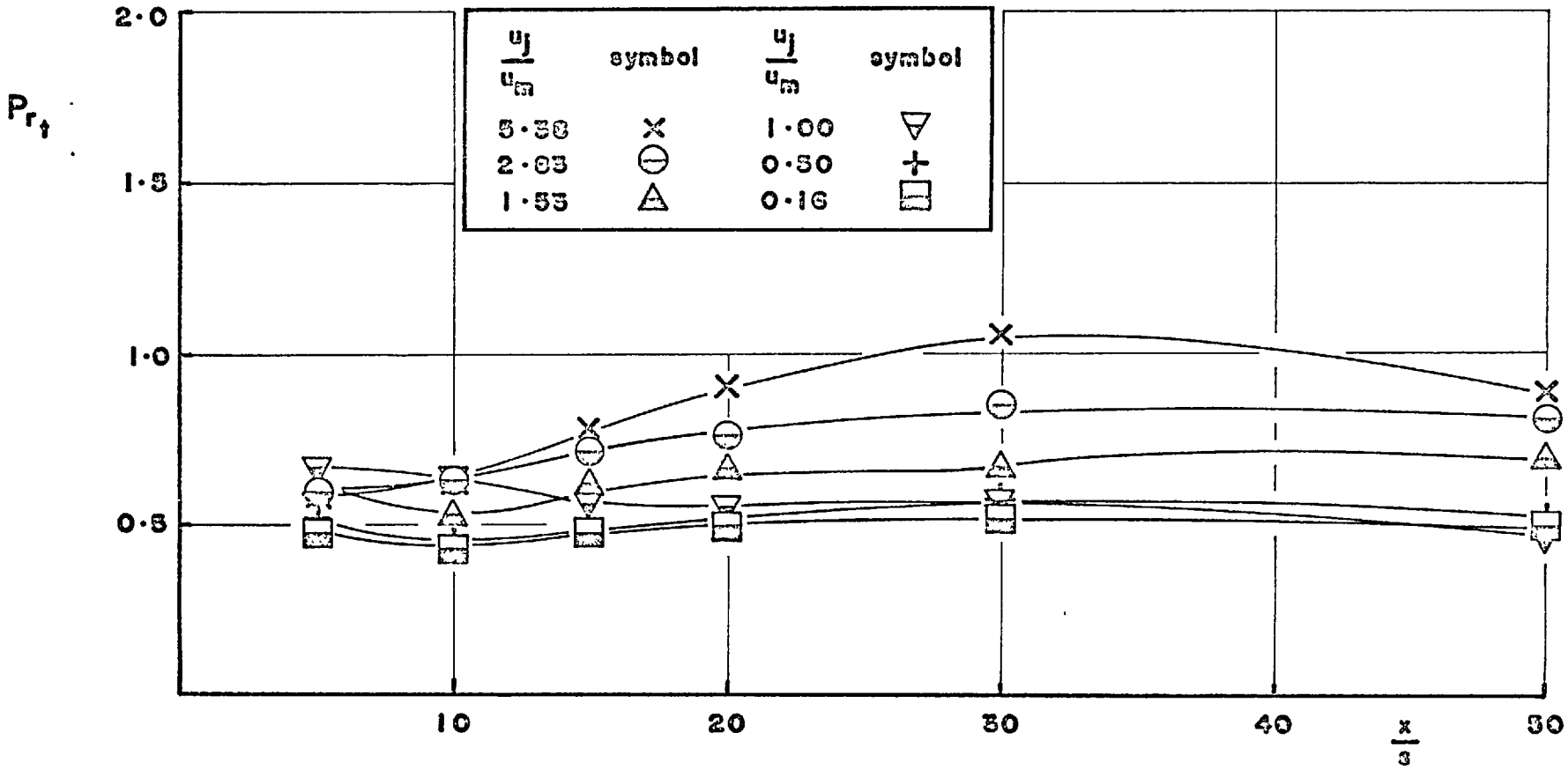


Fig. 5.11(a) Turbulent Prandtl number along axis : Simple theory

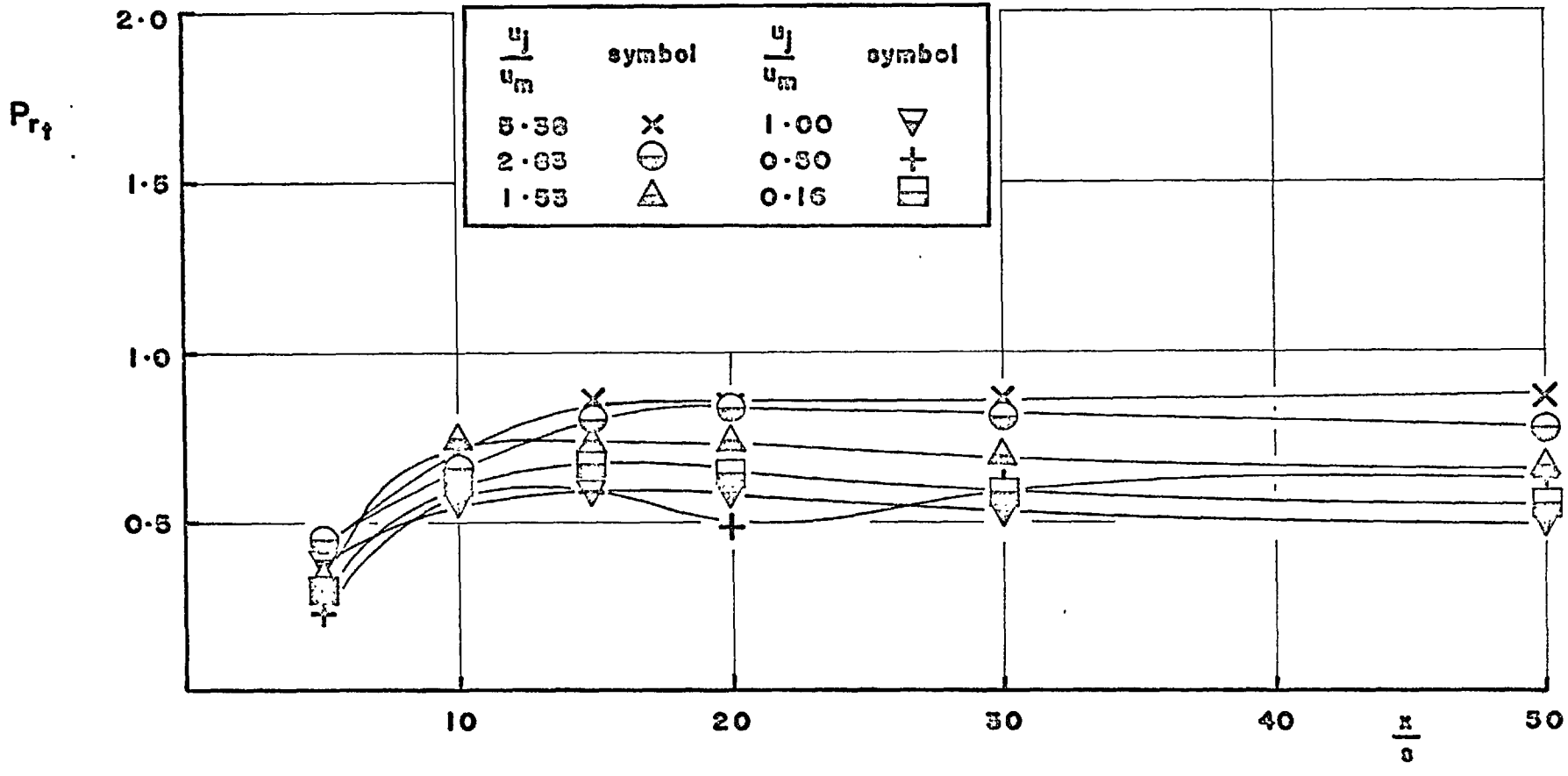


Fig. 5.11(b) Turbulent Prandtl number along axis : Forstall & Shapiro

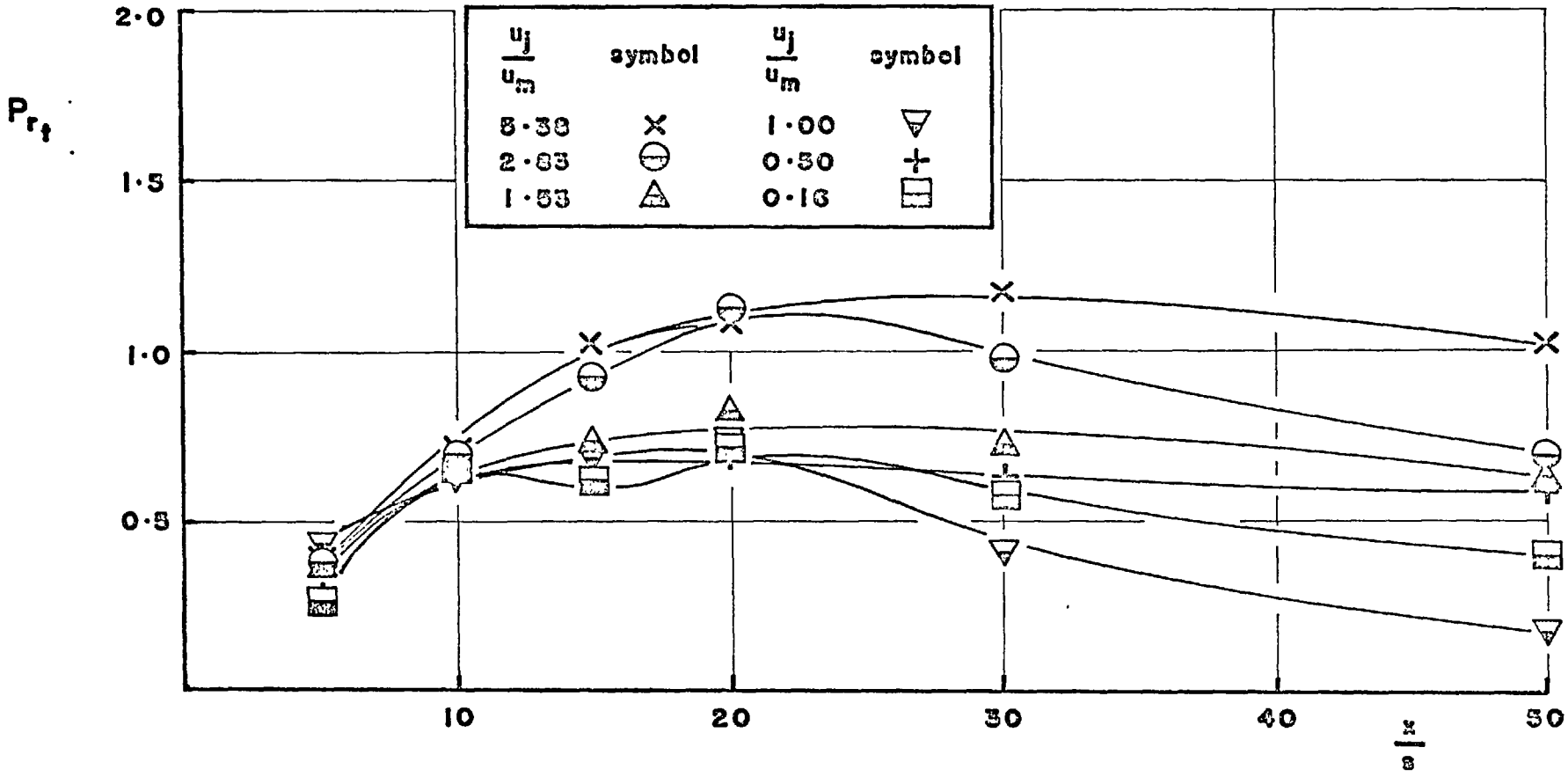


Fig. 5.11 (c) Turbulent Prandtl number along axis : Zakkay et al

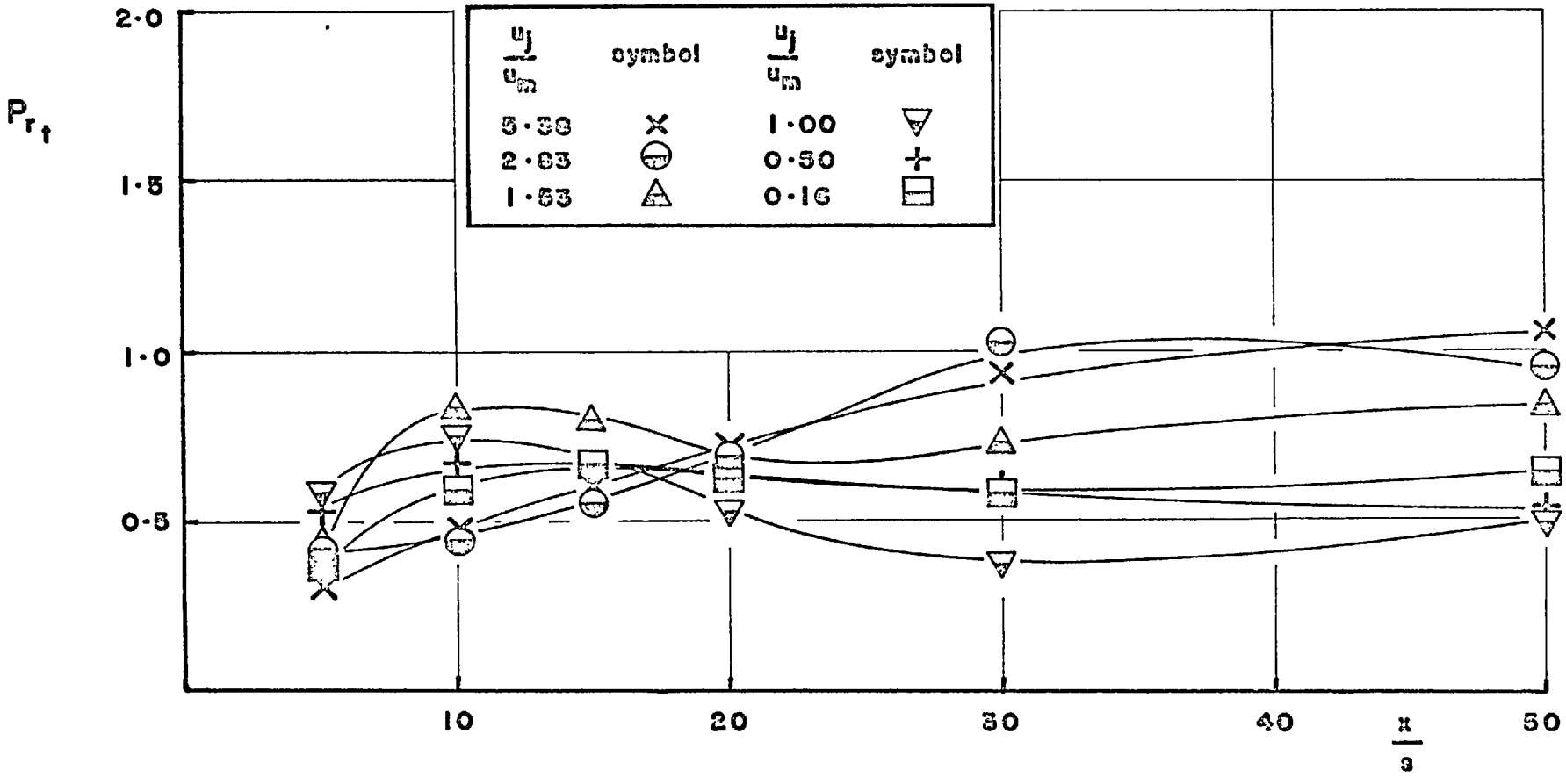


Fig. 5.11 (d) Turbulent Prandtl number along axis : Morkovin

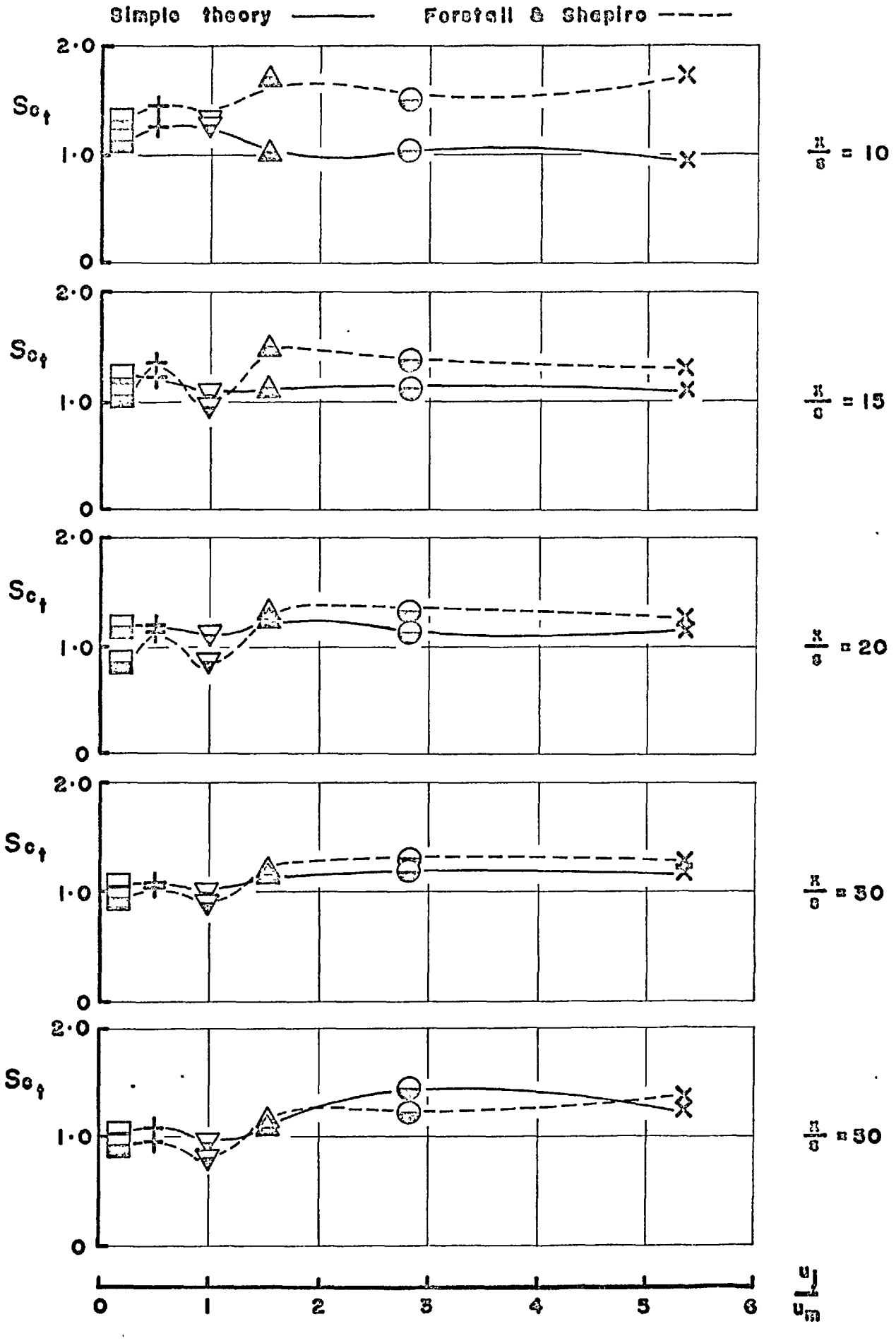


Fig. 5.12 Sc_t against velocity ratio

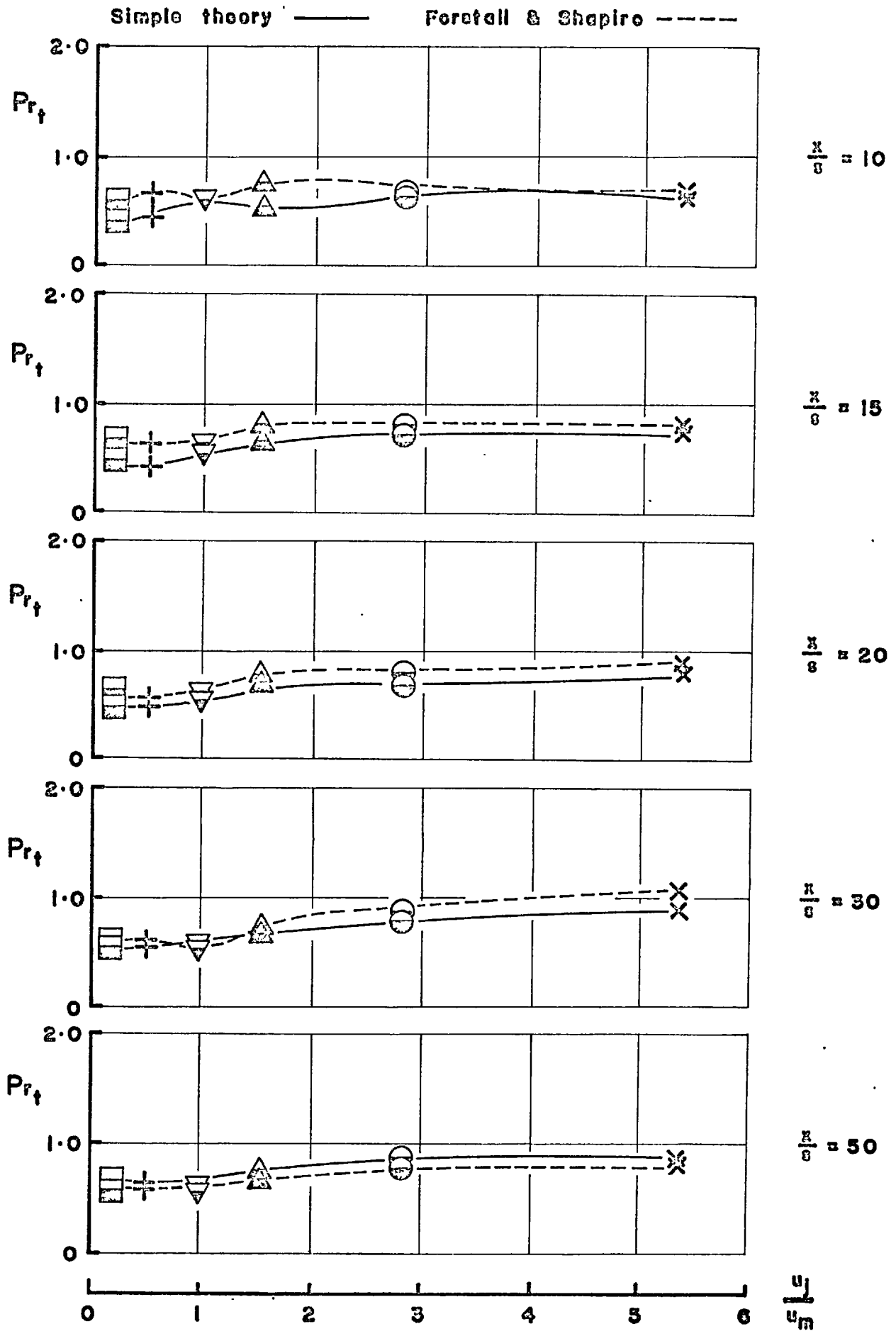


Fig. 5.13 Pr_t against velocity ratio

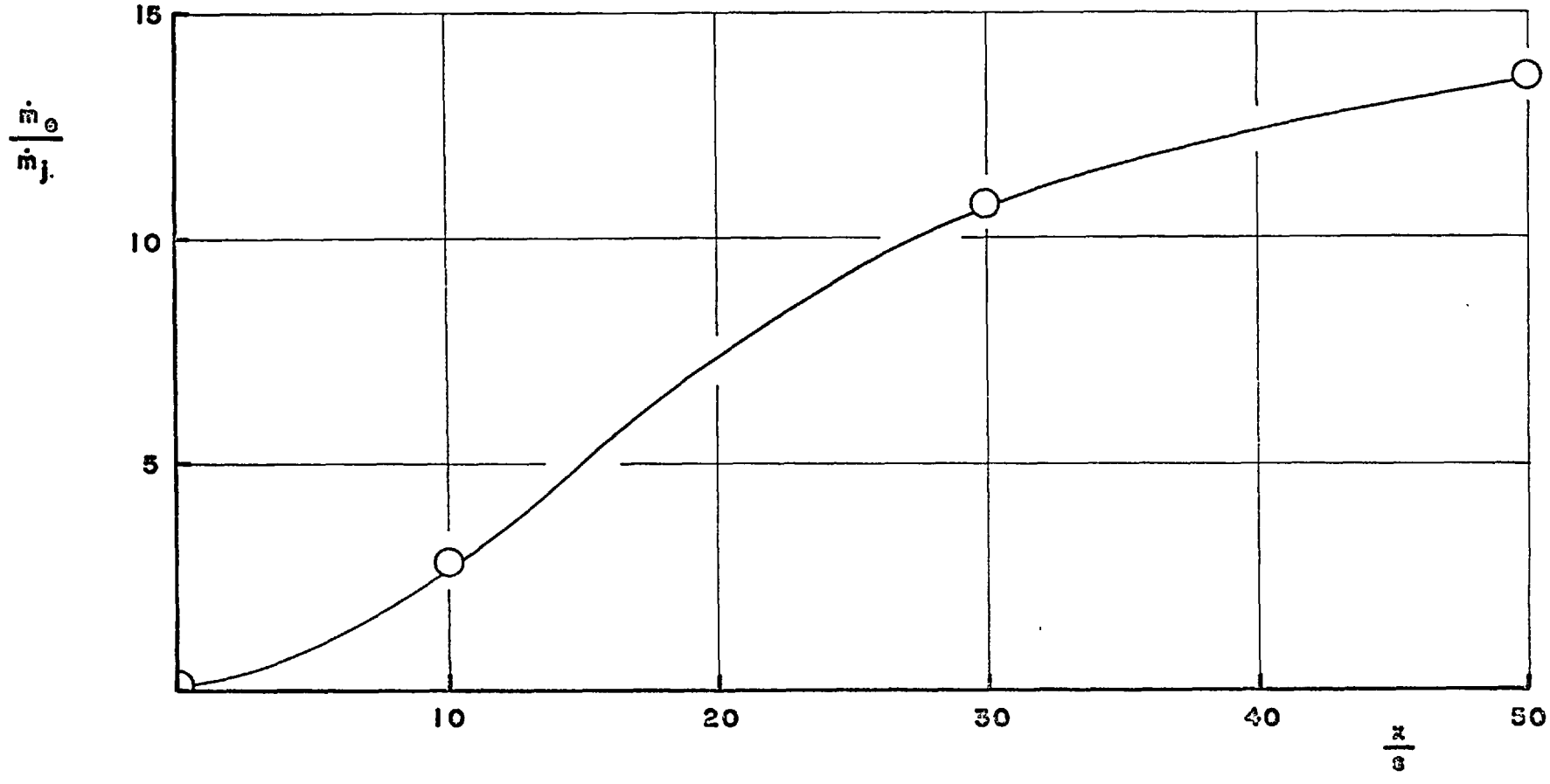


Fig. 5.14 Percentage of mass flow entrained to jet mass flow downstream of slot for $u_j/u_m = 2 \cdot 83$

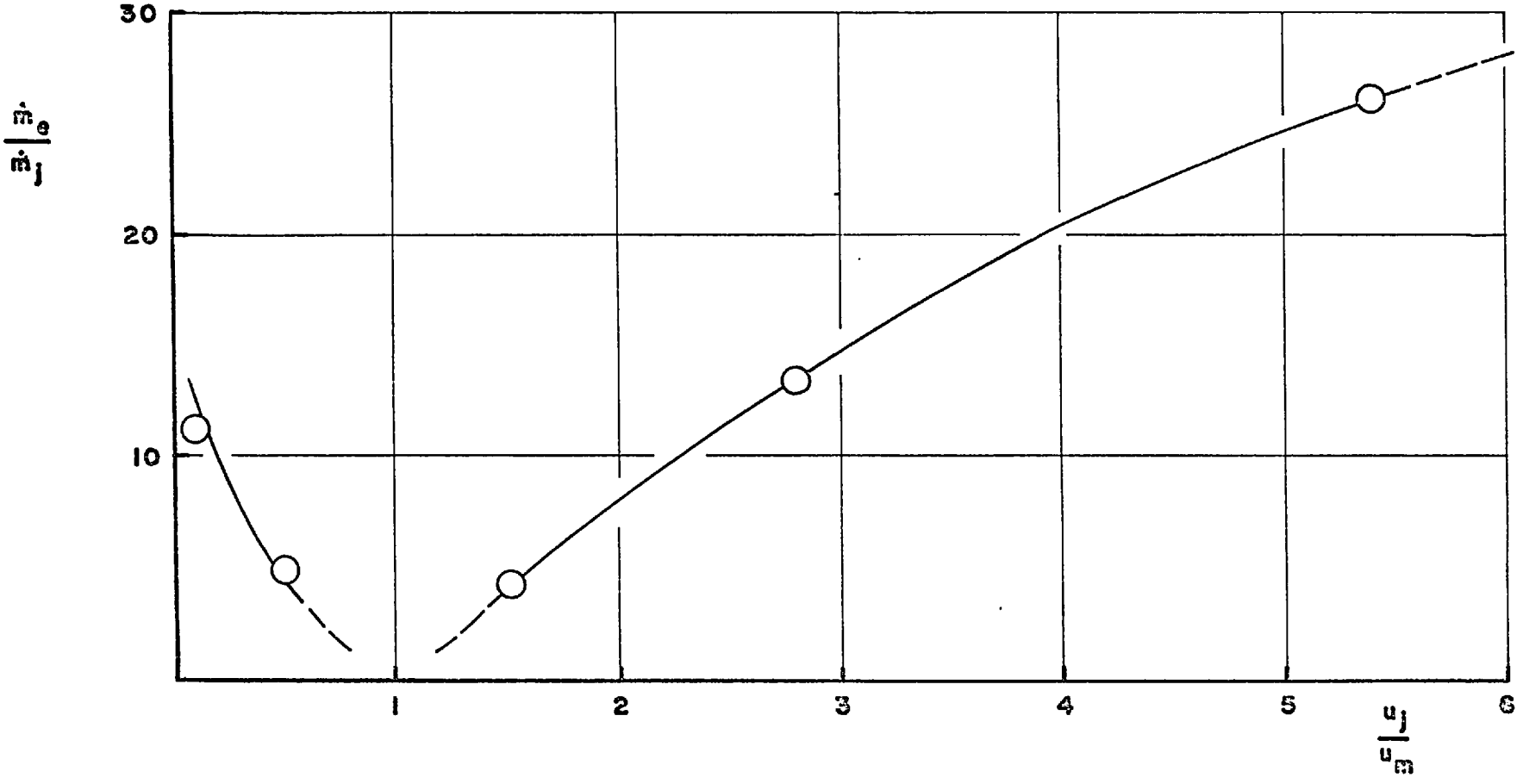


Fig. 5.15 Percentage of mass flow entrained to jet mass flow against velocity ratio